



**MATHEMATICAL MODELS
FOR THE PREDICTION OF
THERMAL ENERGY CHANGES
IN IMPOUNDMENTS**

WATER POLLUTION CONTROL RESEARCH SERIES

The Water Pollution Control Research Series describes the results and progress in the control and abatement of pollution of our Nation's waters. They provide a central source of information on the research, development, and demonstration activities of the Water Quality Office, Environmental Protection Agency, through inhouse research and grants and contracts with Federal, State, and local agencies, research institutions, and industrial organizations.

Inquiries pertaining to the Water Pollution Control Research Reports should be directed to the Head, Project Reports System, Office of Research and Development, Water Quality Office, Environmental Protection Agency, Washington, D.C. 20242.

MATHEMATICAL MODELS FOR THE PREDICTION OF THERMAL
ENERGY CHANGES IN IMPOUNDMENTS

by

Water Resources Engineers, Inc.
Walnut Creek, California

for the

WATER QUALITY OFFICE
ENVIRONMENTAL PROTECTION AGENCY

Project #16130 EXT
Contract # 14-12-422

December 1969

EPA Review Notice

This report has been reviewed by the Water Quality Office, EPA, and approved for publication. Approval does not signify that the contents necessarily reflect the views and policies of the Environmental Protection Agency, nor does mention of trade names or commercial products constitute endorsement or recommendation for use.

TABLE OF CONTENTS

	Page
LIST OF FIGURES	v
LIST OF TABLES	viii
I INTRODUCTION	1
BACKGROUND AND NEED	1
OBJECTIVES	6
ORGANIZATION OF THE RESEARCH EFFORT	8
<i>GENERAL APPROACH</i>	8
<i>REPORT FORMAT</i>	9
<i>AUTHORITY AND RESPONSIBILITY</i>	11
II CLASSIFICATION OF RESERVOIRS	13
PART I -- BASE SIMULATION STUDIES	
III INITIAL MODEL APPLICATIONS	19
HUNGRY HORSE RESERVOIR	21
OBJECTIVES	22
MINOR MODEL REFINEMENTS	22
IV INTERNAL MIXING STUDIES	29

	MIXING PROPERTIES OF RESERVOIRS	30
	EFFECT OF VARYING THE FUNCTIONAL REPRESENTATION OF THE INTERNAL MIXING PROCESS	39
	<i>EXPONENTIAL REPRESENTATION</i>	40
	<i>STEP FUNCTION</i>	46
	<i>REPRESENTATION OF $A(z, t)$ BY A CONTINUOUS FUNCTION</i>	50
	<i>PROPOSED FUNCTIONAL FORM FOR THE EDDY CONDUCTIVITY COEFFICIENT</i>	60
	<i>MODEL SENSITIVITY TO THE DIFFUSION FUNCTION</i>	63
	VERIFICATION OF THE DEEP RESERVOIR MODEL	67
V	SELECTIVE WITHDRAWAL STUDIES	75
	THEORY	75
	SIMULATION OF HUNGRY HORSE RESERVOIR USING SELECTIVE WITHDRAWAL THEORY	85
VI	MULTIPLE OUTLET STUDIES	93
	TEST CASE I	94
	TEST CASE II	98
VII	SUMMARY AND CONCLUSIONS -- PART I	103
	GENERAL	103
	LIMITATIONS	104
	RECOMMENDATIONS	106

PART II -- SIMULATION OF WEAKLY STRATIFIED RESERVOIRS

VIII	INTRODUCTION	109
IX	SEGMENTING THE RESERVOIR	113
	NOMENCLATURE	113
	PROCEDURE	114
	<i>GEOMETRICAL CONSIDERATIONS</i>	114
	<i>RESIDENCE TIME</i>	115
	<i>TRIBUTARY INFLOWS</i>	116
	<i>LONGITUDINAL RESOLUTION OF ISOTHERMS</i>	116
X	INTERFACING ADJACENT RESERVOIR SEGMENTS	119
	MOMENTUM AND BUOYANCY CONSIDERATIONS	120
	INTERFLOW THICKNESS	121
	MASS CONTINUITY	122
	HEAT CONTINUITY	123
XI	APPLICATION TO LAKE ROOSEVELT	127
	GENERAL INFORMATION	127
	PHYSICAL AND THERMAL DATA	128
	METEOROLOGIC DATA	130
	SEGMENTING THE RESERVOIR	133
	SIMULATION RESULTS	138
	<i>GENERAL OBSERVATIONS</i>	138
	<i>SPECIFIC OBSERVATIONS</i>	144
	<i>REMARKS</i>	149

XII	SUMMARY AND CONCLUSIONS -- PART II	151
	GENERAL	151
	RECOMMENDATIONS	152
	CAVEAT	154
XIII	LIST OF REFERENCES	155

LIST OF FIGURES

	Page
FIGURE 1 The Columbia River Basin	4
FIGURE 2 Hungry Horse Reservoir	20
FIGURE 3 Observed Temperature Profiles, Hungry Horse Reservoir, 1965	23, 24
FIGURE 4 Effective Diffusion and Temperature Profiles for Selected Impoundments	32
FIGURE 5 Energy Distribution	34
FIGURE 6 Contribution to Vertical Heat Flux by Individual Heat Transfer Mechanisms, Hungry Horse Reservoir, 1965	41
FIGURE 7 Typical Computed Temperature Profile with $A(z,t)$ Described by Equation 10 and $A(z_T,t) = 5.0 \times 10^{-5} \text{ m}^2 \text{ sec}^{-1}$	44
FIGURE 8 Typical Computer Temperature Profile with $A(z,t)$ Described by Equation 10 and $A(z_T,t) = 1.0 \times 10^{-4} \text{ m}^2 \text{ sec}^{-1}$	44
FIGURE 9 Representation of $A(z,t)$ with a Step Function	47
FIGURE 10 Typical Computed Temperature Profile with $A(z,t)$ Described by Equation 11; Simulation Day is 1 September 1965	50
FIGURE 11 Average Eddy Conductivity Profile for Hungry Horse Reservoir, 1965	52
FIGURE 12 Log of Eddy Conductivity versus log Stability -- Hungry Horse Data	54, 55
FIGURE 13 Typical Temperature and Eddy Conductivity Profile Obtained by Use of Continuous Function for $A(z,t)$	56

FIGURE 14	Relationship between Hypolimnetic Value of Eddy Conductivity Coefficient and Deep Reservoir Hydraulics	59
FIGURE 15	Effect of Eddy Conductivity Parameter Variation on Simulated Reservoir Temperature Profiles; Hungry Horse Reservoir, 1965	64
FIGURE 16	Reservoir Simulation with $A(z,t)$ Defined by Equation 12; Hungry Horse Reservoir, 1965	66
FIGURE 17	Simulated and Observed Thermal Regime for Hungry Horse Reservoir, 1965	68
FIGURE 18	Breakdown of Outlet Discharges and Computed Outlet Temperatures for Hungry Horse Reservoir, 1965	69
FIGURE 19	Simulated and Observed Temperature Profiles for Hungry Horse Reservoir, 1965	70, 71
FIGURE 20	Schematic Sketch of Flow Separation in Stratified Flow	76
FIGURE 21	Schematic Diagram of the Application of Selective Withdrawal Theory to a Stratified Impoundment	77
FIGURE 22	Withdrawal Region for Case of Dividing Streamline Falling Below Reservoir Bottom	80
FIGURE 23	Withdrawal Region for Case of Computed Dividing Streamline Crossing the Thermocline	81
FIGURE 24	Effect of Convective Mixing on the Thermal Profile	82
FIGURE 25	Assumed Reservoir Density Structure for Application of Craya's Criteria	83
FIGURE 26	Comparision of Outflow Temperatures Computed from Debler's Criteria with Measured Cooling Water Temperatures (Fontana Reservoir)	86

FIGURE 27	Simulated Thermal Regime of Hungry Horse Reservoir, 1965, Using Selective Withdrawal Theory	89
FIGURE 28	Simulated Discharge Temperatures for Individual Outlets as Computed with Selective Withdrawal Theory; Hungry Horse Reservoir, 1965	90
FIGURE 29	Simulated Thermal Regime of Hungry Horse Reservoir, 1965, with Modified Reservoir Release Scheme	95
FIGURE 30	Discharges and Discharge Temperatures for Individual Outlets with Modified Reservoir Release Scheme, Hungry Horse Reservoir, 1965	97
FIGURE 31	Simulated Thermal Regime of Hungry Horse Reservoir, 1965, with Addition of Additional Turbine Intake; Hungry Horse Reservoir, 1965	100
FIGURE 32	Discharges and Discharge Temperatures for Individual Outlets with Addition of Additional Turbine Intake; Hungry Horse Reservoir, 1965	101
FIGURE 33	Schematic Illustration of a Reservoir Divided into Segments and Elements	113
FIGURE 34	Relationship of the Interflow Properties of the Model to Those of the Prototype Reservoir	126
FIGURE 35	Plan View of Lake Roosevelt	129
FIGURE 36	Reservoir Segments in Plan View and Typical Cross Sections, Lake Roosevelt	134
FIGURE 37	Reservoir Segments in Profile View, Lake Roosevelt	135
FIGURE 38	Typical Results from Simulation of the Thermal Regime of Lake Roosevelt, 1967	139, 140, 141, 142
FIGURE 39	Typical Shape of Computed Temperature Profile during Cooling Period when Convective Mixing is Suppressed	146
FIGURE 40	Effect of Linearization on the Temperature Distribution of the Interflow	147

LIST OF TABLES

		Page
TABLE 1	Physical and Meteorologic Information, Hungry Horse Reservoir	21
TABLE 2	Hungry Horse Reservoir -- Turbine Intake Temperatures; and Detroit Reservoir -- Tailrace Temperatures	87
TABLE 3	Physical and Thermal Data, Lake Roosevelt	131, 132
TABLE 4	Residence Times for Individual Segments in Lake Roosevelt	136

I. INTRODUCTION

BACKGROUND AND NEED

Water temperature has assumed an important role in water resources planning and management because of its wide-ranging effects on aquatic flora and fauna and its influence on the physical and chemical characteristics of the water itself. Some of the better known effects of water temperature include: effects on fish, particularly on various parts of their life cycle; effects on the temporal and spacial variation in the dissolved oxygen content of the water; effects on the toxicity level of various pollutants; and effects on the taste and odor of drinking water. Details of thermal effects can be found elsewhere (1, 2, 3, 4, 5, 6, 7).

In addition to the above mentioned effects, the water temperature, through its influence on density, affects the hydrodynamic characteristics of the watercourse, particularly in impoundments which are subject to thermal stratification. Through its influence on the hydrodynamic characteristics, the temperature can exert a profound influence on the temporal and spacial variation of water quality characteristics.

Since the influence of temperature on the quality characteristics of a watercourse is so broad, effective water quality planning requires that there exist the capability to predict the temporal and spacial variation of the water temperature under alternative development plans in order to protect the needs of the water users within the watercourse system. However, this is not a simple problem because of the complexity of the mechanisms which govern heat transfer within a waterbody and heat transfer between the waterbody and its surrounding environment. Before the time of World War I, it had been established through the experiences of the industrial complexes in the eastern and midwestern states that cooling water discharges could significantly alter the thermal regime of a river (8); but it has also been recognized, more recently, that a complex of reservoirs and the way in which the water is discharged from them can have significant effects on the thermal regime of the watercourse (9, 10).

In several areas of the country, the build-up of a complex of dams within a watershed coupled with cooling water discharges from industrial and thermal power plant cooling water discharges have changed the thermal regime of the river to such an extent that the native fish populations have either been eradicated, or their loss is impending. The Columbia River Basin in the Pacific Northwest is a typical case in which the existing complex of dams coupled with the discharge of cooling water from the Hanford nuclear power plant has altered the thermal regime of the Lower Columbia River to such an extent that uncontrolled future development may very possibly annihilate the existing anadromous fish run in the River.

The Columbia River Basin, shown in Figure 1, encompasses a drainage area of some 259,000 square miles, 15 percent of which is in Canada. Thus the water resources management problems of the Basin are international in scope. In contrast to the Columbia River in the United States, which is highly developed, the river in its upper reaches in Canada is almost as wild and untamed as it was when the first white explorers saw it. Within the United States the Columbia River below Grand Coulee, and the Lower Snake River, are used primarily for hydropower and navigation. In addition, this portion of the basin supports a sizable commercial and sports fishery. Other dams in the system, including Grand Coulee Dam, are used primarily for hydropower, irrigation, and flood control and storage.

The present power system in the Pacific Northwest is almost all hydro. Consequently, the complex of dams in the Columbia Basin is operated in a manner such that the base power demand plus the peaking power needs are met. This type of operation, however, is nearing an end. Future load growth in the area is expected to triple in the next 20 years and, while hydro peaking capacity can be increased at existing and planned projects, there are only very limited opportunities to develop new projects that would provide significant amounts of additional hydro-energy (11). Thus, future plans call for the construction of thermal nuclear plants to meet the base load demands with the hydro projects being used more and more for peaking power only. According to a recent report (12), practically all of the Columbia River mainstem above the Dalles Dam is considered as preferred nuclear siting areas.

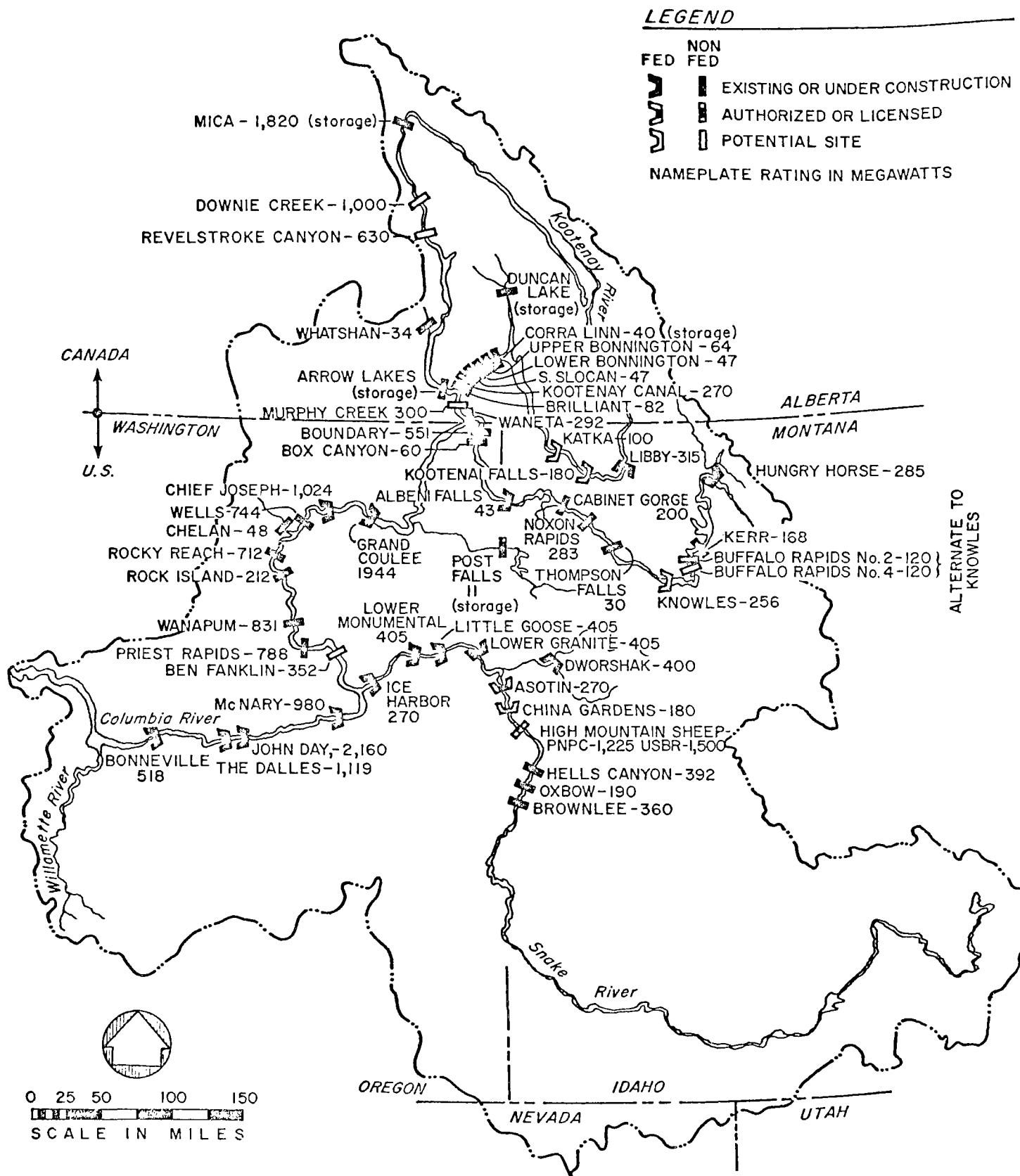


FIGURE 1. The Columbia River Basin

As mentioned above, the present complex of dams in the Columbia Basin, with its present scheme of operation plus the discharge of cooling water from the Hanford nuclear power plant, has already altered the temperature regime of the Lower Columbia sufficiently to endanger the existing fisheries. By the construction of additional dams in Canada and the United States under the Columbia River Treaty (13), the possible addition of nuclear power plants on the mainstem, and the alteration of the operation of the Columbia system, there is a real possibility that the existing fisheries in the Columbia will be lost unless temperature control is integrated into the future planning and development of the Basin.

Recognizing the thermal problems attendant with the present and future development of the Columbia River System, the Federal Water Pollution Control Administration (FWPCA) has undertaken the Columbia River Thermal Effects Project in order to determine the impact of hydroelectric projects and thermal loads on water temperatures in the system from the Canadian border to the river mouth at Astoria. Where appropriate, the Study will utilize established methodology or proven tools to develop the facility for prediction of temperature changes under various climatological, meteorological, or operational conditions. In a number of instances, it will be necessary to direct concurrent research efforts to provide the needed capability.

It has been determined that a mathematical model or "simulation package" for prediction of temperature changes in the river system is an essential tool for the Study. This model or set of models must have the capability to represent with reasonable accuracy the thermal responses of each of the major types of hydraulic

regimes in the system from comparatively simple uniform flow in river reaches to the more complex stratified flows in reservoirs. Capability is also needed to cope with highly unsteady flows associated with power load variations or with tidal influences in the river's estuary.

As an initial step in its program, the Study Team has undertaken the development of a "run-of-the-river" temperature model. This model is expected to be suitable for prediction of temperature changes in reaches of the river system unaffected hydraulically by the backwater of deeper impoundments and in certain of the more shallow reservoirs which may be considered to be well-mixed vertically. However, in order to provide more flexibility for prediction, including those cases where flows are partially or strongly stratified, the Study Team wishes to incorporate into its model package certain components of a deep reservoir model developed by Water Resources Engineers, Inc. (WRE). Further, it wishes that the model be refined and restructured as necessary, so that it can cope with the full range of practical problems to be studied in the many complicated reservoirs identified with the Columbia River System. To this end, FWPCA has contracted with WRE to perform a research and development study whose scope is sufficient to meet the required objectives as stated below.

OBJECTIVES

A general objective of the research reported herein was to devise a generalized mathematical model which would represent, within the practical and reasonable limits of accuracy, the thermal

changes which may be expected under alternative hydrologic, hydraulic and climatologic conditions for operating reservoirs. It is intended that this work support and complement that already completed or underway by the Study Team in its investigation of the Columbia River System.

Specific objectives of the work were to provide for the Columbia River Thermal Effects Project the means for simulation of:

1. thermal energy changes which occur as a result of internal mixing processes in deep, stratified impoundments;
2. temperature changes which may result from the installation and operation of multiple outlets or other physical devices for control of the temperature regime; and
3. thermal energy distributions which result in weakly-stratified reservoirs where so-called "thermal underflows" may occur, i.e., where longitudinal temperature gradients are significant.

These required capabilities were to be supplied to FWPCA in the form of a specific model, or models, compatible with the FWPCA river-run model and to be available for use at the end of the contract period. Further details can be found in the contract proposal (14).

ORGANIZATION OF THE RESEARCH EFFORT

GENERAL APPROACH

At the time that research work was initiated on this contract, WRE had in hand a deep reservoir model which had been recently developed under contract with the Department of Fish and Game of the State of California (15). The model had been successfully verified for deep water bodies having low and moderate discharge to volume ratios by applications to Lake Washington in the State of Washington (16) and to Fontana Reservoir in the TVA system, respectively. The reader who is not familiar with this basic model is encouraged to review reference 15 before proceeding, since the work reported herein is specifically oriented toward the further development of this model.

A review of the initial applications of the model on Lake Washington and Fontana Reservoir established that further refinement of two features of the deep reservoir model would greatly enhance its general applicability. These features were, specifically:

- a. the description of the internal mixing process within a reservoir; and
- b. the methodology for introducing inflows and extracting outflows from the reservoir model.

The accomplishment of objectives 1 and 2 required that the above refinements of the deep reservoir model be made in order to provide FWPCA with a model displaying the capabilities required for its general application. Since the development of these capabilities

can best be accomplished by working with real data, it was appropriate that a prototype test reservoir be selected which displayed strong stratification characteristics and for which there existed a data base adequate for the analyses contemplated. Hungry Horse Reservoir in Montana was chosen as the prototype best suited to the research needs. A set of test simulation runs was conducted on this reservoir for the purpose of refining the description of the internal mixing process and incorporating into the model the theory of selective withdrawal from stratified impoundments. The base simulations also provided opportunity for the identification and correction of any weaknesses in the model. In addition, the reservoir itself served as a test case for verification of the model on a deep reservoir typical of those found in the Pacific Northwest.

The accomplishment of objective 3 required that the generalized model developed in meeting objectives 1 and 2 be restructured to conform to the constraints imposed by a reservoir displaying the characteristics of a weakly-stratified impoundment. This restructured model was then tested on Lake Roosevelt which is a prototype of the weakly-stratified reservoir class.

REPORT FORMAT

Since the successful accomplishment of objective 3 required the meeting of objectives 1 and 2, it was expedient to break the work under this contract into two phases or parts: Part I dealing with the research and development pertaining to the base simulations of the model on a deep reservoir; and Part II addressing itself to the

restructuring of the generalized model developed in Part I of the research, and the results of applying the new model to a weakly-stratified reservoir. Consequently, the report contained herein is also broken into two parts which are titled: Part I--BASE SIMULATION STUDIES; and Part II--SIMULATION OF WEAKLY STRATIFIED RESERVOIRS.

Chapters III through VII constitute Part I of the report. The first four chapters describe, sequentially, the steps taken in meeting objectives 1 and 2. These steps were as follows:

1. An initial set of base simulations were conducted on Hungry Horse Reservoir in order to: a) identify (and correct) any specific weaknesses which might exist in the model; b) establish a better criteria for introducing tributary inflows into the model; and c) explore the effect of varying the functional representation of the internal mixing process.
2. On the basis of the knowledge gained from the base simulations, efforts were concentrated on refining the description of the internal mixing process.
3. The theory of selective withdrawal from stratified impoundments was reviewed and incorporated into the model.
4. Two test cases (one practical, the other hypothetical) were simulated for downstream temperature control.

The summary and recommendations for Part I are contained in Chapter VII.

Part II of the report, which constitutes Chapters VIII through XII, is more application oriented than Part I since the basic unit of the weakly-stratified reservoir model is the deep reservoir model. Part II contains, sequentially:

1. A conceptual description of the weakly stratified reservoir model.
2. The process of adapting the model to the geometric and hydraulic characteristics of the reservoir.
3. The details of restructuring the deep reservoir model.
4. Application of the weakly-stratified reservoir model to Lake Roosevelt.

The summary and recommendations for Part II are contained in Chapter XII.

In addition to the material contained herein, a Supplement to this report has been prepared under separate cover. The Supplement is devoted to a detailed explanation of the use, utility, and details of the computer program employed for simulating the internal temperature structure of thermally stratified impoundments.

AUTHORITY AND RESPONSIBILITY

The work reported herein was performed under Contract No. 14-12-422, dated June 28, 1968, between the Federal Water Pollution Control Administration and Water Resources Engineers, Inc. All aspects of the technical work were conducted by the staff of WRE under the direct supervision of Dr. Gerald T. Orlob, President.

Dr. Larry A. Roesner coordinated the project and was responsible for the theoretical development; Mr. W. R. Norton developed the computer simulation package and contributed substantially to the practical implementation of the theory.

Dr. R. W. Zeller and Mr. John Yearsley, both of whom were members of the FWPCA Study Team, were closely associated with the project throughout its execution and were responsible for supplying all the physical, hydrologic, and meteorologic data used in the development and testing of the reservoir temperature models.

ACKNOWLEDGMENTS

WRE has enjoyed the close liaison and cooperative attitude that existed between itself and the FWPCA during the performance of this work. The establishment of this rapport is directly attributable to Dr. Bruce A. Tichenor, project officer for the FWPCA in this study, Dr. Zeller, and Mr. Yearsley. The attitude and enthusiasm of these gentlemen materially aided the smooth and successful completion of this study.

II. CLASSIFICATION OF RESERVOIRS

In Chapter I, three different types of reservoirs were mentioned and it was inferred that a different approach was required to mathematically model the thermal regime of each type. It is the purpose of the following discussion to define these reservoir types or *classes* somewhat more precisely and to lay down some general guidelines for reservoir classification.

The hydrodynamic and thermal behavior of a fluid system is completely described by the simultaneous solution of three differential equations, namely:

1. the Navier-Stokes equations (equations of motion);
2. the conservation of mass equation; and
3. the conservation of energy equation.

Unfortunately, however, these equations cannot be solved except for a very limited number of steady-state cases. Consequently, real world descriptions of the behavior of prototype systems require that types or *classes* of solutions be formed which describe, in an approximate way, the actual hydrodynamic and thermal processes occurring within the system. As applied to the specific objectives of the work reported herein, these approximate solutions must be formulated in

a manner such that they account for the principal hydrodynamic and thermodynamic processes affecting the internal temperature structure of the reservoir.

Experience with prototype reservoirs indicates that there are three distinct classes of reservoirs, each of which requires a different type of solution for the determination of its internal energy (temperature) distribution. These classes, which were alluded to in the introduction, are:

1. The *deep* reservoir which is characterized by horizontal isotherms;
2. the *weakly-stratified* reservoir, characterized by isotherms which are tilted along the longitudinal axis of the reservoir; and
3. the *completely mixed* reservoir whose isotherms are vertical.

By their very definition, it is apparent that the deep reservoir solution and the completely mixed reservoir solution are one-dimensional, because their thermal properties vary in one direction only. The difference, of course, is that the solution is taken along the vertical axis for the deep reservoir while the completely mixed reservoir solution is taken along the longitudinal axis. In contrast, the solution of the weakly-stratified reservoir requires that both dimensions be considered.

The single most important parameter determining into which class a reservoir will fall, and hence the type of solution required, is the densimetric Froude number which can be written for the reservoir as

$$F = \frac{LQ}{DV} \sqrt{\frac{\rho_0}{g\beta}} \quad (1)$$

where

- L = reservoir length;
- Q = volumetric discharge through the reservoir;
- D = mean reservoir depth;
- V = reservoir volume;
- ρ_0 = reference density;
- β = average density gradient in the reservoir; and
- g = gravitational constant.

This number is the ratio of the inertial force of the horizontal flow to the gravitational forces within the stratified impoundment; consequently, it is a measure of the success with which the horizontal flow can alter the internal density (thermal) structure of the reservoir from that of its gravitational static-equilibrium state.

In deep reservoirs, the fact that the isotherms are horizontal indicates that the inertia of the longitudinal flow is insufficient to disturb the overall gravitational static equilibrium state of the reservoir except possibly for local disturbances in the vicinity of the reservoir outlets and at points of tributary inflow. Thus, F would be expected to be small for such reservoirs. In completely mixed reservoirs, on the other hand, the inertia of the flow and its attendant turbulence is sufficient to completely upset the gravitational structure

and destratify the reservoir. For reservoirs of this class, Fr would be expected to be large. In between these two extreme classes lies the weakly-stratified reservoir in which the longitudinal flow possesses enough inertia to disrupt the reservoir isotherms from their gravitational static-equilibrium state configuration, but not enough to completely mix the reservoir.

For the purpose of classifying reservoirs by their Froude number, β and ρ_0 in equation 1 may be approximated as $10^{-3} \text{ kg m}^{-4}$ and 1000 kg m^{-3} , respectively. Substituting these values and g into equation 1 leads to an expression for Fr as

$$Fr = 320 \frac{L}{D} \frac{Q}{V} \quad (2)$$

where L and D have units of meters, Q is in cms, and V has units of m^3 . From this equation it is observed that the principal reservoir parameters that determine a reservoir's classification are its length, depth, and discharge to volume ratio ($\frac{Q}{V}$).

In developing some familiarity with the magnitude of Fr for each of the three reservoir classes, it is helpful to note that theoretical and experimental work in stratified flow indicates that flow separation occurs in a stratified fluid when the Froude number is less than about $\frac{1}{\pi}$, i.e. for $Fr < \frac{1}{\pi}$, part of the fluid will be in motion longitudinally while the remainder is essentially at rest. Furthermore, as Fr becomes smaller and smaller, the flowing layer becomes more and more concentrated in the vertical direction. Thus, in the deep reservoir it is to be expected that the longitudinal flow is highly concentrated at values of $Fr \ll \frac{1}{\pi}$ while in the completely mixed case Fr must be at least greater than $\frac{1}{\pi}$ since the entire reservoir is in motion and it may be expected in general that $Fr \gg \frac{1}{\pi}$.

Values of Fr for the weakly-stratified case would fall between these two limits and might be expected to be on the order of $\frac{1}{\pi}$. As an illustration, five reservoirs are listed below with their Froude numbers. It is known that Hungry Horse Reservoir and Detroit Reservoir are of the deep reservoir class and can be effectively described with a one-dimensional model along the vertical axis of the reservoir. Lake Roosevelt, which has been observed to fall into the weakly stratified class is seen to have a Froude number on the order of $\frac{1}{\pi}$ which is considerably larger than Fr for either Hungry Horse or Detroit Reservoirs. Finally, Priest Rapids and Wells Dams, which are essentially completely mixed along their vertical axes, show Froude numbers much larger than $\frac{1}{\pi}$, as expected.

RESERVOIR FROUDE NUMBERS

RESERVOIR	LENGTH meters	AVERAGE DEPTH meters	DISCHARGE TO VOLUME RATIO sec^{-1}	Fr	CLASS
Hungry Horse	4.7×10^4	70	1.2×10^{-8}	0.0026	Deep
Detroit	1.5×10^4	56	3.5×10^{-8}	0.0030	Deep
Lake Roosevelt	2.0×10^5	70	5.0×10^{-7}	0.46	Weakly- Stratified
Priest Rapids*	2.9×10^4	18	4.6×10^{-6}	2.4	Completely Mixed
Wells*	4.6×10^4	26	6.7×10^{-6}	3.8	Completely Mixed

*River run dams on the Columbia River below Grand Coulee Dam

The above illustrations tend to confirm the validity of using the densimetric Froude number to classify reservoirs; however, just what values should be used to distinguish the transition points, between the individual reservoir classes, is not clear at this time. The determination of these points requires further investigation.

PART I -- BASE SIMULATION STUDIES

III. INITIAL MODEL APPLICATIONS

HUNGRY HORSE RESERVOIR

All base simulation studies in Part I were performed using Hungry Horse Reservoir in Montana as the prototype. This reservoir is located on the South Fork of the Flathead River in west central Montana and is a major storage reservoir in the Columbia River power system. It has a rated, useable storage capacity of 2.98 million acre-feet and was constructed by the U.S. Bureau of Reclamation during the period 1948-1953. A plan view of the reservoir is illustrated in Figure 2 and information pertinent to energy budget calculations is give in Table 1.

Time and money constraints required that the period of prototype simulation be limited to a single year. Calendar year 1965 was recommended by the FWPCA Study Team as the period during which the data base was most accurate. Although there was only sufficient data to simulate the period from 11 May to 20 October, this time period was of sufficient length to allow simulation of the reservoir from the onset of stratification in the spring, through the summer heating period, and well into the fall cooling portion of the annual cycle. Since these periods are the most critical that the deep reservoir model must be able to simulate, the data were regarded as adequate for the required research and development. Average centerline temperature profiles for the main body of the reservoir,

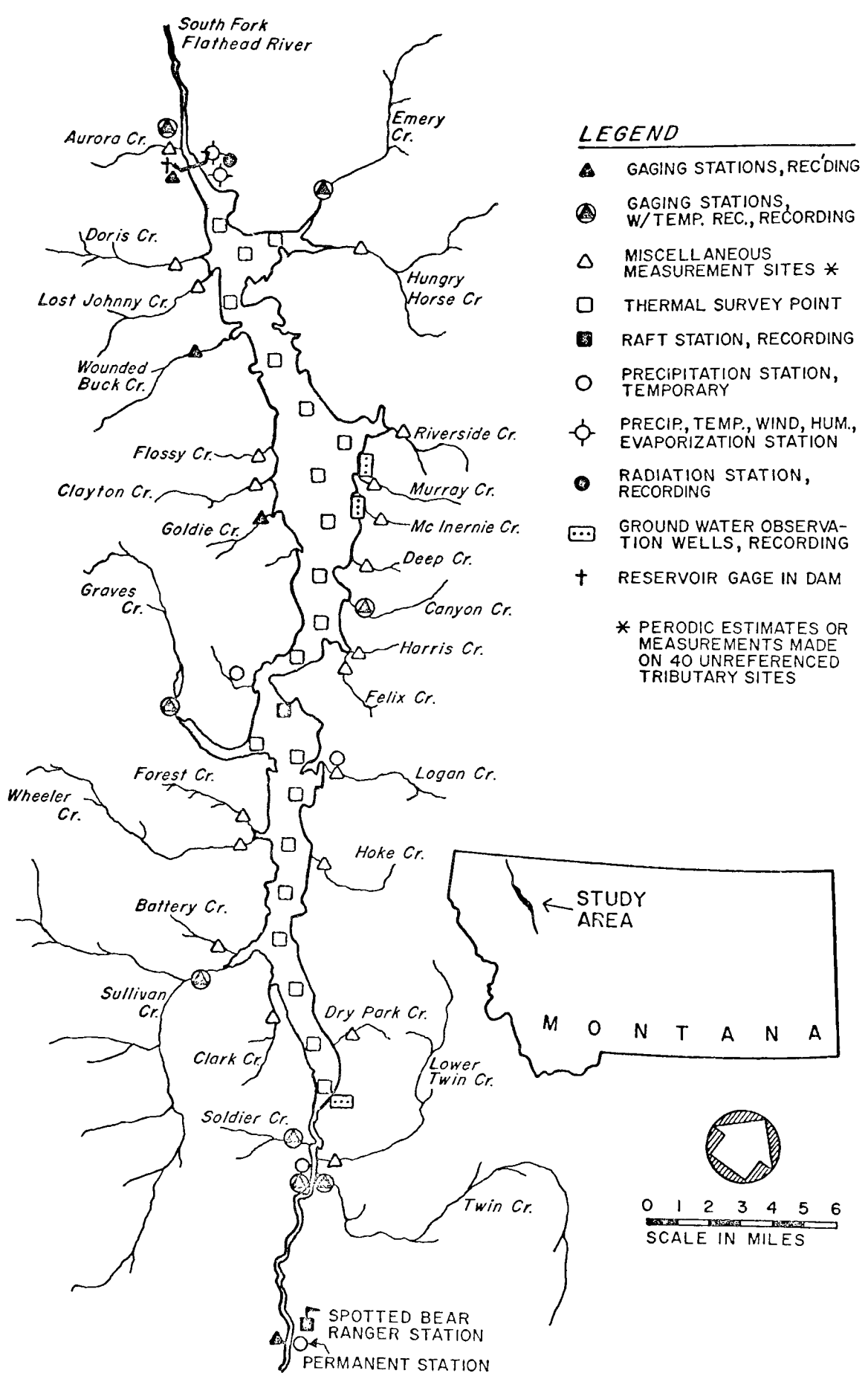


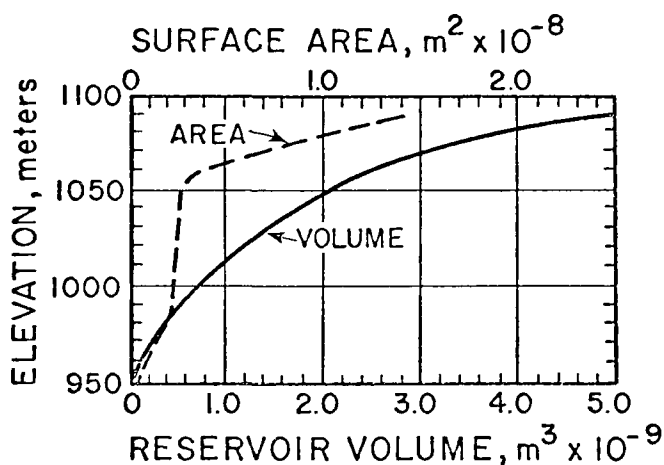
FIGURE 2. Hungry Horse Reservoir

TABLE 1

PHYSICAL AND METEOROLOGICAL INFORMATION
HUNGRY HORSE RESERVOIR

PHYSICAL DATA

Location:	Latitude 48°20', Longitude 114°01'
Elevation:	1085 meters (normal high water surface elevation)
Intake Elevations:	Lower Discharge Tubes - 975 meters Penstock Intakes - 1013 meters
Spillway:	Type - Gloryhole, elevation 1082 meters
Mean Gaged Inflow:	73.2 CMS from 9 tributaries
Mean Ungaged Inflow:	39.3 CMS
Average Reservoir Discharge to Volume Ratio:	0.82 yr ⁻¹



METEOROLOGICAL DATA

Solar Radiation:	computed
Atmospheric Radiation:	computed
Cloud Cover:	data from Kalispell
Barometric Pressure:	data from Kalispell
Wind Speed:	data from Hungry Horse Reservoir
Air Temperature (wet bulb and dry bulb):	data from Hungry Horse Reservoir
Solar Radiation Extinction Coefficient in Water:	supplied by FWPCA, 0.345 m ⁻¹
Evaporation Coefficient:	supplied by FWPCA, 2.1 x 10 ⁻⁹ mps/mb/mps

observed at various times during the simulation period, are illustrated in Figure 3. The ability of the model to reproduce these profiles was taken as the criteria for evaluating its performance.

OBJECTIVES

In the initial model applications a series of base simulations was conducted. The purpose of these simulations was two-fold: first, to identify any specific weaknesses in the model; and second, to explore the effect of varying the functional representation of the internal mixing process. Since the results of investigations on the internal mixing process fall more logically into Chapter IV, this chapter is devoted primarily to the identification and correction of specific weaknesses found in the model.

MINOR MODEL REFINEMENTS

The initial applications of the deep reservoir model revealed that the computer code contained deficiencies in the following areas:

1. Computational efficiency;
2. Adequate detail in the description of the movement of the water surface; and
3. Flexibility in the specification of the simulation time step.

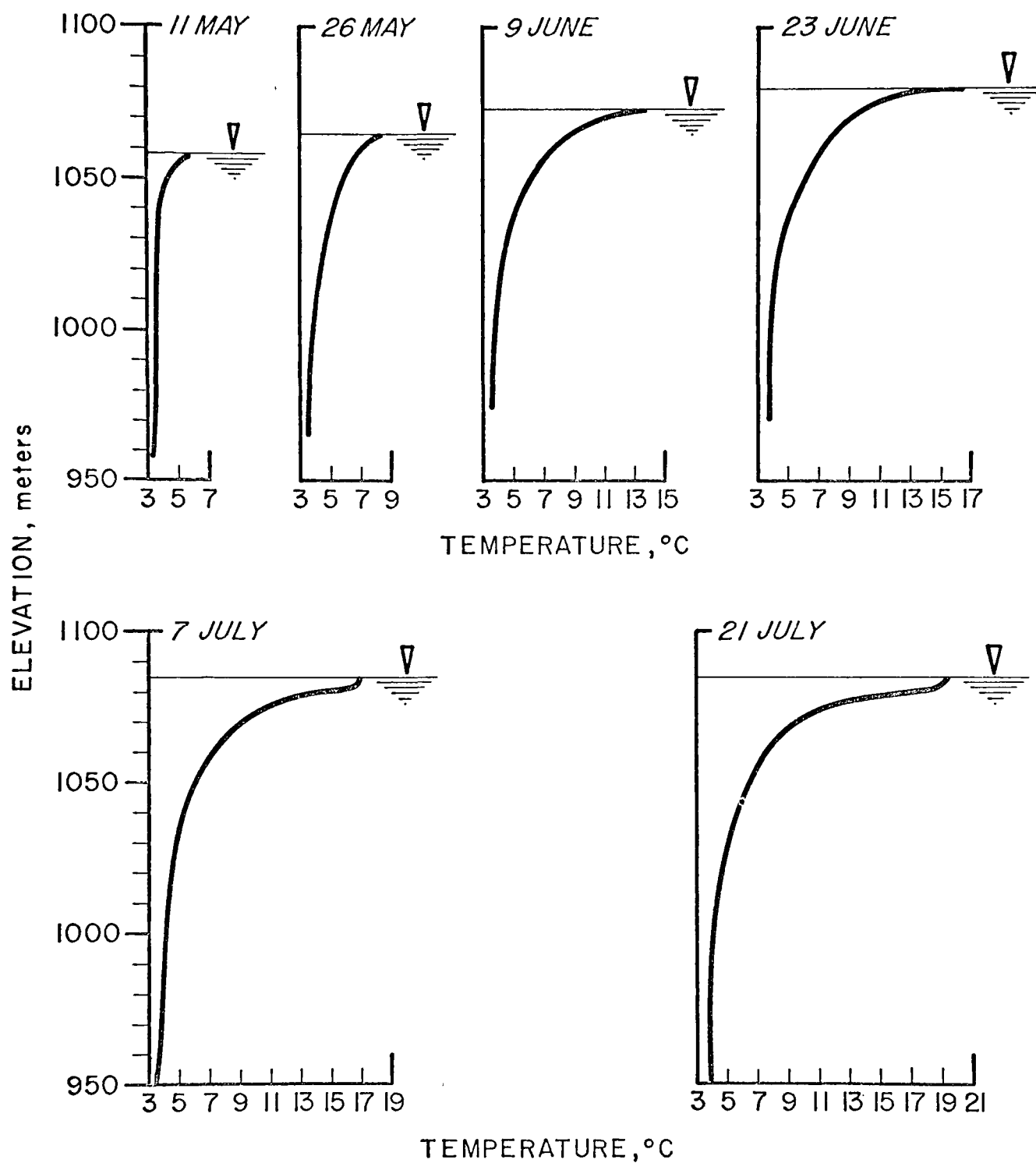


FIGURE 3. Observed Temperature Profiles, Hungry Horse Reservoir, 1965

(Continued next page)

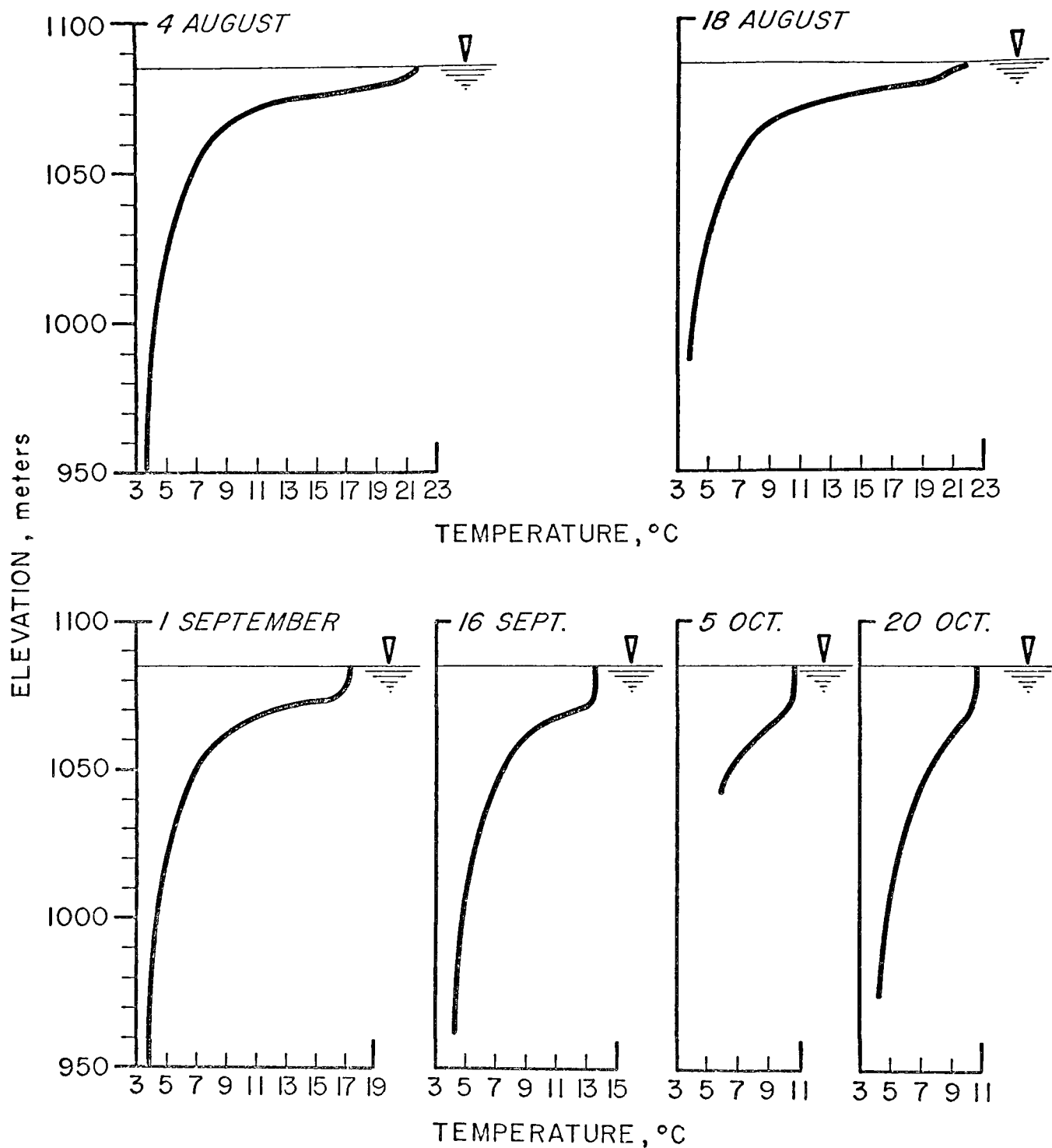


FIGURE 3 (continued). Observed Temperature Profiles, Hungry Horse Reservoir, 1965

COMPUTATIONAL EFFICIENCY

At the time this work was initiated, WRE had only recently completed the basic development and verification of the computer code for deep reservoir simulation. As is often typical of developmental work, computational efficiency was not strongly emphasized. Consequently, a critical review of the computer code revealed that many internal computational refinements could be made to shorten the solution time. It is estimated that the reprogramming effort improved computational efficiency approximately fifty percent which resulted in an overall decrease in computer execution time of about 25 percent.

MOVEMENT OF THE WATER SURFACE

In the original version of the model, each reservoir slice, or *element*, was of equal height. The reservoir surface was taken as the top of the uppermost reservoir element which was completely filled with water; partially filled elements were ignored. As a result of this condition, changes in the water surface elevation were handled in a stepwise fashion with complete elements being added or subtracted from the reservoir as their upper surfaces became submerged or exposed, respectively. With the height of an element typically taken as one meter, changes in water surface elevation were accounted for in steps of approximately three feet.

The step-wise approximation of the water surface elevation has been eliminated by allowing the height of the surface element to be variable (between one and two times the standard element thickness), the upper boundary of the element coincides with the water surface elevation. This refinement is believed to produce a better description of the temperature structure near the reservoir's surface.

VARIATION OF THE SIMULATION TIME STEP

Another refinement was made which allows the use of a simulation time step that is different from the interval between successive observations of the meteorologic and hydrologic input data. In the original version of the model, the simulation interval was restricted to the same duration as the interval between observations of meteorologic input data. In the updated version of the computer code the simulation time step may be either longer or shorter than the interval between data observations; all necessary bookkeeping and time averaging necessary for this feature are handled internally by code. This particular refinement was incorporated in order to facilitate reservoir simulation in instances when advective heat transfer violates the basic assumptions of the model. This problem occurs when, for a given time step, the mass volume of flow through a reservoir element is greater than the volume of the element.

Experience indicates that the most critical period with regard to advection violations is in the spring of the year when the tributary inflows to the reservoir are at their maximum; this situation may also be expected to develop during periods when reservoir release rates are high. One of the easiest ways to rectify this violation is to shorten the simulation time step, a manipulation that is now trivial since the required data conversions are handled internally.

TRIBUTARY INFLOWS

As stated in the introduction, the method of introducing inflows to the reservoir was known to need refinement. The original method was to place the entire flow of a tributary into that reservoir

element whose density was nearest to that of the tributary flow. The main objection to this criteria was that the inflow was artificially constrained between the upper and lower planes bounding the element, while in reality the vertical distribution of the flow varies with both the degree of stratification and the quantity of flow.

In order to account for the effects of stratification and the magnitude of inflow, the following scheme has been adopted. First, the elevation, z_0 , is located where the density of the reservoir is equal to that of the inflow. Next, the vertical thickness of the inflow, D , is computed from equation 27-B in Chapter X. The inflow is then distributed between the elevations $z_0 + \frac{1}{2} D$ and $z_0 - \frac{1}{2} D$, assuming a uniform velocity distribution.

The base simulations did not reveal a need for additional refinements. It was concluded from these studies that the successful refinement of the description for the internal mixing process plus the incorporation of selective withdrawal theory into the model would produce a general deep reservoir model with the capabilities required to satisfy objectives 1 and 2.

IV. INTERNAL MIXING STUDIES

Of the total effort expended in Part I of the research, the major portion of it was devoted to the study and refinement of the description of the internal mixing process in deep reservoirs. The expenditure of this amount of effort was anticipated at the outset of the work because internal mixing is a basic feature of the deep reservoir model. Thus, its proper description is imperative to the proper representation of the vertical distribution of heat within a stratified impoundment.

In this chapter, a qualitative overview of the experience and theory relating to internal mixing in reservoirs is presented in the first section. The second section reports the results of varying the functional representation of the mixing process, and describes the form that was chosen as best suited to the description of the process. The last section describes the verification of the deep reservoir model on Hungry Horse Reservoir as simulated with the newly developed functional representation of the internal mixing process.

MIXING PROPERTIES OF RESERVOIRS

The two major factors which govern mixing in reservoirs are gravity and turbulence. Gravity may cause or enhance mixing or it may suppress mixing depending upon whether the density stratification in the reservoir is unstable or stable, respectively. Turbulence, on the other hand, can only promote mixing. When gravity alone is responsible for mixing, the mixing process is called "natural convection," while mixing in the presence of turbulence, with or without gravitational effects, is referred to as "forced convection."

Ordinarily, forced convection is the phenomenon of primary concern in the evaluation of the mixing properties of reservoirs, although at certain times, when the surface of the reservoir is cooling, natural convection plays a primary role in epilimnetic mixing. Since experience with the deep reservoir model has revealed no problems in the present method of describing natural convection, this phenomenon will not be discussed here. Details of its role in distributing heat along the vertical axis of the reservoir can be found in reference 15.

Mixing implies the transfer of materials or properties within a system from points of high concentration to points of low concentration, and *vice versa*. For a system which is experiencing forced convection, it is a rule of experience that the time rate of transport, F , of a property, S , through the system is (other things being equal) proportional to the rate of change of concentration of this property with distance, z . In equation form this rule is

expressed as

$$F = -A \frac{\partial S}{\partial z} , \quad (3)$$

where A is the coefficient of proportionality. The mixing process as defined by equation 3 is often called "effective diffusion," "eddy diffusion," or the "diffusion analogy" since it is identical in form to the equation describing the process of molecular diffusion. The difference between the two processes, however, is that for molecular diffusion, A is constant, while for turbulent transfer, A is a function of the dynamic character, or the turbulence level, of the system. In general, A is a temporal and spatial variable, and thus will be referred to as A(z,t). Equation 3 rewritten for heat flow along the reservoir vertical axis is

$$H = -\rho c A(z,t) \frac{\partial T}{\partial z} , \quad (4)$$

where

- H = heat flux, $HL^{-2}T^{-1}$;
- ρ = density of water, ML^{-3} ;
- c = heat capacity of water, $HM^{-1}D^{-1}$;
- A(z,t) = coefficient of eddy conductivity, L^2T^{-1}
- T = temperature, D;
- z = elevation in the reservoir, L; and
- t = time, T.

The proper or correct choice of A(z,t) is a difficult task because it represents the prototype response to many unknown and/or poorly defined random inputs. However, experience with the coefficient (see Figure 4) has disclosed some of its general properties:

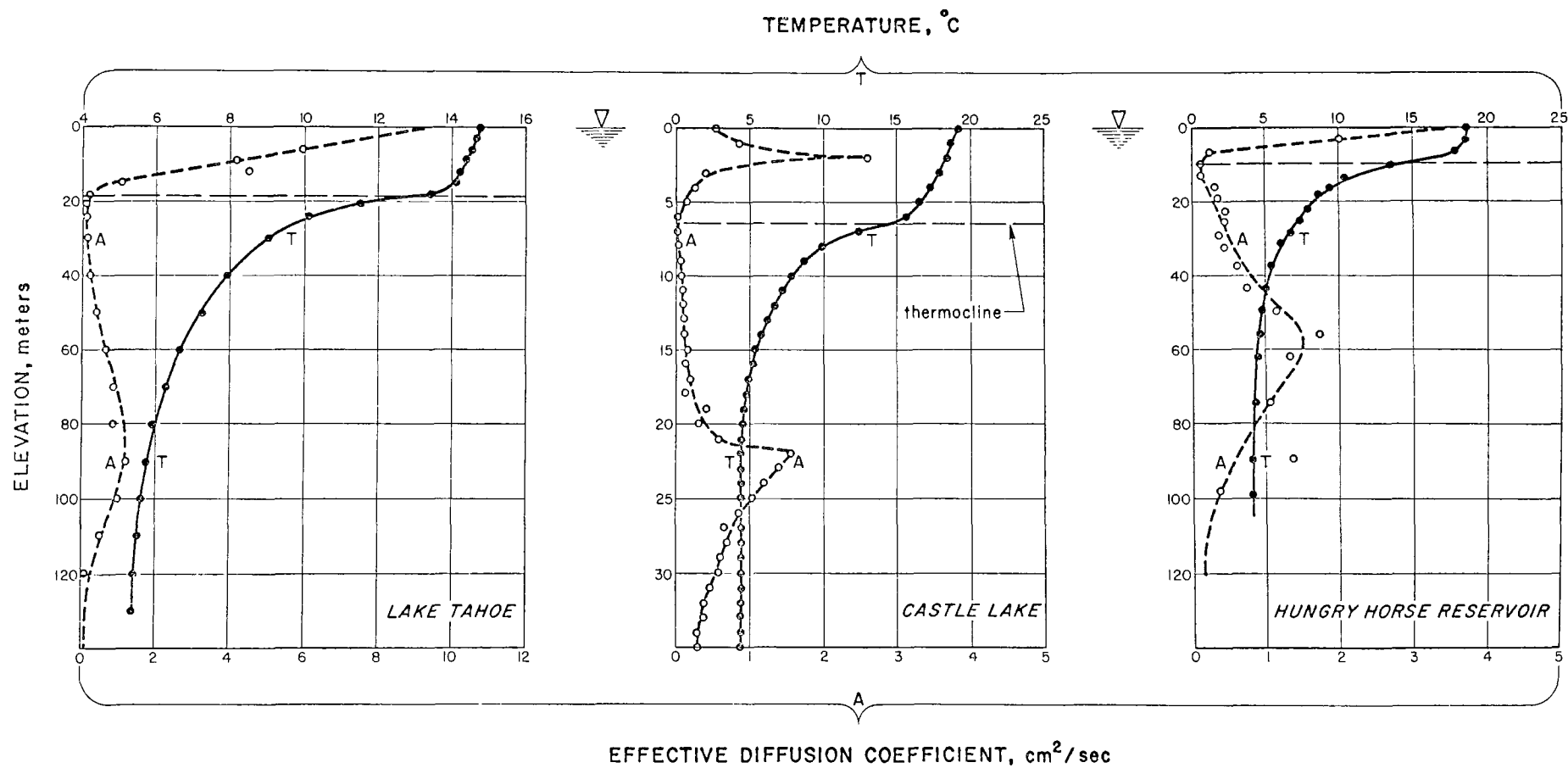


FIGURE 4. Effective Diffusion and Temperature Profiles for Selected Impoundments (from Reference 15)

1. Effective mixing in the epilimnion is usually greatest near the surface but declines rapidly with depth as the thermocline is approached.
2. The effective diffusion coefficient is minimal at, or very near the position of the maximum temperature gradient, the so-called "thermocline."
3. In the hypolimnion the effective diffusion coefficient increases with depth in a more or less erratic manner, reaching a maximum at about mid-depth, thereafter decreasing as the bottom is approached.
4. The value of $A(z,t)$ is vastly greater than the coefficient of thermal diffusivity for heat transfer by molecular conduction ($\kappa \approx 1.4 \times 10^{-7} \text{ m}^2/\text{sec}$).

While it is impossible to give a detailed theoretical description for the observed behavior of $A(z,t)$, the following arguments are proposed as a possible explanation. A horizontal current with an average velocity, u , at elevation, z , has a kinetic energy per unit mass of $KE = u^2/2$. If it is assumed that the horizontal flow in a reservoir is basically a boundary layer flow (except in the region of the outlets and at points of tributary inflow), the vertical distribution of KE would then appear as shown in Figure 5-A. This amount of energy is expended through turbulence; however, in a stratified reservoir it is not all available for turbulent mixing as it is a non-stratified impoundment, for the following reason: In a stably stratified reservoir the vertical differences in density cause a buoyant restoring force to be exerted on any parcel of fluid which is displaced from its position of static equilibrium. Thus, of the

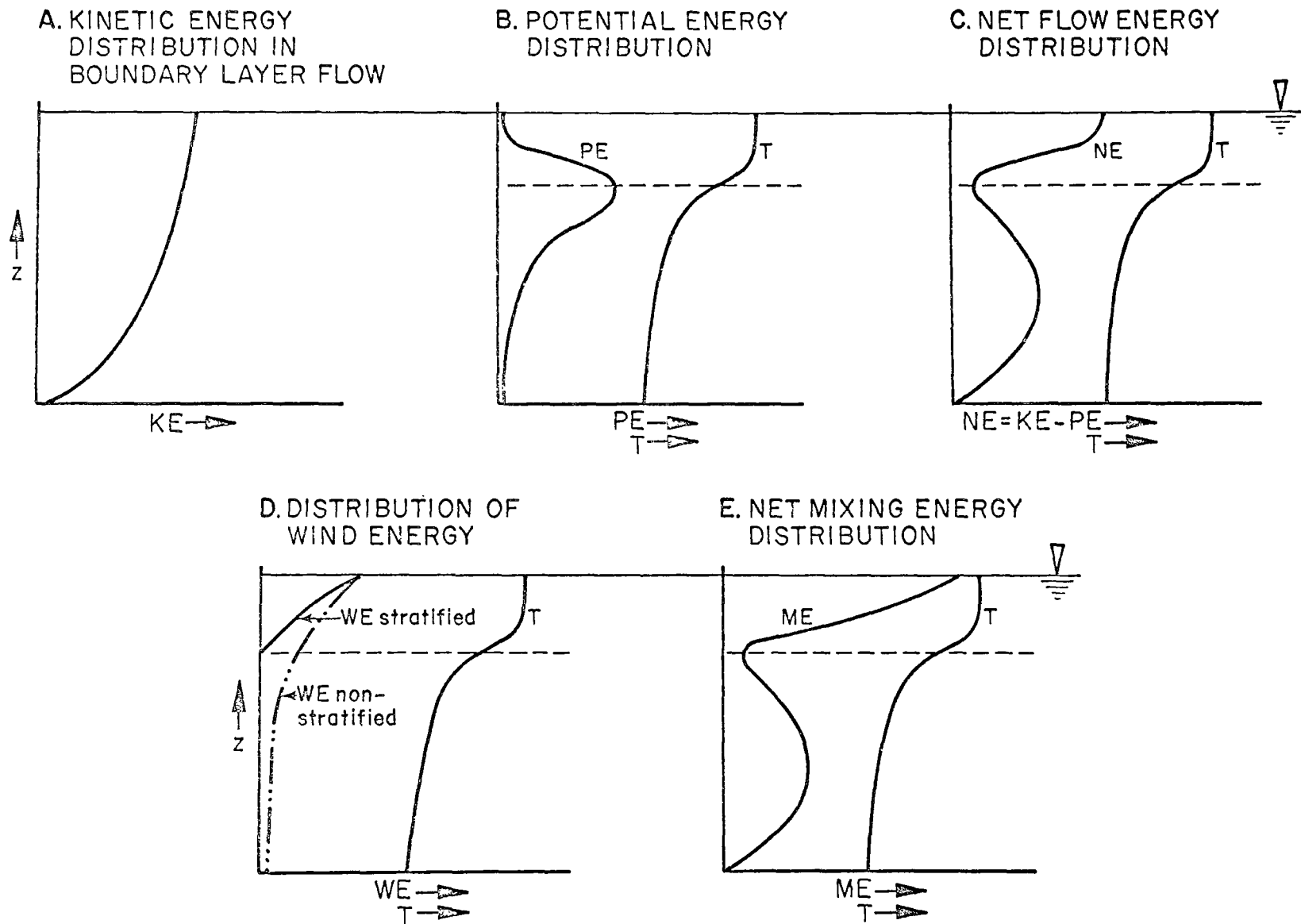


FIGURE 5. Energy Distribution

total KE available, only that energy which is in excess of that required to overcome the buoyancy forces is available for mixing.

For a reservoir with a temperature profile of the form shown in Figure 5-B, the vertical distribution of the work per unit volume that is required to overcome the density stratification is given by the curve PE which is shown in the same Figure. Thus, the net amount of turbulent energy NE which is available for mixing is the difference, $KE - PE$, with the restriction, $NE \geq 0$. A typical curve of NE for the temperature profile given in Figure 5-B is shown in Figure 5-C.

In addition to turbulence induced by the boundary layer flow, mixing in the upper layers of the reservoir is contributed to by the wind. Following arguments of Eckman as related by Hutchinson (3), the energy input per unit volume, WE, should experience an exponential decay with depth as shown in Figure 5-D. In the case of a stratified reservoir, the same arguments apply for reduction of the diffusion coefficient due to stratification as applied to the boundary layer flow. As such, it is generally thought that the effects of wind mixing do not persist below the thermocline.

Figure 5-E, which is the vertical distribution of the energy available for mixing, ME, follows from the linear combination of NE for the boundary layer flow and WE resulting from wind mixing. It is observed that the combined effect produces a form of ME which is similar in its shape to the prototype forms of $A(z,t)$ illustrated in Figure 4. This is an expected result since the value of $A(z,t)$, at any elevation, z , is a direct measure of the turbulent energy available for mixing at that elevation.

While the preceding discussion has been devoted to a qualitative description of the functional form of the eddy conductivity coefficient, the pertinent energy processes can be expressed mathematically. For the sake of completeness, these relationships are given below. Details can be found in reference 17.

If the energies illustrated in Figure 5 are now thought of as the rate of energy expenditure per unit time and per unit mass, then KE becomes the equivalent rate per unit mass at which kinetic energy is transferred from mean motion to turbulent motion and is expressed as

$$KE = A_{\tau} \left(\frac{\partial u}{\partial z} \right)^2 \quad (5)$$

where A_{τ} is the eddy viscosity coefficient and u is the mean horizontal velocity at elevation, z . The subscript, τ , has been added to distinguish this coefficient from the eddy conductivity coefficient, $A(z,t)$. Similarly, defining PE as the average work done by turbulent motion against gravity, or buoyancy, per unit mass and unit time leads to

$$PE = -gA(z,t) \frac{1}{\rho} \frac{\partial \rho}{\partial z} \quad , \quad (6)$$

where g is the gravitational acceleration. Combining equations 5 and 6 gives the value of NE, the energy available per unit mass and per unit time for the vertical transport of heat, i.e. mixing;

$$NE = \left[A_{\tau} \left(\frac{\partial u}{\partial z} \right)^2 + gA(z,t) \frac{1}{\rho} \frac{\partial \rho}{\partial z} \right] \quad , \quad (7)$$

subject to $NE \geq 0$.

If the effect of wind is neglected, the following observation can be made. Since KE is the rate at which turbulent energy is supplied to the system and PE is the rate at which turbulent energy is used to overcome the gravitational stability of the system, then, in order to maintain turbulence in the system, KE must be larger than PE. From equations 5 and 6, it follows that

$$\frac{-g \frac{1}{\rho} \frac{\partial \rho}{\partial z}}{(\frac{\partial u}{\partial z})^2} < \frac{A_{\tau}}{A(z,t)} \quad (8)$$

The dimensionless quantity on the left-hand side of equation 8 is called the "gradient Richardson number," R_i (18). The function, $-\frac{1}{\rho} \frac{\partial \rho}{\partial z}$, is commonly referred to as the "gravitational stability," E , of a stratified water body. If this relationship is substituted into equation 8, there results for the description of the Richardson number,

$$R_i = \frac{gE}{(\partial u / \partial z)^2} \quad (9)$$

The efficacy of using the Richardson number as a measure of the energy available for vertical mixing has been the subject of much discussion. The problem revolves around the ratio, $A_{\tau}/A(z,t)$, which is, at best, difficult to define. If $R_i < \frac{A_{\tau}}{A(z,t)}$, then mixing will occur; conversely, if $R_i > \frac{A_{\tau}}{A(z,t)}$, turbulent mixing will not occur. Without

going into further detail, suffice it to say that a small Richardson number indicates maintenance or increase of turbulence, whereas a large value indicates suppression or extinction of turbulence. In addition to the problem of defining the critical value of R_i (where $R_i = \frac{A_\tau}{A(z,t)}$), the lack of a theory describing the details of the reservoir's internal flow structure precludes an accurate evaluation of the velocity gradient. Hence, the evaluation of the Richardson number, itself, is a formidable task.

Under the assumption that energy input by the wind is an exponential function of the depth, WE is described simply as

$$WE = WE_0 e^{-\alpha d} \quad , \quad (10)$$

where WE_0 = energy input per unit volume per unit time at the water surface;

α = decay constant; and

d = depth below the water surface.

The value of α is chosen so that WE is very small (say, 0.01 WE_0) at the depth of the thermocline. WE_0 is a function of the wind stress at the water surface. Some direction in the assessment of its magnitude can be found in Hutchinson (3).

Finally, through the combination of equation 7 and 10, it is possible to write an expression for the amount of turbulent energy in the reservoir that is available for mixing. This expression is

$$ME = WE_0 e^{-\alpha d} + [A_T (\frac{\partial u}{\partial z})^2 + gA(z,t) \frac{1}{\rho} \frac{\partial \rho}{\partial z}] \quad (11)$$

The examination of equation 11 and the prototype behavior of $A(z,t)$ as illustrated in Figure 4 reveals that while the behavior of a thermally stratified reservoir seems to follow certain laws, it is apparent that the overall complexity of real impoundments precludes an explicit, detailed representation in mathematical form. Thus, certain simplifications must be made. The simplifications made in defining the temporal and spacial variation of the eddy conductivity coefficient, $A(z,t)$, are described in the following section.

EFFECT OF VARYING THE FUNCTIONAL REPRESENTATION OF THE INTERNAL MIXING PROCESS

The functional representation of the vertical transport of heat as a result of the internal mixing process was defined in the last section by equation 4. It is apparent from this equation that any variation in its functional form can be accomplished only by varying the functional description of the eddy conductivity coefficient, $A(z,t)$. Consequently, this section is devoted to describing the results of using different functional representations for $A(z,t)$.

The functional representation of $A(z,t)$ must, of necessity, be empirical in nature since the eddy conductivity coefficient describes the prototype response to many unknown and/or poorly defined random influences. However, on the basis of the theory and prototype experience described above, it is observed that the choice of a functional form to represent the eddy conductivity coefficient must be based on the ability

of the function to display the following characteristics:

1. $A(z,t)$ is large in the epilimnion;
2. $A(z,t)$ is small at the thermocline, or preferably, $A(z,t)$ should decrease as the stability, E , increases (recall $E = -\frac{1}{\rho} \frac{\partial \rho}{\partial z}$); and
3. $A(z,t)$ is large in the hypolimnion, being of the same order of magnitude as its value in the epilimnion.

At this point, it is worth mentioning that Hungry Horse Reservoir was an ideal prototype for studying internal mixing. Because of its small discharge-volume ratio, only a small portion of the vertical heat transfer occurred by advection. Consequently, "eddy diffusion" played a major role in the vertical distribution of heat. This fact can be readily observed in Figure 6 where the solar, vertical advection, and diffusion fluxes within the reservoir are graphed as a function of elevation for a typical day.

EXPONENTIAL REPRESENTATION

The first functional representation of $A(z,t)$ to be tested was the original function proposed in the Fish and Game Report (reference 15). Summarily, this representation was:

$$A(z,t) = A_0(t) e^{-\eta(z_s - z)} \quad , \quad z \geq z_T \quad , \quad (12-A)$$

$$A(z,t) = A(z_T,t) \quad , \quad z_T > z \quad , \quad (12-B)$$

where $A_0(t)$ = value of the eddy conductivity coefficient at the water surface;

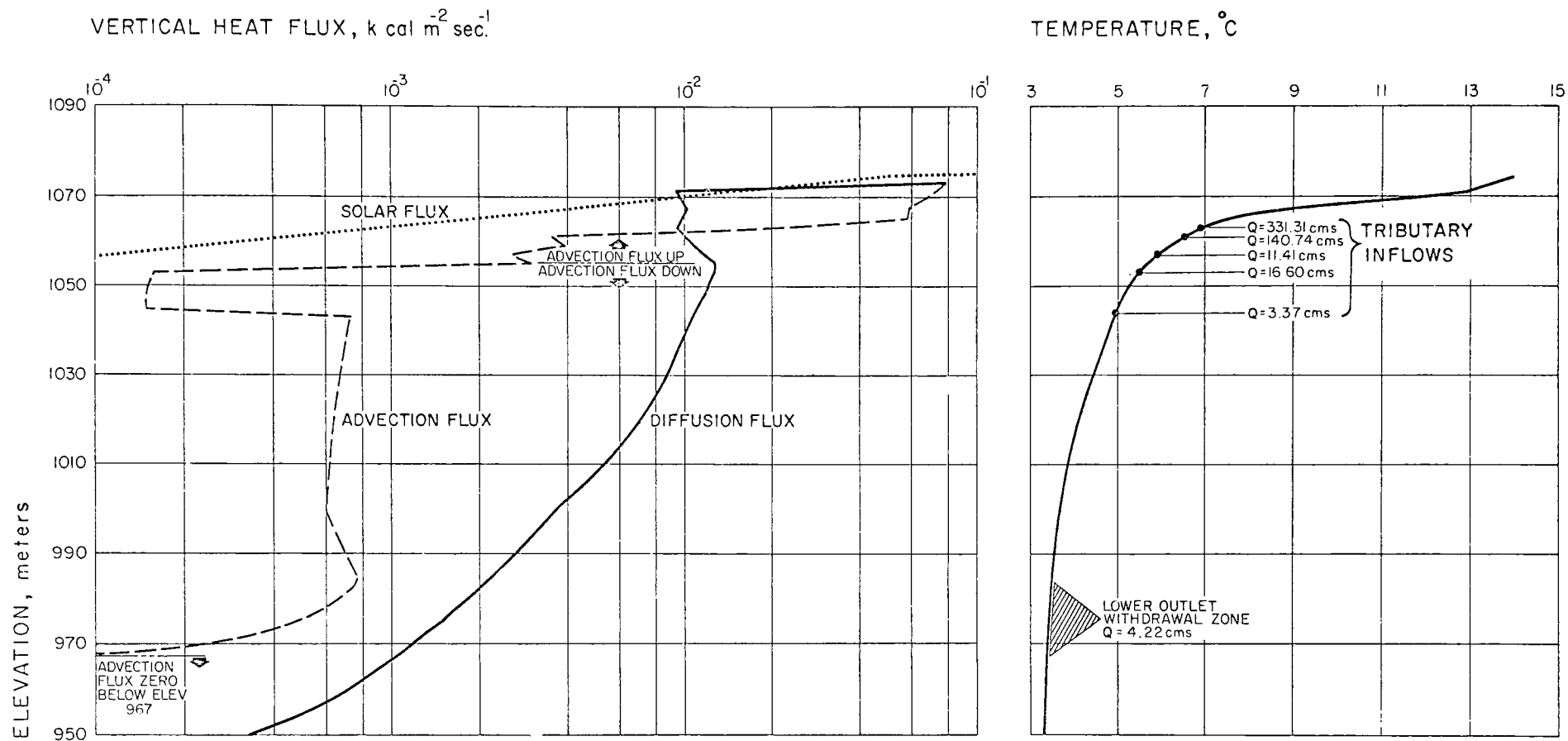


FIGURE 6. Contribution to Vertical Heat Flux by Individual Heat Transfer Mechanisms, Hungry Horse Reservoir, 1965

η = decay coefficient;

z_T = elevation of the thermocline; and

z_s = elevation of the water surface.

Examination of equation 12 reveals that the function as defined in equation 12-A displays characteristic 1 and characteristic 2 above the thermocline. Equation 12-B, however, tends to be in violation of characteristic 2 below the thermocline and does, in fact, violate characteristic 3. Although the weakness of equation 12-B was realized in the original derivation of the function, it was not thought to be a significant weakness for the following reasons. In the hypolimnion, the thermal gradients are very small; thus, according to equation 4, the vertical rate of turbulent heat transport will also be small. Furthermore, this rate would be significantly small, in comparison to the rate of heat transfer by other mechanisms, so that the error resulting from the use of equation 12-B would not be a significant percentage of the total rate of heat transport.

For testing the functional representation of $A(z,t)$ as hypothesized in equation 12, Hungry Horse Reservoir proved to be an ideal prototype. Examination of the observed temperature profiles for the reservoir, as illustrated in Figure 3, reveals that for most of the simulation period the thermocline (defined as the elevation at which $\frac{\partial^2 T}{\partial z^2} = 0$) is either at, or very near, the water surface. Thus, the model was required to simulate a region in which the functional representation of $A(z,t)$ was known to be weak, i.e., through most of the simulation period, $A(z,t)$ was described by equation 12-B.

As originally proposed, the determination of $A_0(t)$ in equation 12-A would be made on the basis of experience and/or by deducing its value from the prototype data. In addition, the value of the eddy conductivity coefficient at the thermocline, $A(z_T, t)$, had to be obtained in the same manner. Once these two values were established, η could be determined by the ratio, $A(z_T, t)/A_0(t)$, and the elevation z_T , of the thermocline. In the initial simulations, however, A_0 and $A(z_T)$ were assumed constant, i.e., time invariant, and various values and combinations of values were evaluated for their ability to reproduce the prototype behavior.

The results of the test simulations demonstrated that the weakness involved in using equation 12-B was a drawback to its general use in reservoir simulation. In particular, it was found that an accurate representation of the temperature profile in the clinolimnion (the region of the reservoir between the thermocline and the "knee" of the temperature curve in the hypolimnion) was not possible with this function. Without going into details concerning the individual test runs, the problems involved with such a functional representation for $A(z, t)$ below the thermocline can be described as follows. First, if $A(z_T)$ is chosen as the prototype value of $A(z, t)$ at the thermocline, its value is very small. The use of such a small value for the entire reservoir below the thermocline over-suppresses the turbulent rate of heat transport down through the reservoir; i.e. it "traps" the heat in the surface layers. This results in very high computed surface temperatures and temperatures that are too cold in the reservoir depths. A typical case is illustrated in Figure 7 where the value of $A(z_T, t)$ was taken as $5.0 \times 10^{-5} \text{ m}^2 \text{ sec}^{-1}$. Increasing the value $A(z_T)$ to a value such that the computed surface temperatures were about the same as the observed values allowed too much heat to pass through the region of steep gradients but still did not allow enough heat to pass through to the lower reservoir depths. A typical profile computed by using this approach is shown in Figure 8.

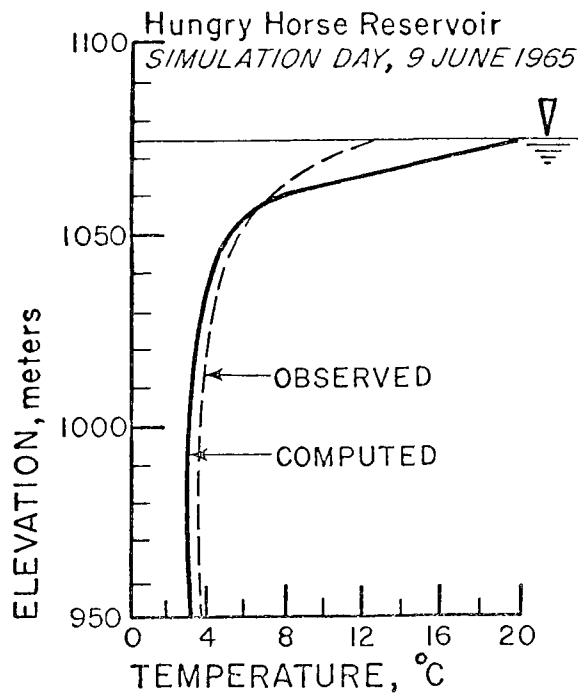


FIGURE 7. Typical Computed Temperature Profile with $A(z,t)$ Described by Equation 12 and $A(z_T,t) = 5.0 \times 10^{-5} \text{ m}^2 \text{ sec}^{-1}$

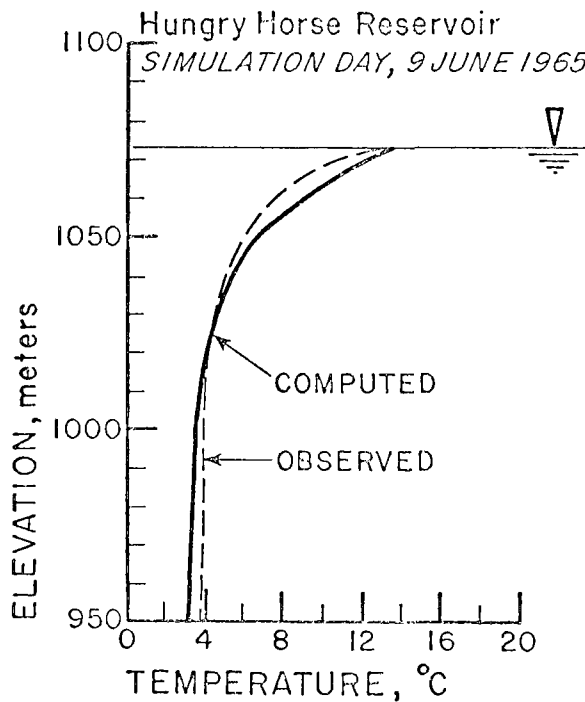


FIGURE 8. Typical Computed Temperature Profile with $A(z,t)$ Described by Equation 12 and $A(z_T,t) = 1.0 \times 10^{-4} \text{ m}^2 \text{ sec}^{-1}$

The conclusions drawn from these test simulations were:

1) the amount of heat transferred by deep reservoir turbulence can be a significant portion of the total heat transfer; and 2) in the region of steep thermal gradients below the thermocline, i.e. the clinolimnion, $A(z,t)$ must have a value substantially less than that value used for the hypolimnion.

In reflecting upon the functional form of $A(z,t)$ as proposed by equation 12, it is observed that the function is primarily oriented to the description of turbulence induced by wind action. This conclusion becomes obvious when equation 12-A is compared with equation 10 and Figure 5-D. A review of the circumstances under which equation 12 was formulated confirms that such a formulation was not accidental. The prototype reservoir upon which the original function was developed was Fontana Reservoir in the TVA System. In this reservoir, a primary factor in the development and persistence of the epilimnetic region is wind mixing. Moreover, the reservoir itself has a moderate discharge to volume ratio (2.3 yr^{-1}). Thus, while wind mixing is one of the primary movers of heat in the epilimnion, the high discharge to volume ratio for the reservoir indicates that the prime mover of heat in the hypolimnion is vertical advection. For such a case, the reasoning which underlies the formulation of equation 12-B is sound.

In contrast to Fontana, Hungry Horse Reservoir is almost completely opposite in its characteristics. First of all, wind mixing (at least during the simulation period in 1965) is insignificant. Examination of the meteorological inputs for the simulation period reveals that the development of the epilimnetic region resulted from convective mixing as a result of surface cooling, not from wind mixing. With regard to hydrologic and geometric characteristics, Hungry Horse is of the low discharge-volume type having an average ratio of about 0.8 yr^{-1} . With such a small ratio it is not surprising that turbulent heat transfer in

the hypolimnion should represent a significant portion of the total heat transport.

In summary, the initial test simulations revealed that equation 12-B was inadequate for defining the eddy conductivity coefficient below the thermocline. The adequacy of equation 12-A in describing $A(z,t)$ above the thermocline could not be evaluated since the epilimnion was formed by natural convective mixing rather than by wind action.

STEP FUNCTION

On the basis of the experience derived from testing the exponential representation of $A(z,t)$, it was decided to investigate the use of a step function for its adequacy in describing the vertical variation of the eddy conductivity coefficient. The advantage of such an approach was that the capability would exist to assign one value of $A(z,t)$ to the epilimnetic region, another value to the region of the thermocline, i.e. the region of steep thermal gradients, and a third value to the hypolimnetic region. Such a function would display all the characteristics required of the eddy conductivity function. The generalized mathematical formulation for this type of functional representation was proposed as follows:

$$A(z,t) = A_E(t) \quad z > z_E \quad (13-A)$$

$$A(z,t) = A_T(t) \quad z_E > z > z_H \quad (13-B)$$

$$A(z,t) = A_H(t) \quad z_H > z \quad (13-C)$$

Schematic diagrams of this functional form are given in Figure 9 for the case of the thermocline at the surface and for the case of the thermocline below the surface.

Key: — — — PROTOTYPE BEHAVIOR / — PROPOSED REPRESENTATION

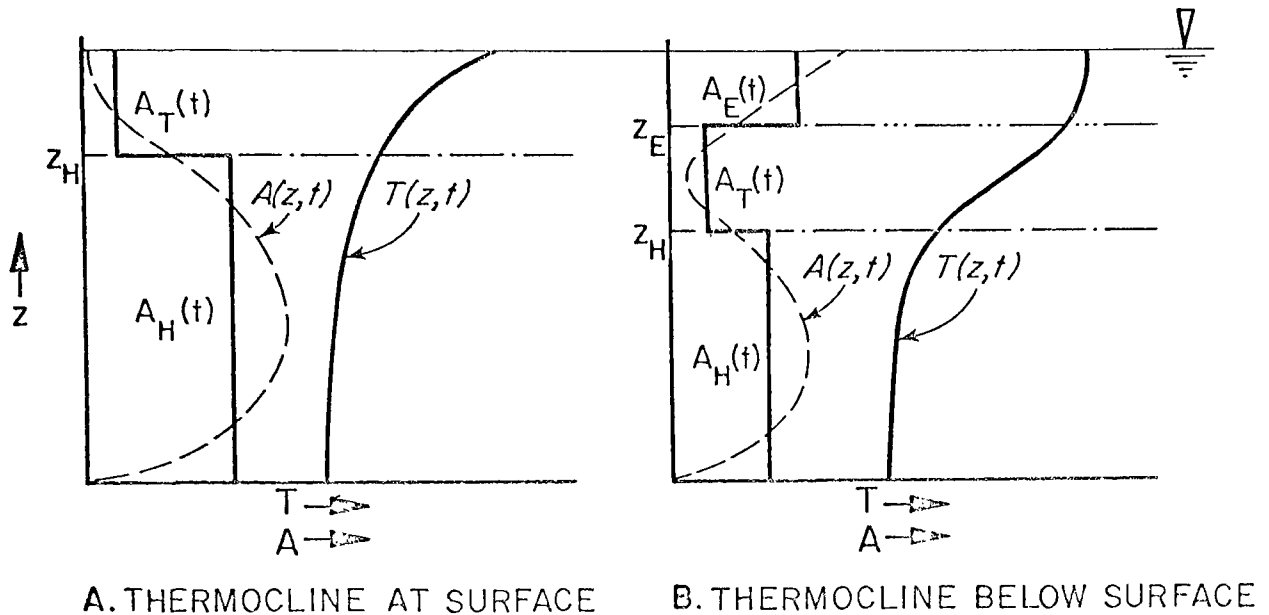


FIGURE 9. Representation of $A(z,t)$ with a Step Function

The functional form of the eddy conductivity function as proposed in equation 13 essentially divides the reservoir along its vertical axis into three zones with $A(z,t)$ exhibiting certain distinct characteristics in each zone. Re-examination of the above section on MIXING PROPERTIES OF RESERVOIRS reveals these characteristics to be as follows:

ZONE	DEFINITION OF ZONE	CHARACTERISTIC FEATURES OF $A(z,t)$
(1)	$z < z_H$	$A_H(t)$ is primarily a function of the intensity of the deep reservoir turbulence; it is only slightly dependent upon the gravitational stability of the reservoir.
(2)	$z_H < z < z_E$	$A_T(t)$ is primarily a function of the gravitational stability.
(3)	$z_E < z$	$A_E(t)$ is primarily dependent upon the amount of wind mixing.

Although in general, A_E , A_T and A_H are all time variant functions, they were fixed at constant values in this set of test simulations since the interest was more in how this type of functional representation would shape the temperature profiles (or the vertical heat distribution) rather than how precisely individual observed thermal profiles could be matched.

One of the questions that arose in connection with the functional representation as given by equation 13 was how to choose the value of z_E and z_H . Since $A(z,t)$ is functionally dependent upon the stability of the system, especially in Zone 2, it was decided that z_H and z_E should also be based on stability criteria. Through a series of trial simulations, it was found that the best results were obtained when these elevations were taken to be the elevations in the reservoir where the stability was 4×10^{-5} meters $^{-1}$.

The functional representation of $A(z,t)$ as a step function was found to substantially improve the modeling capability over that which was possible through the use of equation 12. However, since there was an order of magnitude difference between the value of A_T and those of A_H and A_E , a problem developed at the switching elevations, z_H and z_E . The problem was specifically this: for any given temperature gradient at the elevation z_E or z_H the substitution of equation 13 into equation 4 indicates that the rate of heat transfer on either side of these two elevations will differ by an order of magnitude, since A_T is an order of magnitude smaller than A_H or A_E . Consequently, immediately above z_E there will be a "stacking" of heat which creates large thermal gradients at that point; at the elevation z_H , on the other hand, the large value of A_H causes a "draining" of the heat at that elevation, thus creating very low temperature gradients. The result of this situation is to cause a series of "bumps" in the computed temperature profile. While this is not necessarily harmful to the performance of the model, it is undesirable from an operational point of view. An example of the type of profile obtained under this type of functional representation for the eddy conductivity coefficient is illustrated in Figure 10. The diffusion coefficients for this case were $1 \times 10^{-4} \text{ m}^2/\text{sec}$ for A_E and A_H and $5 \times 10^{-6} \text{ m}^2/\text{sec}$ for A_T .

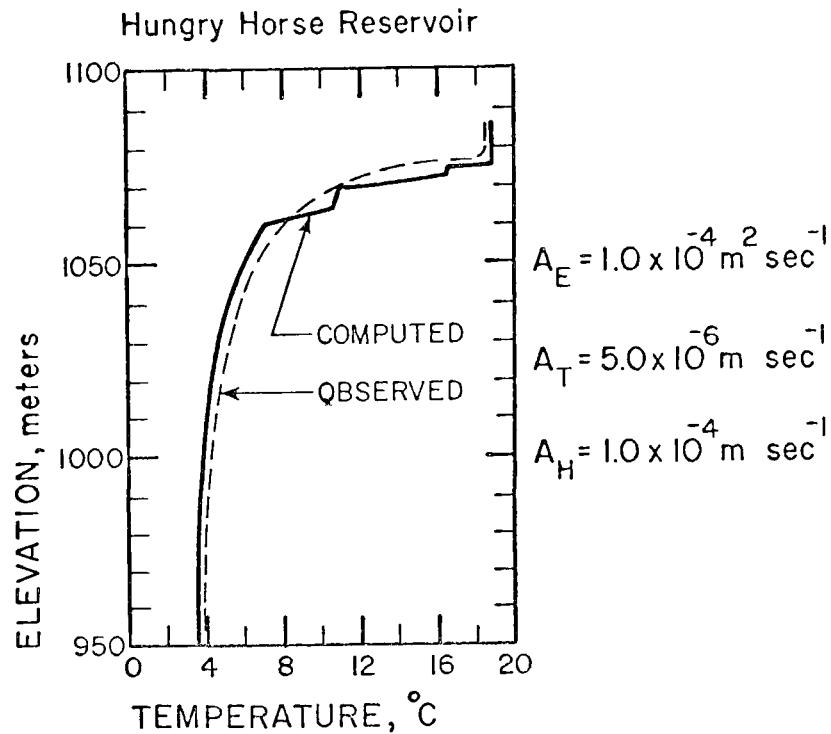


FIGURE 10. Typical Computed Temperature Profile with $A(z,t)$
Described by Equation 13; Simulation Day is
1 September 1965

REPRESENTATION OF $A(z,t)$ BY A CONTINUOUS FUNCTION

The results of using the step function to represent the spatial variation of the eddy conductivity coefficient were encouraging. It appeared that, if the abrupt step changes could be smoothed out of the describing function, a good representation of the spatial behavior of $A(z,t)$ would be obtained.

Reviewing the mechanics of turbulent heat transfer in a stratified water body reveals that a precise definition of the spatial variation of $A(z,t)$ is most important in Zone 2 because the temperature gradients are steepest and the spatial variation of the eddy conductivity

coefficient is greatest in this region. Thus, it was desirable to represent $A(z,t)$ in Zone 2 with a continuous function, $A_T(z,t)$, that would have a minimum value at the thermocline and would be equal to $A_E(t)$ and $A_H(t)$ at the elevations z_E and z_H , respectively. Since $A_T(z,t)$ is primarily a function of the stability, it follows that such a relationship should be sought in the prototype data.

The first step in looking for a continuous function of $A_T(z,t)$ was to use the observed prototype temperature profiles and simulate the reservoir "backwards" to obtain the eddy conductivity coefficients required to produce these profiles. The details of this method of solution can be found in reference 15. Through the employment of this methodology, the average spatial variation of $A(z,t)$ was found for the following time periods:

May 11 - May 26
May 26 - June 9
June 9 - June 23
June 23 - July 7
July 7 - July 21
July 21 - August 4
August 4 - August 18
August 18 - September 1
September 1 - September 16
September 16 - October 5

Linear plots of the average spatial variation of $A(z,t)$ during these time periods are shown in Figure 11. Note the scale change in the $A(z,t)$ axis at 10.

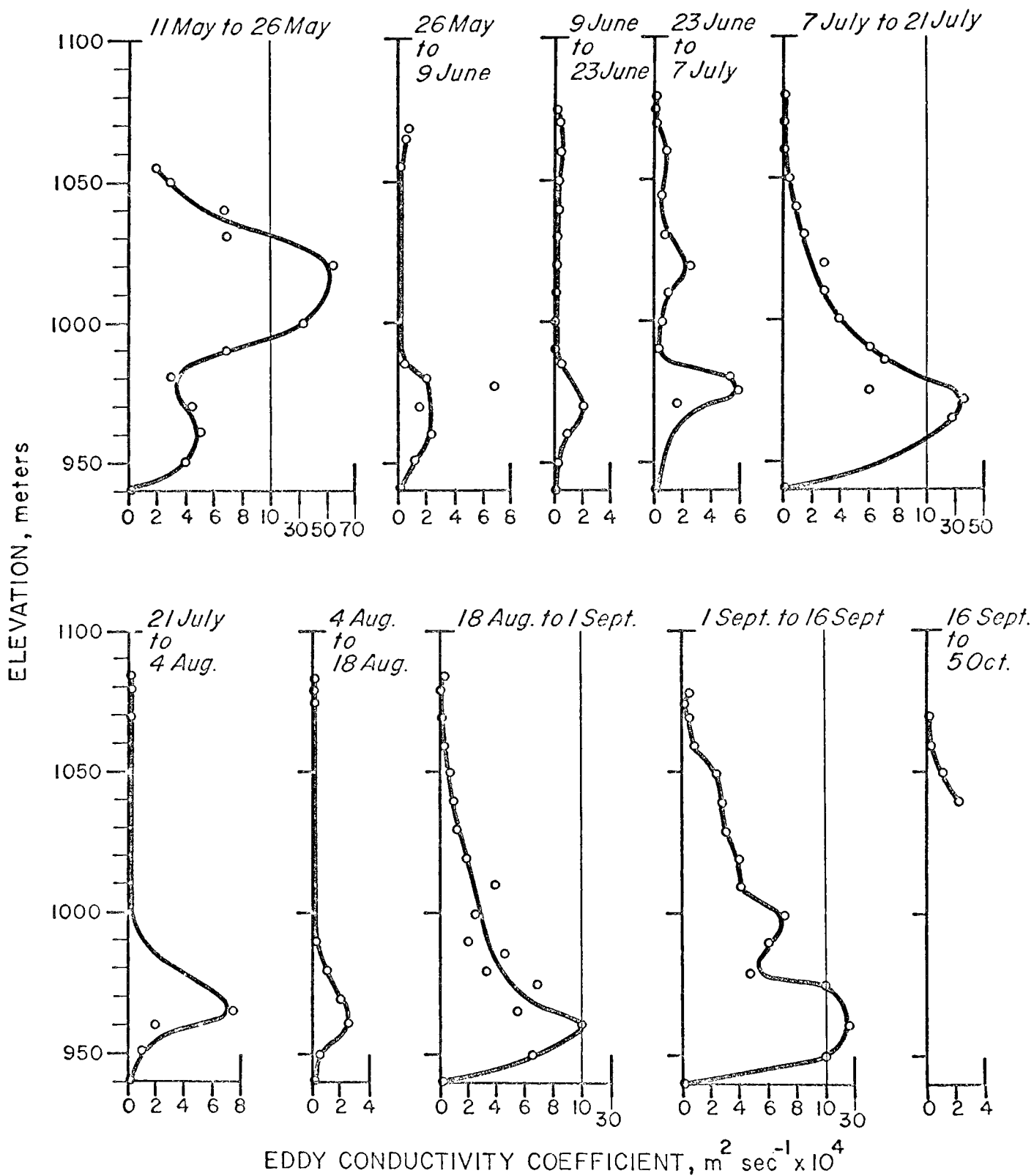


FIGURE 11. Average Eddy Conductivity Profiles for Hungry Horse Reservoir, 1965

It is observed that while these forms are similar to those shown in Figure 4 below the thermocline, there is no significant increase in $A(z,t)$ above the thermocline. The reasons for this behavior have been explained previously.

The search for a functional relationship between $A_T(z,t)$ and the stability, E , culminated in plot of $\ln A(z,t)$ versus $\ln E$. These plots of the Hungry Horse data, for the time periods given above, are illustrated in Figure 12. It is quite evident from Figure 12 that $A(z,t)$ is primarily a function of the stability when E is greater than about 10^{-6} m^{-1} (for a stability of $E = 10^{-6} \text{ m}^{-1}$, the corresponding temperature gradient is approximately $0.06 \text{ }^\circ\text{C m}^{-1}$). Moreover, the relationship in this region is of the form

$$A(z,t) = bE^{-a} \quad (14)$$

If the average functional variation indicated by the dotted line in Figure 12 is used, the value associated with a is 0.7 and b is $1.48 \times 10^{-8} \text{ m}^{1.3} \text{ sec}^{-1}$.

The use of equation 14 as a definition for $A_T(z,t)$ in Zone 2 strengthens the deep reservoir model in several ways. First of all, in addition to providing a continuous spatial description of the eddy conductivity coefficient, it also yields a temporal description of the coefficient in this zone since $A_T(z,t)$ is a function of the temporal and spatial variation of the stability, E . Second, by the use of equation 14 the step changes in $A(z,t)$ at the elevations z_H and z_E are eliminated since z_H is now defined as the elevation at which

Legend: ○ 11 MAY - 26 MAY 1965 ○ 9 JUNE - 23 JUNE 1965 △ 7 JULY - 21 JULY 1965
 △ 26 MAY - 9 JUNE 1965 □ 23 JUNE - 7 JULY 1965

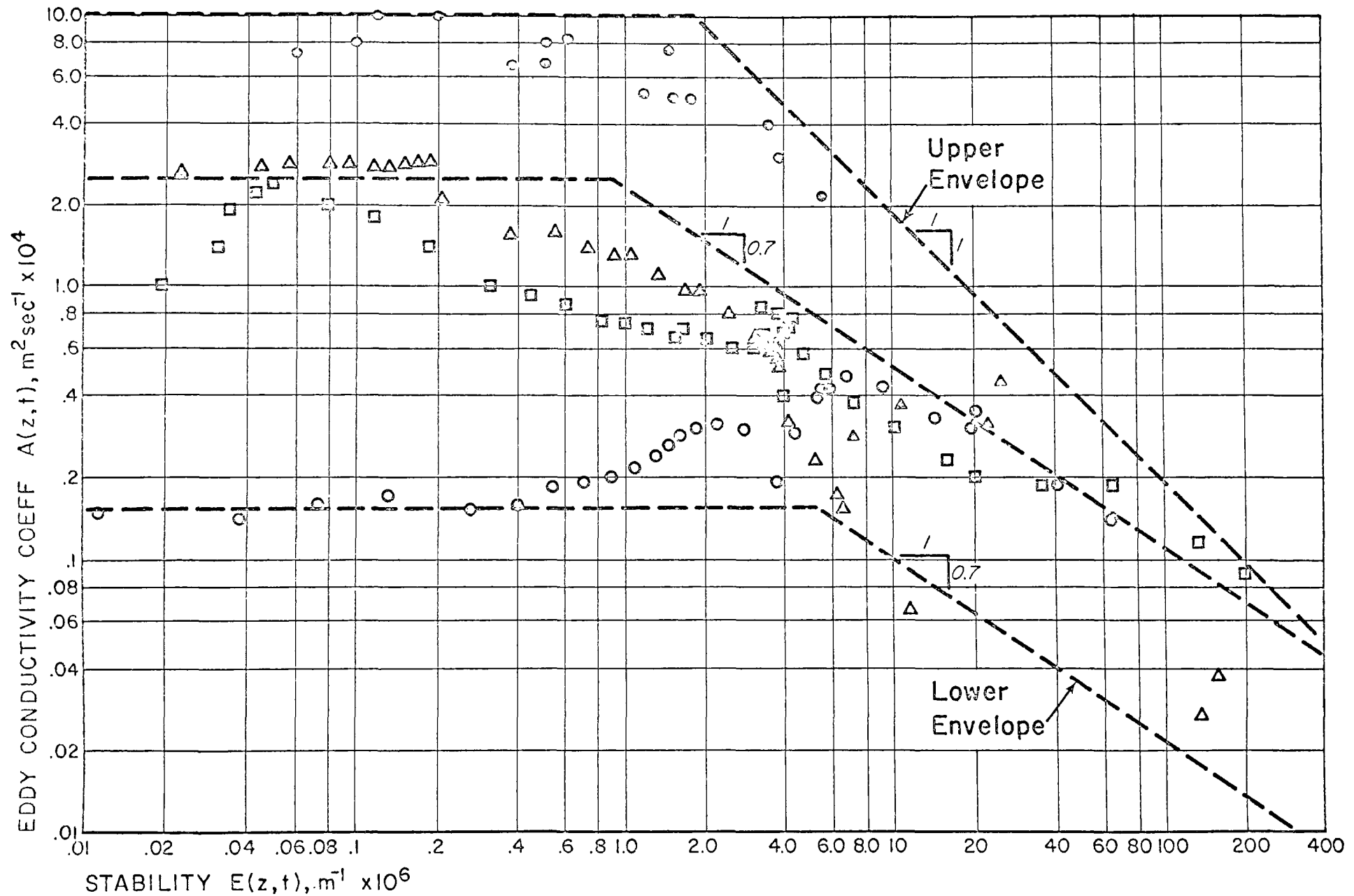


FIGURE 12. Log of Eddy Conductivity versus Log Stability--Hungry Horse Data
 (Continued next page)

Legend: ○ 21 JULY - 4 AUG. 1965

○ 18 AUG. - 1 SEPT. 1965

△ 16 SEPT. - 5 OCT. 1965

△ 4 AUG. - 13 AUG. 1965

□ 1 SEPT. - 16 SEPT. 1965

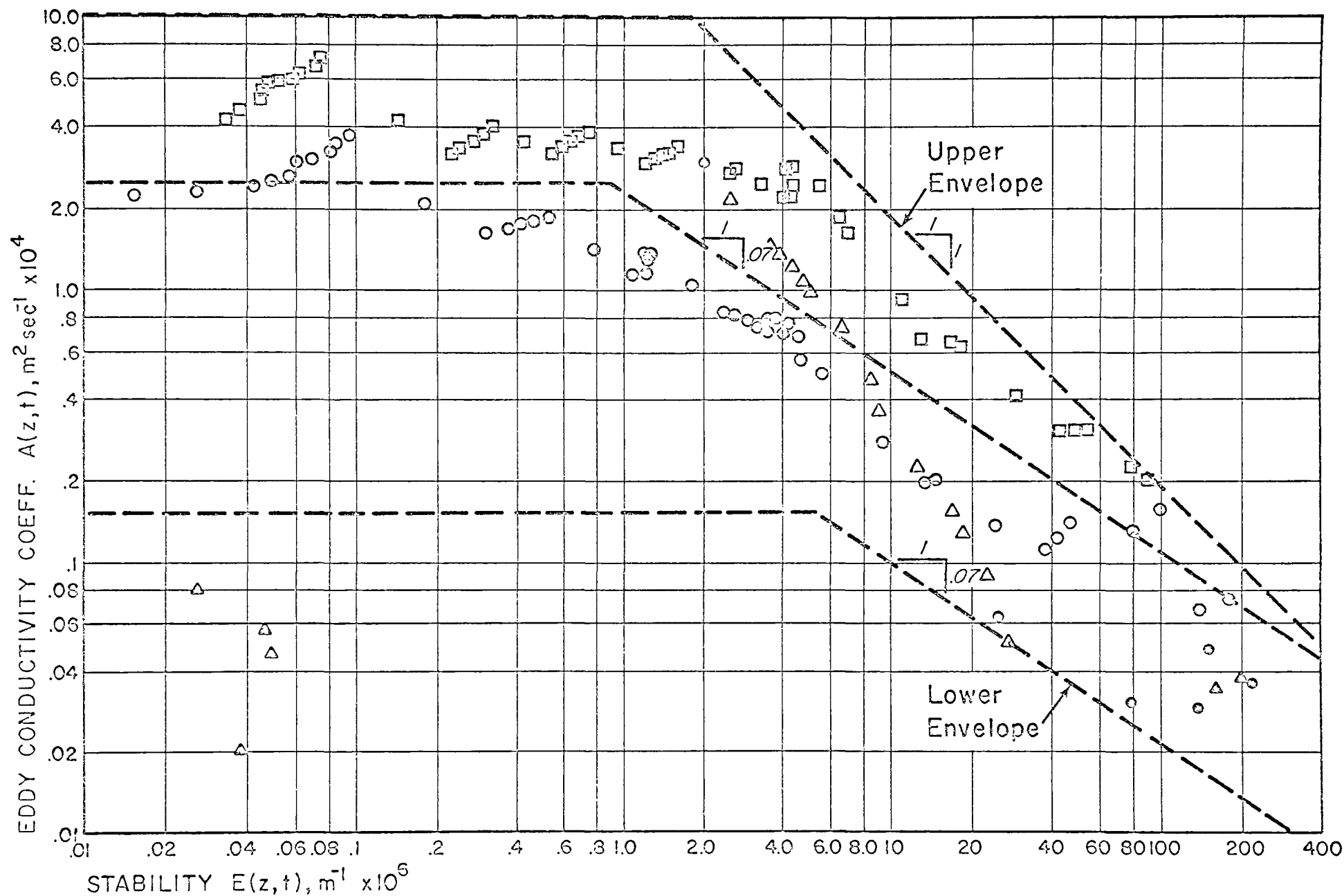


FIGURE 12 (cont'd). Log of Eddy Conductivity versus Log Stability--Hungry Horse Data

$$E_H = \left[\frac{b}{A_H(t)} \right]^{\frac{1}{a}} \quad \text{and } z_E \text{ is the elevation at which } E_E = \left[\frac{b}{A_E(t)} \right]^{\frac{1}{a}}$$

Third, with the more precise definition of $A_T(z,t)$ the modeling capabilities in the region of steep thermal gradients are significantly improved. An example of the application of this refined approach to the definition of $A(z,t)$ is illustrated in Figure 13. Note, again, the scale change in the $A(z,t)$ axis at 10.

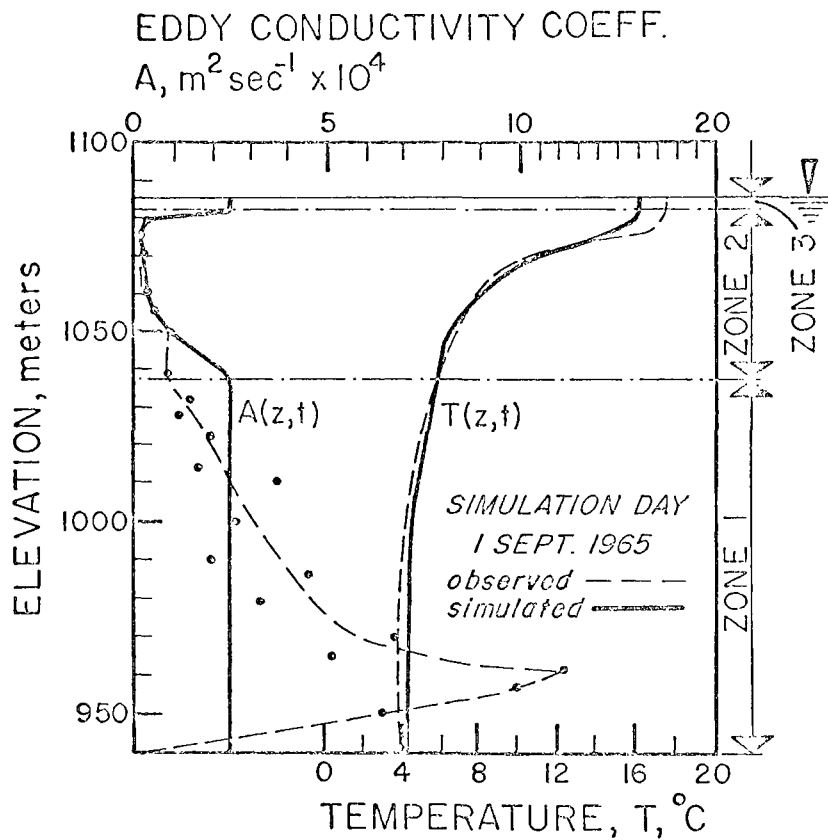


FIGURE 13. Typical Temperature and Eddy Conductivity Profile Obtained by Use of Continuous Function for $A(z,t)$

Having formulated the description of $A_T(z,t)$ in Zone 2, there remained the problem of defining $A_E(t)$ in Zone 3 and $A_H(t)$ in Zone 1. Since wind mixing was not observed in the prototype data, no further development of $A_E(t)$ was possible; thus, the effort was directed toward a temporal description of $A_H(t)$.

The value of $A_H(t)$ reflects the level of deep reservoir turbulence, or more precisely, the rate of dissipation of energy by turbulence. According to Hutchinson (3), the hypolimnetic turbulence in lakes is due almost entirely to the internal seiche current system. While this is probably true during the summer months, turbulence is also supplied to the hypolimnion in the fall and spring by the deceleration of the tributary inflows which enter the hypolimnion. In addition, in operating reservoirs, the energy contained in the transient momentum flows that are established through operation of the outlets must be dissipated through turbulence in the hypolimnion.

In searching for some relationship between $A_H(t)$ and the above-mentioned parameters, the following scheme was tried:

$$A_H(t) = f [(\Delta Q_{out})_{ave} + (Q_{in})_{net}] \quad (15)$$

where $(\Delta Q_{out})_{ave}$ = average of the absolute values of the daily change in discharge through outlets below the thermocline; and
 $(Q_{in})_{net}$ = average inflow minus the average outflow below the thermocline; positive values or zero.

The time over which the flows were averaged was 14 to 15 days which corresponds to the time interval between successive measurements of the

thermal profile in the reservoir. Figure 14-A is a linear plot of observed values of $A_H(t)$ versus $(\Delta Q_{out})_{net} + (Q_{in})_{net}$. Since more energy is dissipated through deceleration of flows than through acceleration, it was felt that a better fit might be obtained by the equation:

$$A_H(t) = f_1 [(-\Delta Q_{out})_{ave} + (Q_{in})_{net}] \quad , \quad (16)$$

where $(-\Delta Q_{out})_{ave} =$ average daily decrease in discharge through outlets below the thermocline, i.e.

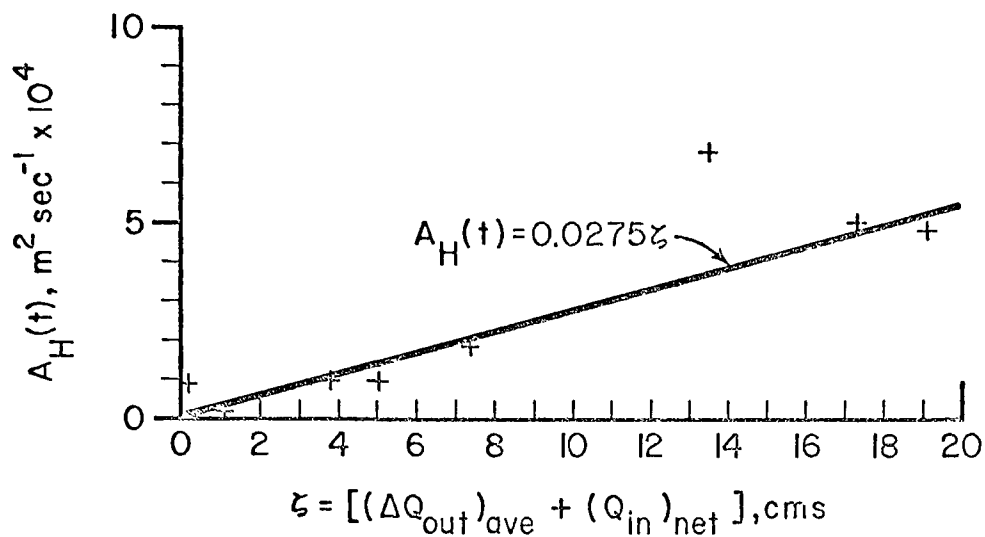
$$(-\Delta Q_{out})_{ave} = \frac{\sum \text{all negative values of } \Delta Q_{out}}{\text{period}} .$$

Equation 16 is illustrated in Figure 14-B. Comparison of the two plots in Figure 14 indicates that equation 15 describes best the temporal variation of $A_H(t)$. From Figure 14-A the value of $A_H(t)$ may be expressed as

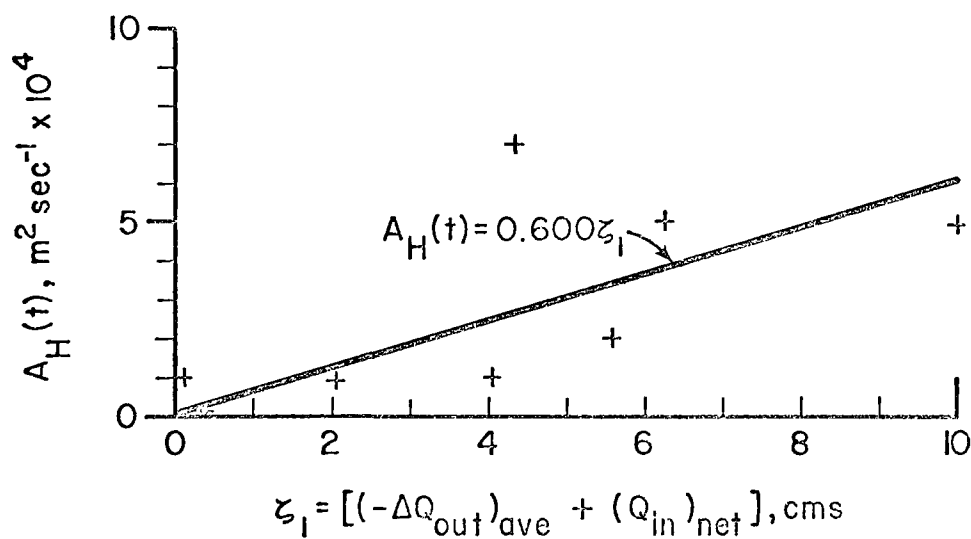
$$A_H(t) = 0.0275\zeta \quad , \quad (17)$$

where $\zeta = [(\Delta Q_{out})_{ave} + (Q_{in})_{net}]$, $m^3 \text{ sec}^{-1}$; and $A_H(t)$ has units of $m^2 \text{ sec}^{-1}$.

Equation 17 gives a general description of $A_H(t)$ in Hungry Horse Reservoir. The applicability of this equation to deep reservoirs in general, however, requires further testing. Although the functional relationship appears to be sound, it is almost certain that the constant 0.0275 will not be the same from reservoir to reservoir. Its value will most likely be primarily a function of the volume of the reservoir, because for a given value of ζ , the turbulent energy dissipated per unit



A. RELATIONSHIP BY EQUATION 15



B. RELATIONSHIP BY EQUATION 16

FIGURE 14. Relationship between Hypolimnetic Value of Eddy Conductivity Coefficient and Deep Reservoir Hydraulics

volume (upon which $A(z,t)$ is based) will be directly proportional to the reservoir volume.

PROPOSED FUNCTIONAL FORM FOR THE EDDY CONDUCTIVITY COEFFICIENT

Briefly summarizing the results of the research effort reported in this section, the most important finding was, by far, the log-log relationship between $A(z,t)$ and the stability E , as expressed by equation 14, in the region of steep thermal gradients. Although this formulation is based on the observed behavior of a single reservoir, some credibility is afforded to its general applicability by the fact that this same relationship was found to hold for Detroit Reservoir in Oregon, which was analyzed under a separate contract with the U. S. Army Corps of Engineers. Regarding the functional form of $A_H(t)$ as given in equation 17, the conclusions are not firm; thus the equation cannot be regarded as a general function without further substantiation. The evaluation of $A_E(t)$, of course, could not be accomplished due to the lack of observed wind mixing.

On the basis of the existing theory and the results reported in this section, the functional form of the eddy conductivity coefficient is proposed as follows in equation 18. Some discussion of the proposed form is given below.

$$A(z,t) = A_0 e^{-n(z_s - z)} \quad z_E < z \quad , \quad (18-A)$$

$$A(z,t) = bE^{-a} \quad z_H < z < z_E \quad , \quad (18-B)$$

$$A(z,t) = c \quad z < z_H \quad (18-C)$$

where z_E and z_H are the elevations at which $E \approx 10^{-6}$ meters⁻¹ and $E = (b/c)^{1/a}$, respectively. The value of η is chosen so that

$$e^{-\eta(z_S - z_E)} = \frac{b}{A_0} (10^{-6})^{-a}$$

Equation 18-A is based on the theory of wind mixing in the epilimnion. The value chosen for z_E , although somewhat arbitrary at this point, was chosen on the basis of the log-log plots of Figure 12, the rationale being that the linear log-log relationship between $A(z,t)$ and E should cease to exist at about the same value of E in the epilimnion as that observed in the hypolimnion. The proper choice of A_0 is purely speculative at this time; however, some insight into estimating its value may be derived from research reported by Hutchinson (3).

Inspection of the linear portion of the eddy conductivity-stability curves in Figure 12 indicates that, while the upper envelope curve has a slope of -1.0 in this region, the average slope for all curves is about -0.7. Consequently, the value proposed for \underline{a} is 0.7. It is worth noting that this same value for the average slope was observed for Detroit Reservoir.

The value of \underline{b} in equation 18-B was purposely left unspecified because there is some question as to whether this value might not be a function of the hypolimnetic turbulence level. It would seem that the greater the hypolimnetic turbulence, the larger the value of E at which the log-log relationship between $A(z,t)$ and E begins to exist. While no clear evidence of this fact was found in Hungry Horse, it must be borne in mind that this reservoir has a very small discharge to volume ratio and hence this variation would not be as apparent as in a reservoir with a larger ratio. On the other hand, Detroit Reservoir, which has an average dis-

charge-volume ratio, three times larger than that of Hungry Horse (see Chapter II), was found to have a value of $2.0 \times 10^{-8} \text{ m}^{1.3} \text{ sec}^{-1}$ for \underline{b} . Thus, for the present, it is suggested that the value of \underline{b} be taken as $1.5 \times 10^{-8} \text{ m}^{1.3} \text{ sec}^{-1}$.

For reasons previously given, $A(z,t)$ in equation 18-C was described as constant rather than by equation 17. In addition to these previous arguments, consideration of the limited amount of time variation in the hypolimnetic value of the eddy conductivity coefficient coupled with the small temperature gradients in this region tend to negate the need for a temporal and/or spatial description of the coefficient in deep reservoirs. On the basis of the Hungry Horse analyses, it is suggested that until more experience is gained with the hypolimnetic value of A_H , that the value be assumed to be $2.5 \times 10^{-4} \text{ m}^2 \text{ sec}^{-1}$. This value is in agreement with average values observed in deep lakes (3) and the oceans (17). A value of $0.3 \times 10^{-4} \text{ m}^2 \text{ sec}^{-1}$ for A_H , which was found in Detroit Reservoir, lies within range of minimum observed values.

In summary, the following values are recommended for the parameters in equation 18:

$$\begin{aligned} a &= 0.7, \\ b &= 1.5 \times 10^{-8} \text{ m}^{1.3} \text{ sec}^{-1}, \\ c &= 2.5 \times 10^{-4} \text{ m}^2 \text{ sec}^{-1}. \end{aligned}$$

Finally, in the absence of a better definition, it is suggested that the value of A_0 be taken as equal to c and that η be taken as zero, i.e., $A_E(z) = c$.

MODEL SENSITIVITY TO THE DIFFUSION FUNCTION

The proposed functional form of the eddy conductivity coefficient, as given in equation 18, contains four parameters, A_0 , a , b , and c . In order to acquire some feeling for the sensitivity of the deep reservoir model to variations in these parameters, three test simulations were performed with $A(z,t)$ defined as follows:

1. by the upper envelope curve shown in Figure 12 with
 - $a = 1.0$,
 - $b = 1.8 \times 10^{-9} \text{ m sec}^{-1}$,
 - $c = 1.0 \times 10^{-3} \text{ m}^2 \text{ sec}^{-1}$;
2. by the average curve shown in Figure 12 with values of a , b , and c as given above; and
3. by the lower envelope curves shown in Figure 12 with
 - $a = 0.7$,
 - $b = 3.1 \times 10^{-9} \text{ m}^{1.3} \text{ sec}^{-1}$,
 - $c = 1.5 \times 10^{-5} \text{ m}^2 \text{ sec}^{-1}$.

Typical temperature profiles produced in these three simulations are shown in Figure 15. Examination of this Figure reveals that while the average curve gives the best representation of the observed profiles, use of the lower envelope curve results in computed profiles that, for the most part, are within 1 °C of the observed values. The upper envelope curve, on the other hand, produces the worst simulation; one that is not acceptable within the reasonable limits of accuracy.

These simulations, while not providing conclusive evidence regarding the sensitivity of the model to individual parameter variation,

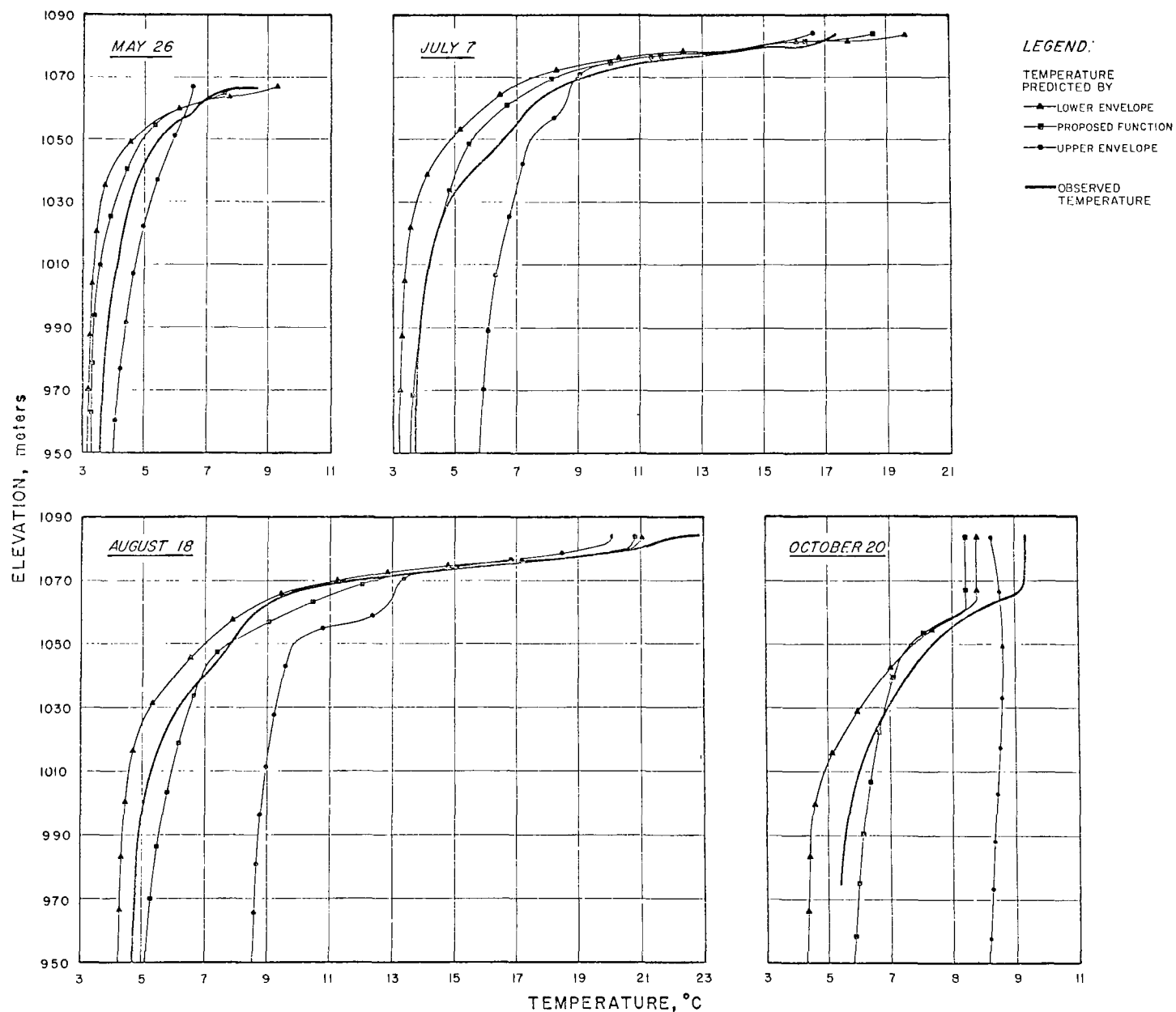


FIGURE 15. Effect of Eddy Conductivity Parameter Variation on Simulated Reservoir Temperature Profiles; Hungry Horse Reservoir, 1965

are constructive in that they show that the model is not over-sensitive to parameter variations within the ranges defined by the lower envelope curve and the proposed curve. Within the parameter ranges defined by the proposed curve and the upper envelope curve, however, parameter variation should be approached with caution since the model appears to be more sensitive to the parameter values within these ranges.

At the request of the FWPCA Study Team, one additional simulation was run in order to demonstrate the difference between the functional form of the eddy conductivity coefficient as proposed in equation 18 and the functional form as proposed in the original model development (see equation 12). One deviation from this original form was made in that $A(z,t)$ above the thermocline was taken as constant and smaller than that value used below the thermocline. This modification was made in order to retain sufficient heat within the surface layers of the reservoir so that the simulated surface temperatures would be approximately the same as those observed. At the suggestion of the Study Team, the following values of $A(z,t)$ were assigned:

$$\begin{aligned} A(z) &= 1.0 \times 10^{-5} \text{ m}^2 \text{ sec}^{-1} \text{ above the thermocline; and} \\ A(z) &= 2.5 \times 10^{-4} \text{ m}^2 \text{ sec}^{-1} \text{ below the thermocline.} \end{aligned}$$

Typical profiles resulting from this simulation are illustrated in Figure 16. In deference to the originally proposed function, there are other combinations of values for $A(z)$ which will produce better results. However, this simulation does illustrate the difficulties encountered in using equation 12 to describe the functional form of $A(z,t)$. In particular, it demonstrates the difficulty in simulating the clinolimnetic portion of the temperature profile as a result of assuming $A(z,t)$ constant in this region.

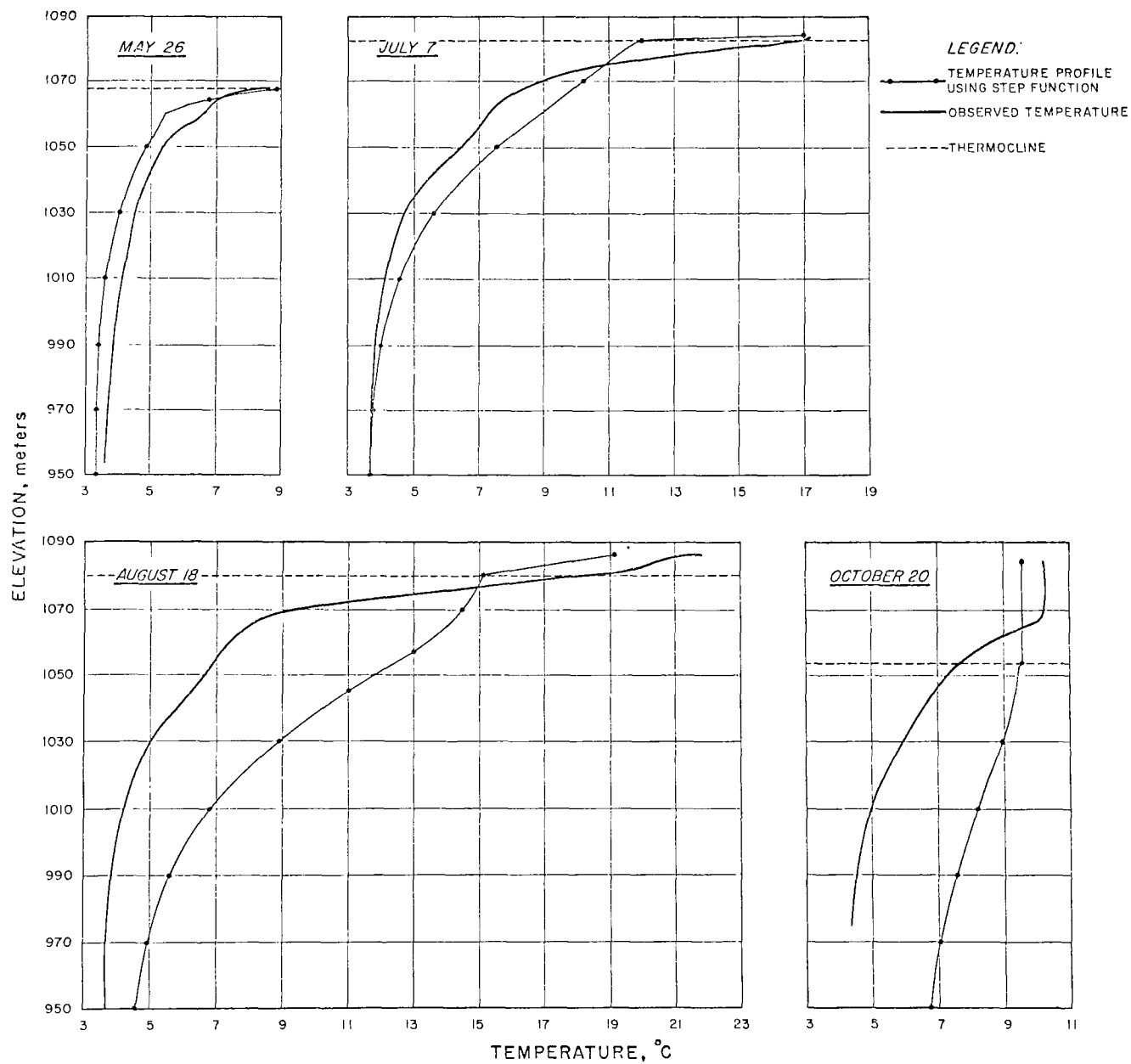


FIGURE 16. Reservoir Simulation with $A(z,t)$ Defined by Equation 12; Hungry Horse Reservoir, 1965

VERIFICATION OF THE DEEP RESERVOIR MODEL

Verification of the applicability of the deep reservoir model to reservoirs in the Northwest, and a final test of the functional form of the eddy conductivity as proposed in equation 18, were achieved simultaneously by the simulation of Hungry Horse Reservoir for the period 11 May to 20 October, 1965. The values used for the eddy conductivity parameters \underline{a} , \underline{b} , and \underline{c} were the recommended values; A_0 was taken equal to c and $\eta = 0$. The time increment between successive computations was one day. The results of this simulation, which are illustrated graphically in Figures 17, 18, and 19, show good agreement between the simulated and observed data.

Figure 17-B shows a comprehensive summary of the behavior of Hungry Horse Reservoir as observed and as predicted by the model during the 173-day period. Isothermal lines, which are superimposed on an elevation-time field, give a pictorial representation of the changing thermal energy distribution throughout the simulation period. The primary value of this plot for comparison purposes is to show the time and space relationships between the observed reservoir behavior and the model simulation. The relationship between computed results and observed results at any point in time is best illustrated by comparison of the thermal profiles which are shown in Figure 19.

The time-space relationship shown in Figure 17-B adequately demonstrates the capability of the model to describe the same progression of events as were observed in the reservoir. The primary difference between the model results and the observed behavior is that the model tends to enter the cooling cycle about one to two weeks early. The exact

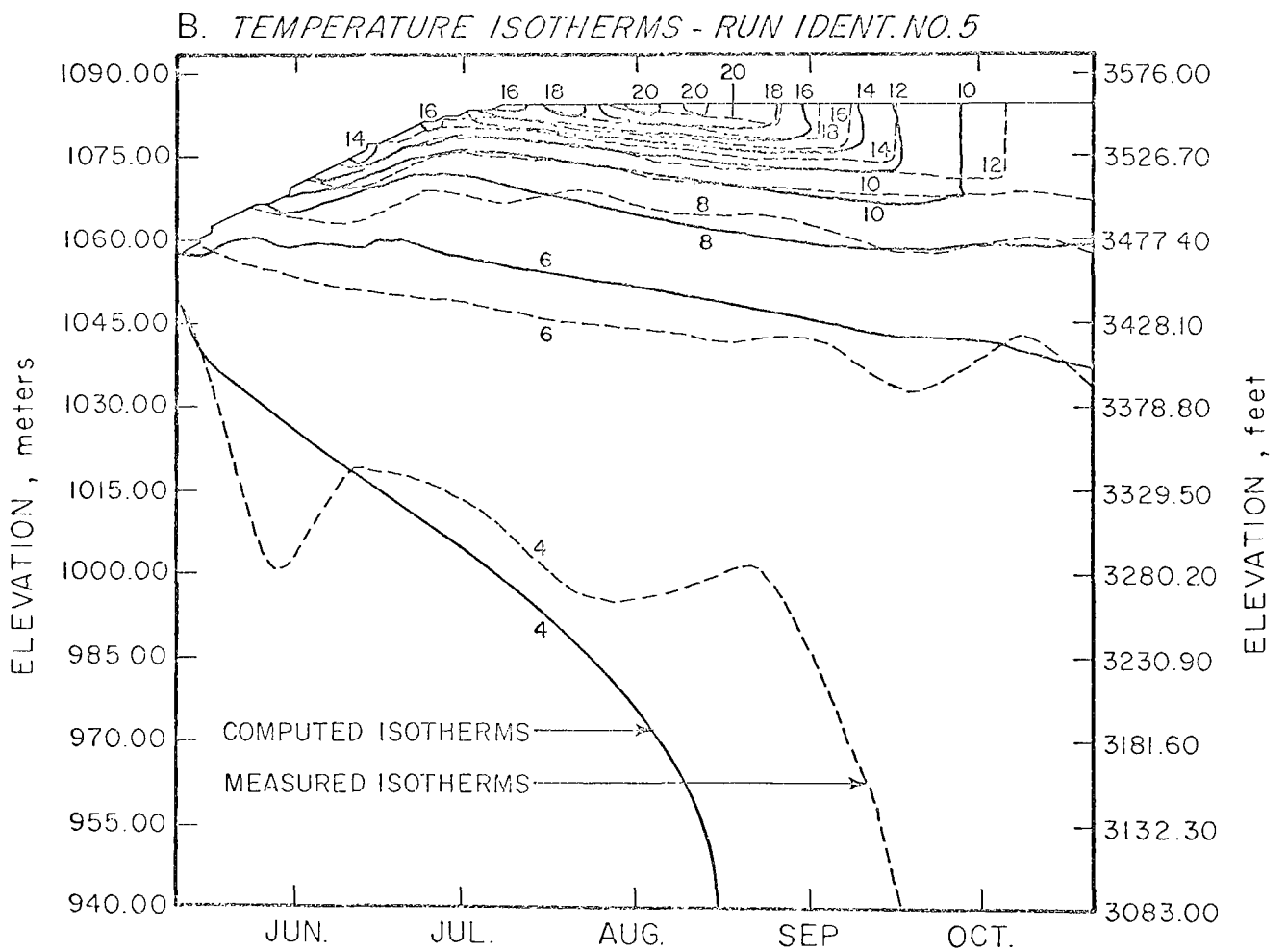
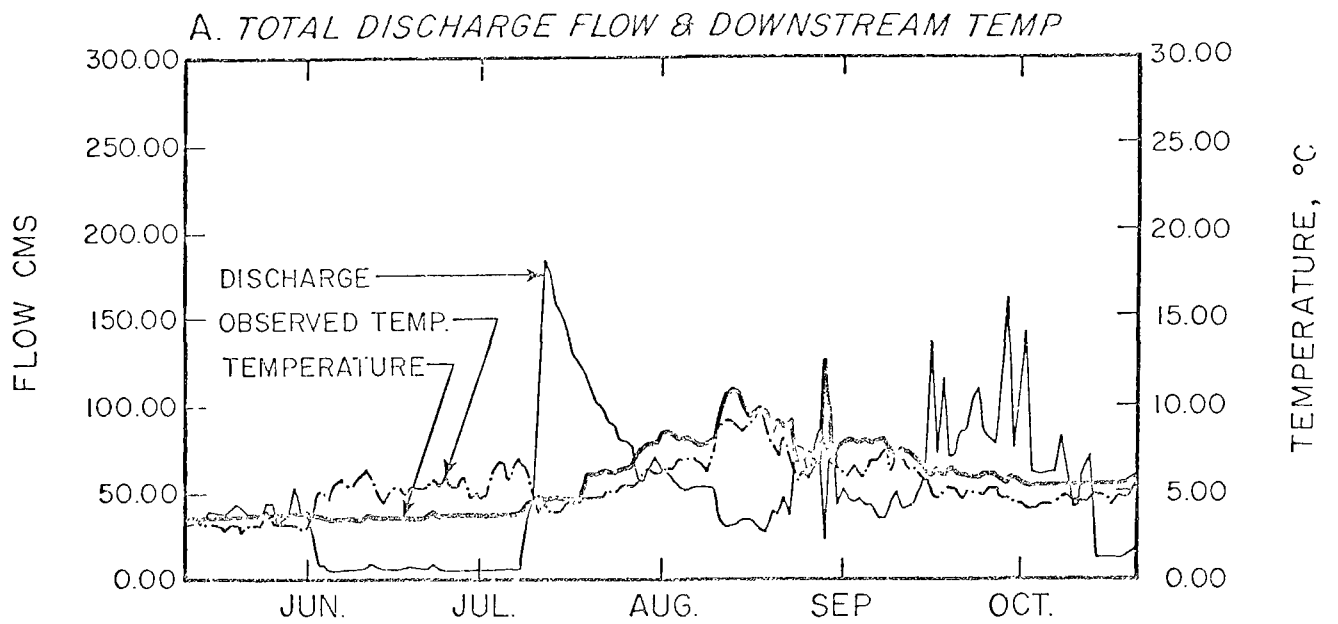


FIGURE 17. Simulated and Observed Thermal Regime for Hungry Horse Reservoir, 1965

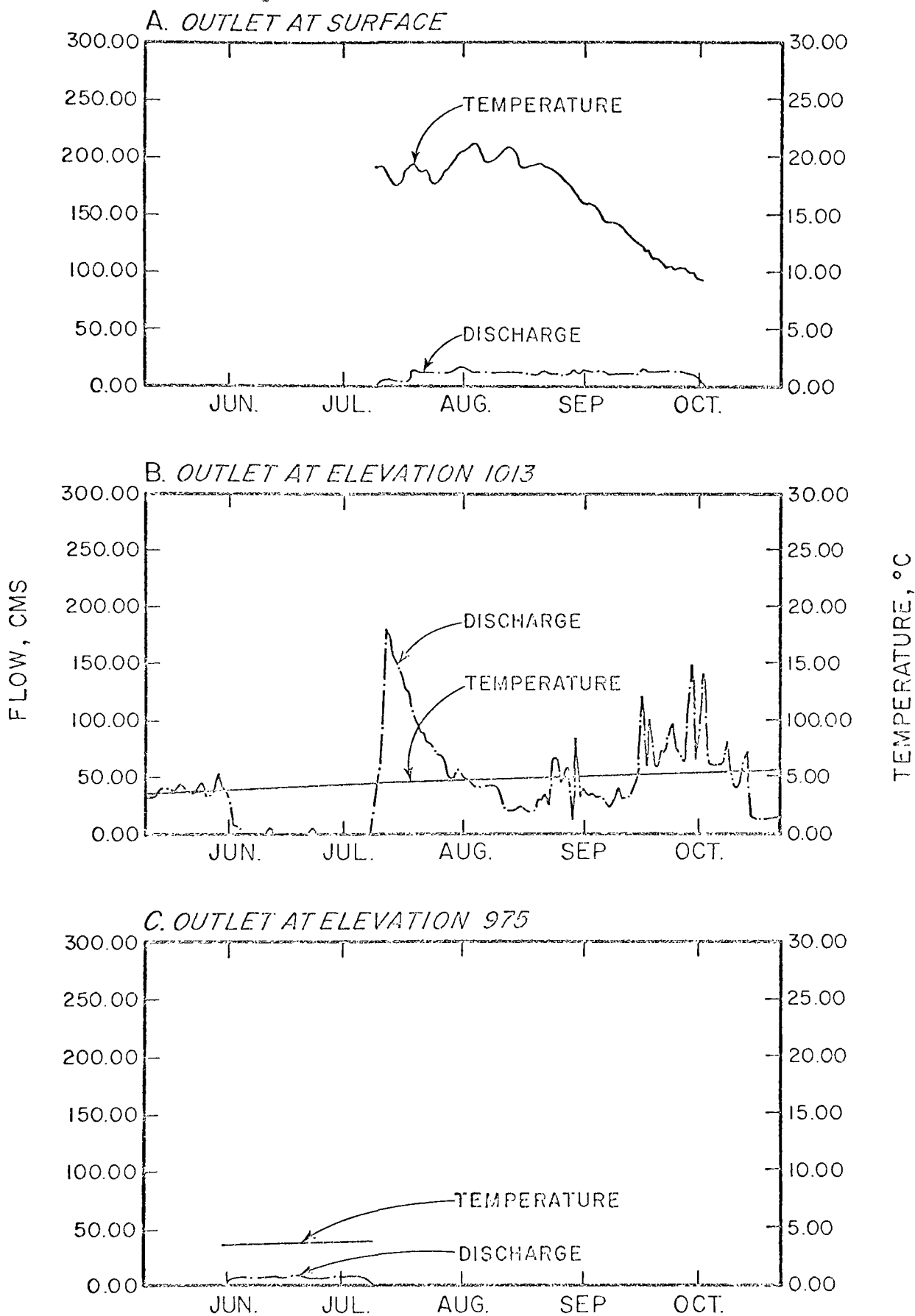


FIGURE 18. Breakdown of Outlet Discharges and Computed Outlet Temperature for Hungry Horse Reservoir, 1965

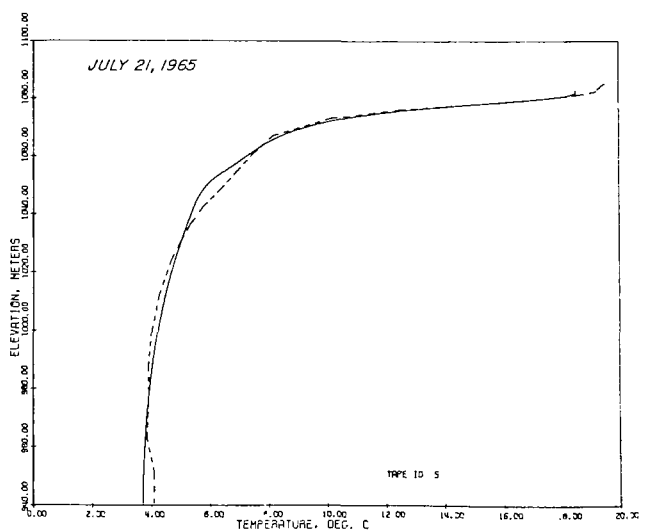
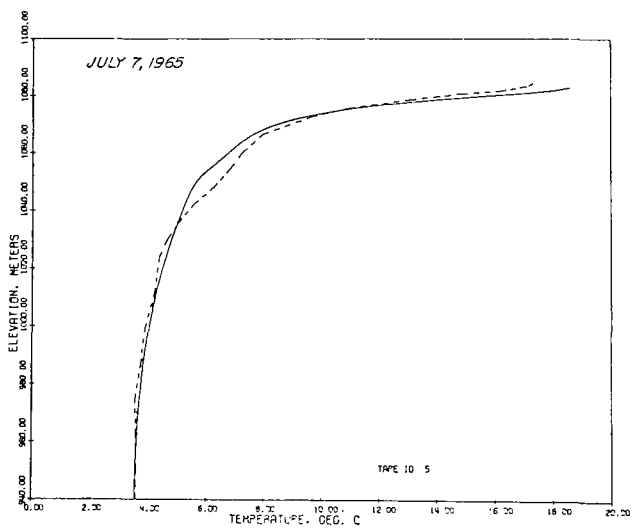
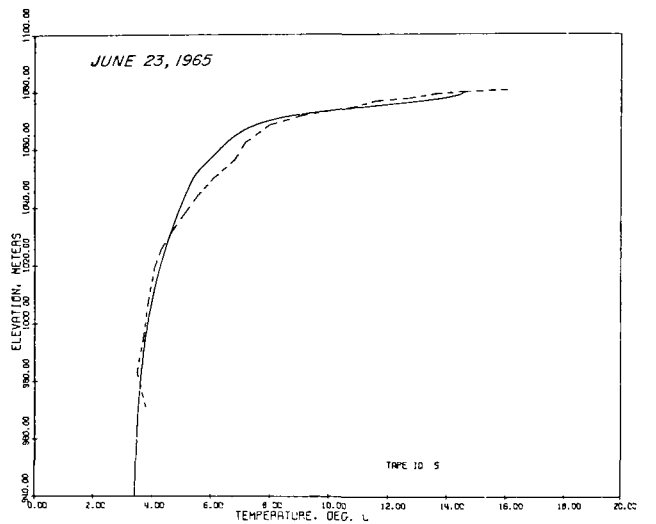
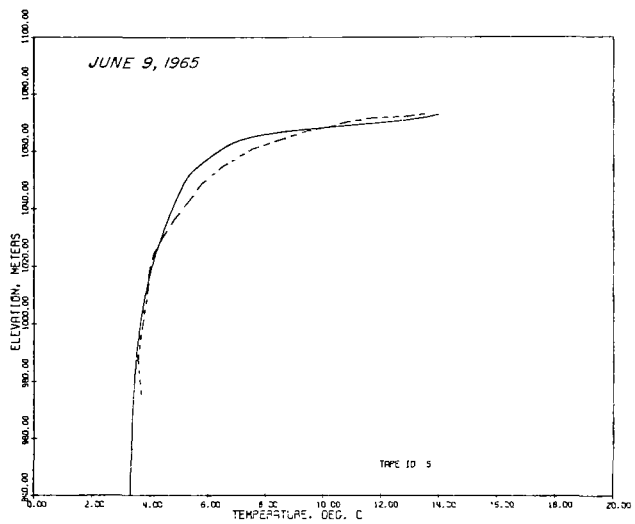
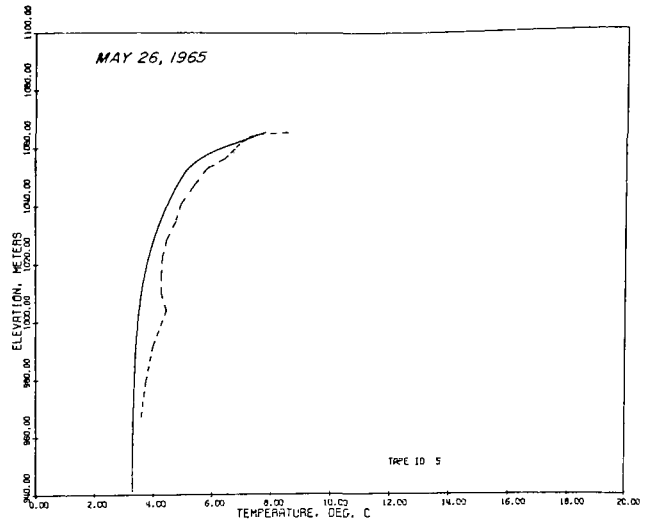
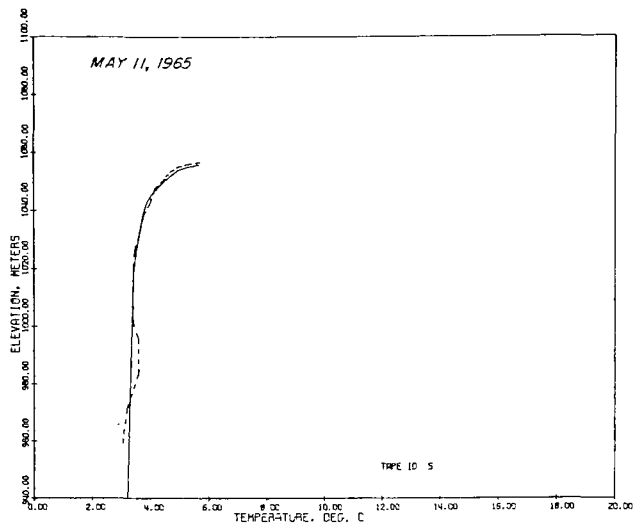


FIGURE 19. Simulated and Observed Temperature Profiles for Hungry Horse Reservoir, 1965

(Continued next page)

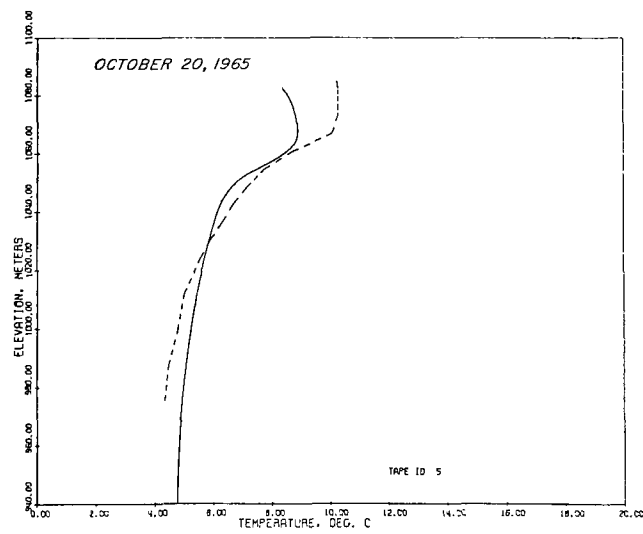
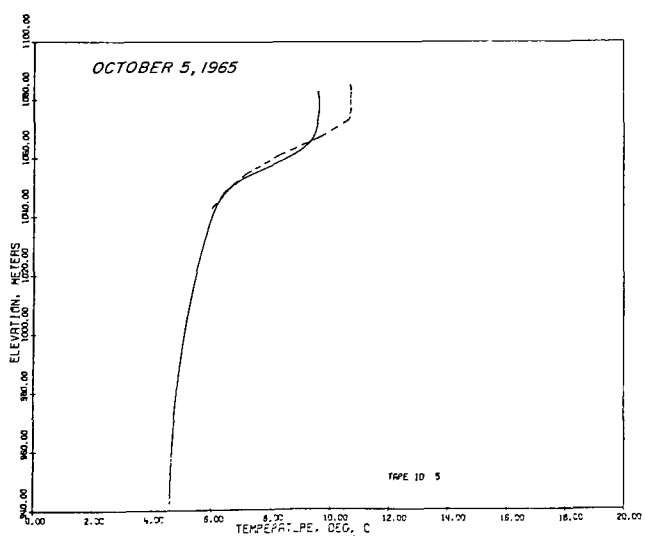
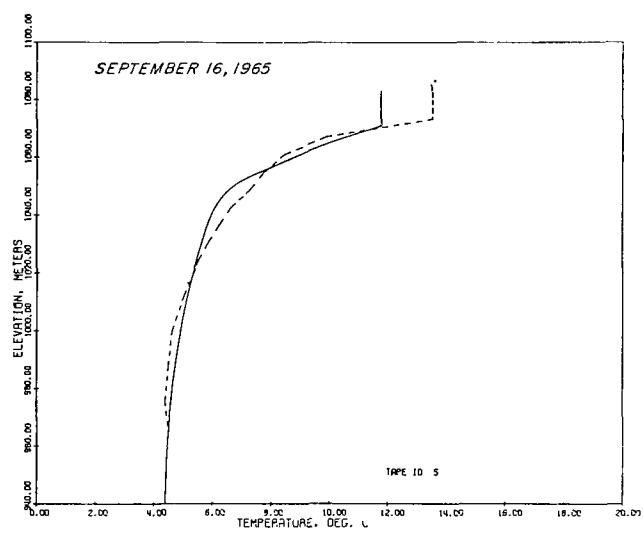
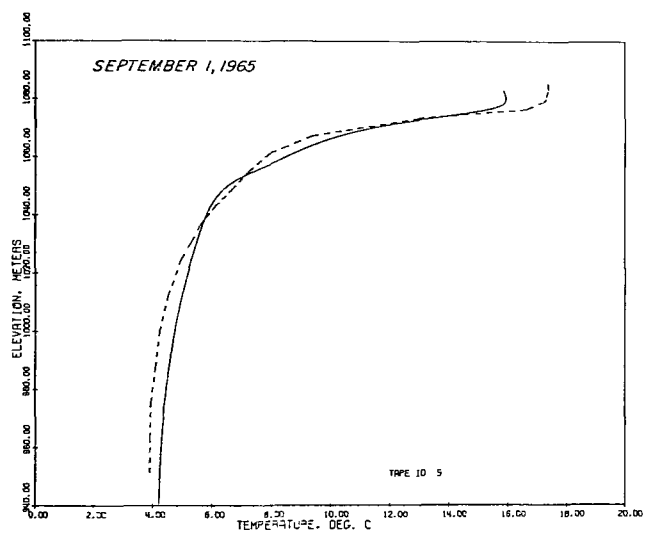
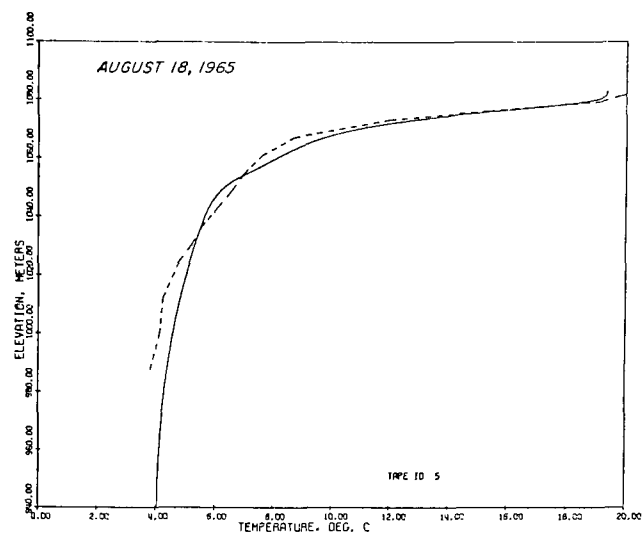
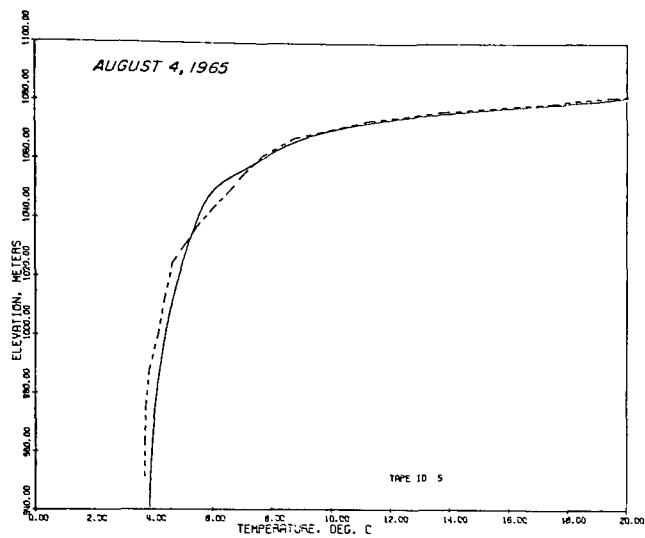


FIGURE 19 (cont'd). Simulated and Observed Temperature Profiles for Hungry Horse Reservoir, 1965

reason for this cannot be stated due to the complexity of the interaction between the reservoir and the meteorological factors. One reasonable explanation, however, could be that the surface of the reservoir becomes more turbid in the fall, thus trapping more short-wave solar radiation in the surface layers than occurs earlier in the year. Such a condition would warm the surface layers and consequently retard the rate of surface cooling. However, even with the early cooling, Figure 19 shows that the maximum variation in the computed and observed epilimnetic temperatures is less than 2°C.

It should be noted that while the spatial variations between the computed and observed 4°C and 6°C isotherms is quite large, the actual difference between the observed and computed temperatures is small (Figure 19 indicates the differences to be less than 0.6°C). This apparently anomolous behavior is due to the very small thermal gradients in the hypolimnion.

Figure 17-A supplies complimentary data to Figure 17-B in that it gives the time history of the net thermal and hydraulic characteristics of the reservoir discharge. The observed temperature line shown in the Figure is the average daily stream temperature as recorded 1.5 miles below the dam. Except for the month of June and the first part of July, the recorded temperatures are always lower than the computed temperatures. Communication with persons familiar with the gage indicates that it probably contains a negative bias. The high recorded temperatures during June apparently resulted from the temperature probe being in slack water during the low discharge period. Even though the absolute agreement between the observed and computed temperatures cannot be compared,

the observed temperatures are valuable in assessing the capability of the model to produce the observed day-to-day behavioral pattern of the downstream temperature. Examination of Figure 17-A indicates that the behavioral pattern of the predicted temperature is in excellent agreement with that observed, thus demonstrating the model's capability to simulate the day-to-day variation in the downstream temperature.

Figure 18 provides a breakdown of the composite information contained in Figure 17-A. In this simulation run, the method of flow withdrawal from the reservoir was that used in the original derivation of the model, i.e. the withdrawal depth is taken to be the thickness of the element whose elevation corresponds to the elevation at the centerline of the outlets (in this case, the element thickness was one meter). Consequently, the temperatures shown in Figure 18 are the reservoir temperatures at the elevation of the outlet. These particular plots will be more useful in comparing the element withdrawal technique to the selective withdrawal technique which is the subject of the following chapter.

In summary, the verification run as described above adequately demonstrates the validity of equation 18 in describing the internal mixing process. Moreover, this simulation serves as verification that the model is generally applicable for the simulation of deep reservoirs in the Pacific Northwest.

V. SELECTIVE WITHDRAWAL STUDIES

THEORY

When water is withdrawn from a stratified impoundment, it does not necessarily follow that the entire fluid bulk will contribute to the outflow as is the case for a non-stratified body. The theoretical analysis of Yih (19) showed that there is a tendency for flow separation when the densimetric Froude number becomes less than $1/\pi$. That flow separation does, indeed, occur at low Froude numbers has been confirmed experimentally by Debler (20).

For the flow situation shown in Figure 20, the densimetric Froude number F is defined by Debler as

$$F = \frac{q}{d^2} \sqrt{\frac{\rho_0}{g\beta}} \quad (19)$$

where

- q = volumetric discharge per unit width of the channel;
- d = height of the dividing streamline far back from the outlet
- ρ_0 = density at the channel bottom;
- $\beta = -\frac{\partial \rho}{\partial z}$; and
- g = gravitational constant.

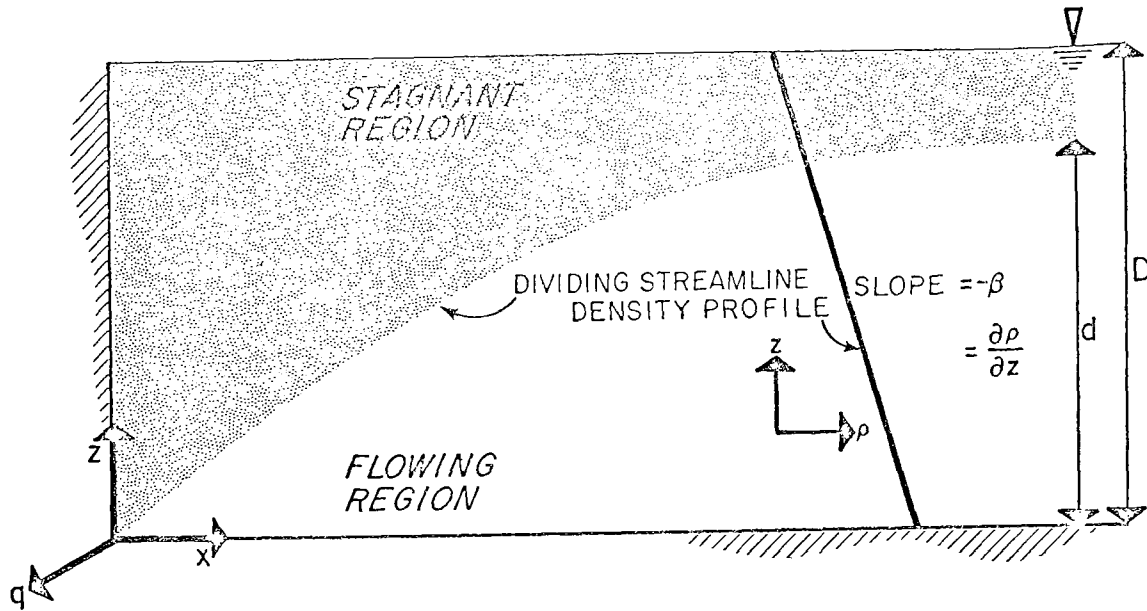


FIGURE 20. Schematic Sketch of Flow Separation in Stratified Flow

Through the performance of a set of experimental runs, Debler established that the Froude number of the divided flow was a constant, with a value of about 0.24. On the basis of this result, the withdrawal depth, d , can then be defined as

$$d = 2.0 \left[q \sqrt{\frac{\rho_0}{g\beta}} \right]^{1/2} \quad (20)$$

This equation is recommended by Brooks and Koh (21) for determination of the withdrawal thickness close to the dam (Brooks and Koh recommend 1.9 for the constant rather than 2.0). Farther back from the dam, they recommend using the results of Koh's theory (reported in the same publication) which incorporates viscous broadening of the withdrawal layer for the case of steady turbulent flow. However, since transients in the withdrawal currents caused by fluctuating release rates are very persistent,

they can significantly alter the steady flow solutions, especially far back from the dam. Consequently, it was felt that the use of equation 20 would provide as good an approximation to the withdrawal zone as could be obtained by application of the more sophisticated viscous broadening theory.

In applying equation 20 to an operating reservoir, reference is made to Figure 21 which shows a dam with three outlets. Each outlet has a volumetric discharge Q . To convert these discharges to a discharge per unit width, the reservoir width, w , at the elevation of the outlet is used. Equation 20 for this case is assumed to define the half-width of the withdrawal layer. The value of ρ_0 is taken as the density at the centerline of the outlet and β is taken as the negative value of the density at the centerline of the outlet.

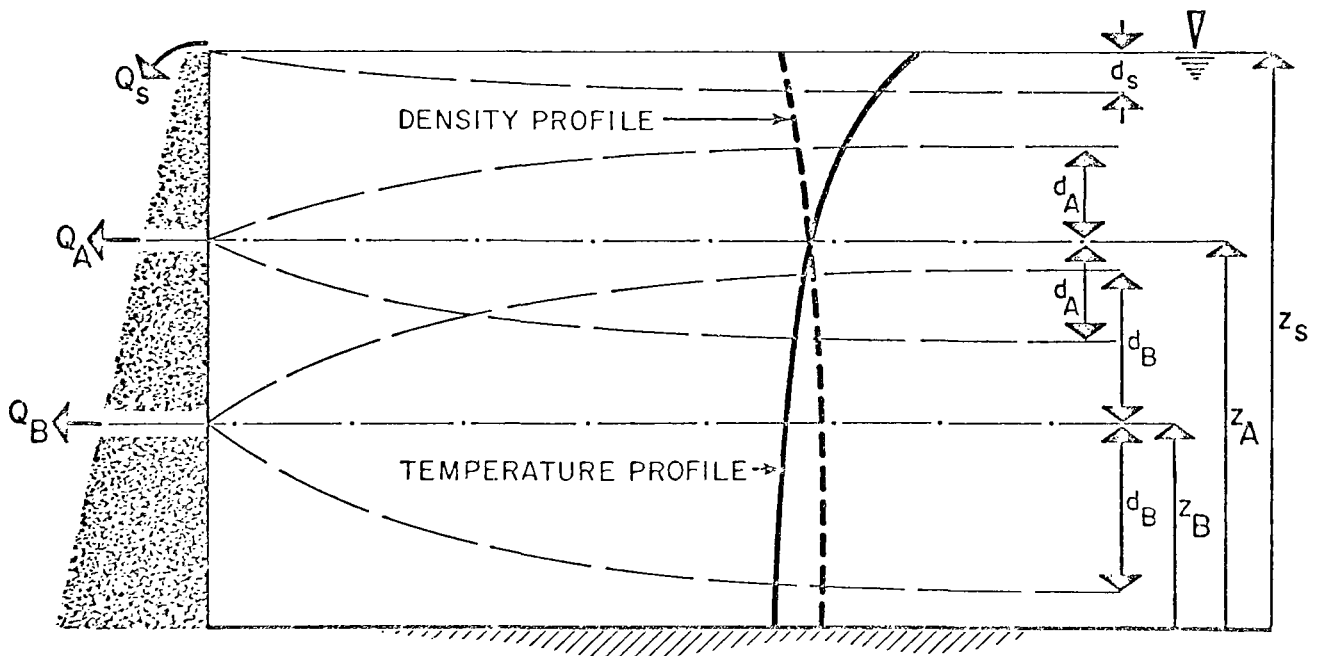


FIGURE 21. Schematic Diagram of the Application of Selective Withdrawal Theory to a Stratified Impoundment

By the use of these definitions for ρ_0 and β , it is observed that the ratio $\frac{\rho_0}{\beta} = \left(\frac{1}{\rho_0} \beta\right)^{-1}$ is the reciprocal of the stability, E , at the centerline of the outlet. Thus equation 20 can be rewritten as

$$d = 2.0 \left[\frac{q}{\sqrt{gE}} \right]^{1/2} \quad (21)$$

Applying equation 21 to the outlet configuration shown in Figure 21, the value of q is taken as follows:

$$\begin{aligned} \text{surface outlet} \quad q &= \frac{Q_s}{w_s} \\ \text{submerged outlets} \quad q &= \frac{1/2 Q_A}{w_A}, \quad q = \frac{1/2 Q_B}{w_B} \end{aligned}$$

To apportion the flow within the withdrawal zones, the inviscid theory of Yih (22) is used in which the velocity within the flow field is defined as

$$u(z) = \sqrt{\frac{\rho_0}{\rho}} U' \quad (22)$$

where U' is a constant called the "associated velocity." However, considering the degree of density stratification encountered in prototype reservoirs, the variation in the ratio $\frac{\rho_0}{\rho}$ over the withdrawal depth is insignificant; hence, the velocity within the withdrawal zone is defined simply as

$$u(z) = \text{constant}. \quad (23)$$

In applying equation 23 to the flow field, it is assumed that the principle of superposition holds for regions in which the withdrawal layers overlap. If the effect of channel side-slope is neglected, the withdrawal layer configuration shown in Figure 21 has a spatial velocity distribution given as

$$u(z) = \frac{Q_B}{w_B(2d_B)} , \quad z_B - d_B \leq z \leq z_A - d_A ; \quad (24-A)$$

$$u(z) = \frac{Q_A}{w_A(2d_A)} + \frac{Q_B}{w_B(2d_B)} , \quad z_A - d_A \leq z \leq z_B + d_B ; \quad (24-B)$$

$$u(z) = \frac{Q_A}{w_A(2d_A)} , \quad z_B + d_B \leq z \leq z_S - d_S ; \quad (24-C)$$

$$u(z) = \frac{Q_S}{w_S d_S} , \quad z_S - d_S \leq z \leq z_S . \quad (24-D)$$

Although the selective withdrawal scheme as outlined above is generally applicable, some situations can be encountered in its application that require special attention. The first of these is the case in which the dividing streamline for a submerged outlet falls above the water surface or below the reservoir bottom. This situation is likely to be encountered with deep outlets early in the year when the stratification is weak, i.e., the stability is small. There is no theoretical precedent for dealing with this case; consequently, the most simple approach is used for the sake of computational convenience. The solution is to confine the withdrawal zone to that region which falls between the dividing streamline, which lies in the fluid, and the water surface or the reservoir bottom, depending upon which boundary was crossed. The velocity is then distributed uniformly over the revised withdrawal depth. This scheme is illustrated

in Figure 22 for the case in which the computed streamline falls below the reservoir bottom.

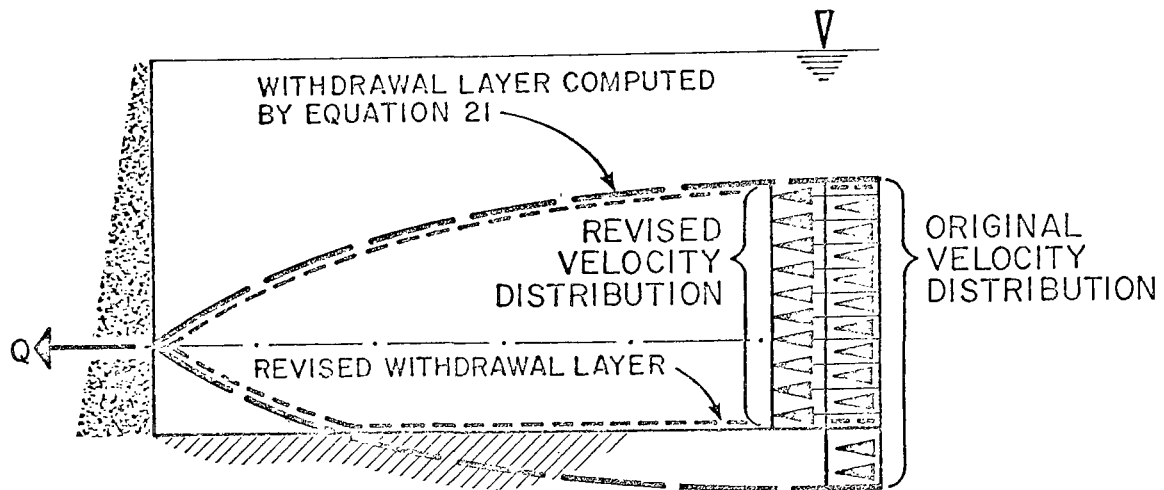


FIGURE 22. Withdrawal Region for Case of Dividing Streamline Falling Below Reservoir Bottom

A second situation, which can be encountered, is that the dividing streamline, computed for an outlet on one side of the thermocline, falls on the other side of the thermocline. An example of such a case is shown in Figure 23. The objection to this condition is based on the fact that the withdrawal depth is a function of stability which is assumed constant over the withdrawal depth. The case illustrated in Figure 23 is clearly in violation of this assumption. Since the withdrawal depth varies inversely with the stability, the upper withdrawal region should be smaller than the computed value. It is reasonable and convenient to limit the upper withdrawal zone to the elevation of the

thermocline as shown in the Figure. A similar correction is made for outlets in the epilimnion whose lower streamline falls below the thermocline. The flow distribution for these cases is adjusted in a manner analogous to that for the case of the dividing streamline crossing a reservoir boundary.

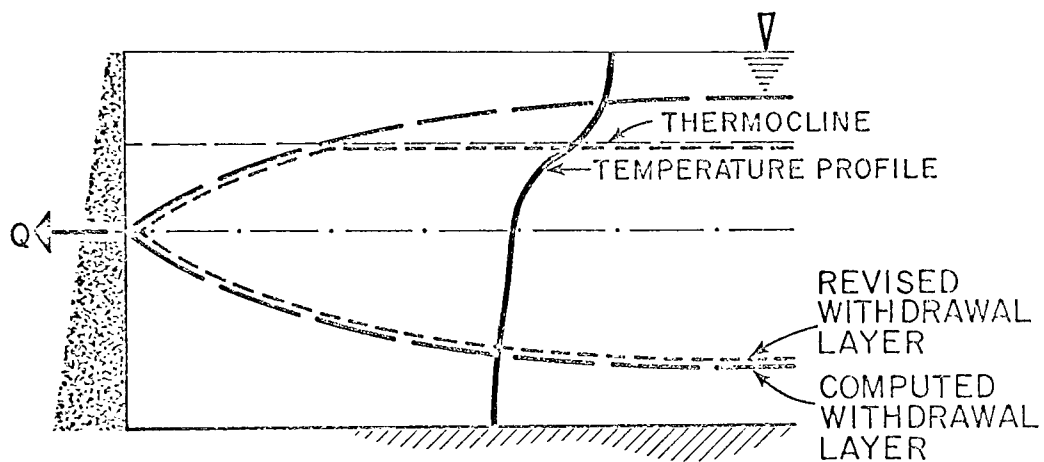


FIGURE 23. Withdrawal Region for Case of Computed Dividing Streamline Crossing the Thermocline

A special situation is encountered with the onset of fall cooling when epilimnetic mixing by natural convection becomes predominant. The result of this mixing is to cause the reservoir in the epilimnetic region to be isothermal as illustrated in Figure 24; hence, the stability in this region is zero and Debler's criteria is no longer applicable to outlets above the thermocline. To account for this situation, the theory of Craya (23) as reported by Yih (22) has been used.

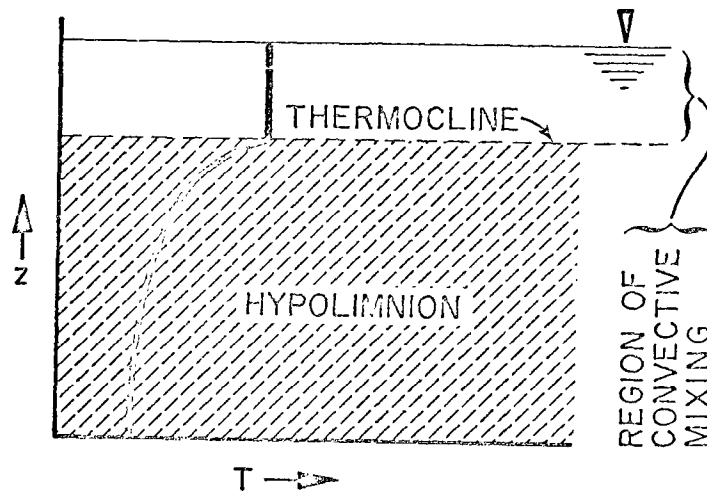


FIGURE 24. Effect of Convective Mixing on the Thermal Profile

To use Craya's approach, it is assumed that the density structure of the reservoir is a step function whose value is ρ above the thermocline and $\rho + \Delta\rho$ below the thermocline as illustrated in Figure 25.

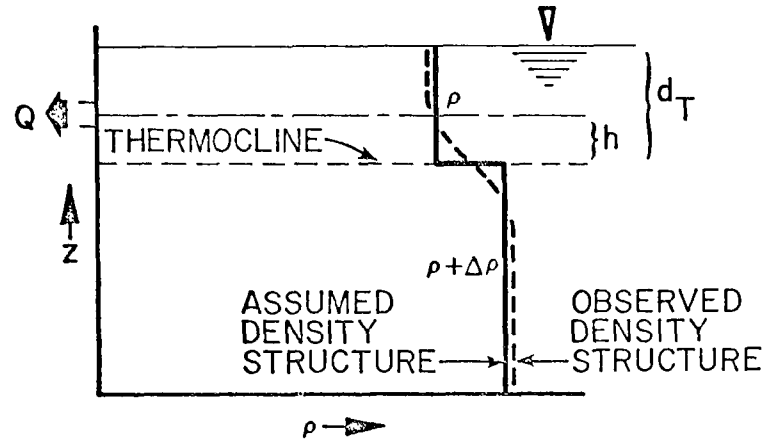


FIGURE 25. Assumed Reservoir Density Structure for Application of Craya's Criteria

Using the notations of this Figure, the critical epilimnetic discharge at which water will begin to be withdrawn from the hypolimnion of the reservoir is

$$\frac{Q_A}{w_A} = q_c = 1.52 \sqrt{gh^3 \frac{\Delta\rho}{\rho}}, \quad 2h \leq d_T, \quad (25)$$

for submerged outlets, and

$$\frac{Q_S}{w_S} = q_c = 0.75 \sqrt{gd_T^3 \frac{\Delta\rho}{\rho}}, \quad (26)$$

for surface outlets. The velocity distribution in the epilimnion is assumed to be uniform.

If q is greater than q_c for any outlet or combination of outlets, Debler's criteria (equation 21) is used to compute the depth of withdrawal from the hypolimnion, taking $q - q_c$ for the discharge and the value of E immediately below the thermocline for the stability. The velocity distribution is then adjusted so that it is uniform throughout the entire withdrawal depth. While there is no precedent for using Debler's criteria for the excess flow, there does not appear to be any existing theory which is more appropriate in this kind of situation.

Although some parts of the selective withdrawal theory related above might be challenged on theoretical grounds, it must be recognized that the approach to the incorporation of selective withdrawal theory into the deep reservoir model has of necessity had a pragmatic orientation due to the need to produce a functional tool which could provide required answers when applied to prototype situations. Nevertheless, WRE believes that the theory related above represents the best approach available at the present time. Moreover, it points out the need for additional research and development of a practical nature in the area of withdrawal from stratified impoundments. The incorporation of the above theory, as it stands, is regarded as being another step forward in refining the deep reservoir model. The use of this theory should enhance the model's capabilities particularly in simulating the individual discharge temperatures from the reservoir outlets.

In order to test the validity of the proposed selective withdrawal scheme, it was desirable to compare computed withdrawal temperatures with observed temperatures. The only observed withdrawal temperatures

on Hungry Horse were the cooling water temperatures for the turbines and the accuracy of these temperatures was not known. Consequently, Fontana Reservoir was chosen to test the theory since the observed data was more reliable. The data for the computations was taken from reference 24. The comparison of the computed turbine intake temperatures with the observed turbine cooling water temperatures for Fontana Reservoir is shown in Figure 26 (the cooling water temperatures had been correlated and adjusted to the reservoir temperatures during a period when the reservoir was isothermal). It appears that the computed outflow values contain a small amount of bias, tending on the average to be about 1°F too cool. Very rarely are they biased more than 2°F. At the present time the reason for this bias is not known; however, it is felt that the predictions are close enough to the observed temperatures to adequately satisfy the modeling requirements.

As a further test, a few trial computations were made on Hungry Horse Reservoir and Detroit Reservoir. The results shown in Table 2 indicate that the prediction is satisfactory.

SIMULATION OF HUNGRY HORSE RESERVOIR USING SELECTIVE WITHDRAWAL THEORY

Having incorporated the selective withdrawal theory into the deep reservoir model, the simulation run illustrated in Figures 27 and 28 was executed. The only difference between this run and the verification run in Chapter IV is that the verification run used the original method of element withdrawal while the run illustrated here had the selective withdrawal theory incorporated. To facilitate the comparison of these two simulations, Figures 17 and 18 have been overlaid on Figures 27 and 28, respectively,

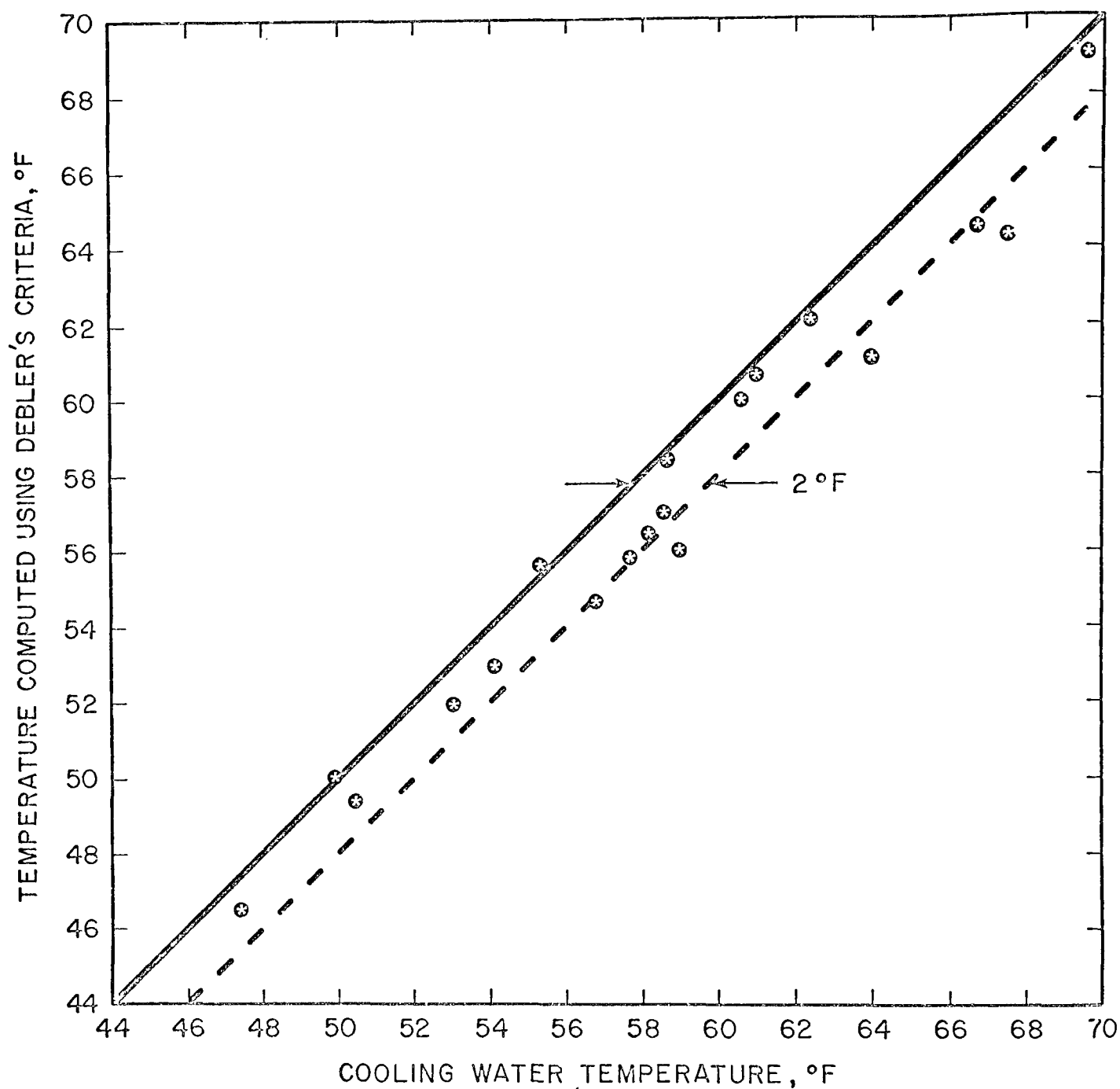


FIGURE 26. Comparison of Outflow Temperatures Computed from Debler's Criteria with Measured Cooling Water Temperatures (Fontana Reservoir)

TABLE 2

HUNGRY HORSE RESERVOIR
TURBINE INTAKE TEMPERATURES

DATE	COMPUTED, °C	COOLING WATER TEMPERATURE, °C
21 July 1965	4.4	4.5
18 August 1965	4.3	5.0

DETROIT RESERVOIR
TAILRACE TEMPERATURES

DATE	TURBINE INTAKE TEMPERATURE COMPUTED, °F	SPILLWAY TEMPERATURE COMPUTED, °F	TAILRACE TEMP., °F COMPUTED	OBSERVED
20 May 1964	42	47	44	43
7 November 1958	54	NO DISCHARGE	54	54
10 November 1958	52	NO DISCHARGE	52	53

Examination of the results indicates that the effects of including the selective withdrawal theory into the model are something less than dramatic. The most obvious result is a minor alteration of the thermal regime of the reservoir in that the vertical rate of heat transfer is slightly increased, i.e., the isotherms for the selective withdrawal case are somewhat deeper than in the element withdrawal case. In addition, the onset of the convective cooling cycle is slightly retarded.

The complexity of the reservoir mechanics precludes any simple explanation for this observed behavior. It can only be hypothesized that the selective withdrawal scheme induces larger thermal gradients into the reservoir with the result that the rate of turbulent heat transfer is increased.

It was expected that the use of selective withdrawal would cause a decrease in the computed net outflow temperature during the period of spillway operation, since some of the cooler water below the surface would be included in the spillway discharge; however, this was not the case. In fact, the selective withdrawal scheme produced slightly higher outflow temperatures than did the element withdrawal scheme. The reason for this is hypothesized as follows. During the period of spillway operation, the element withdrawal scheme takes all of the surface spill from the surface element of the reservoir, thus tending to expose the cooler underlying water. The selective theory, on the other hand, causes a portion of the spill to be drawn from elements below the surface; consequently, not as much of the warm surface water is removed, and the reservoir's surface has a tendency to remain warmer. Unless the spillway

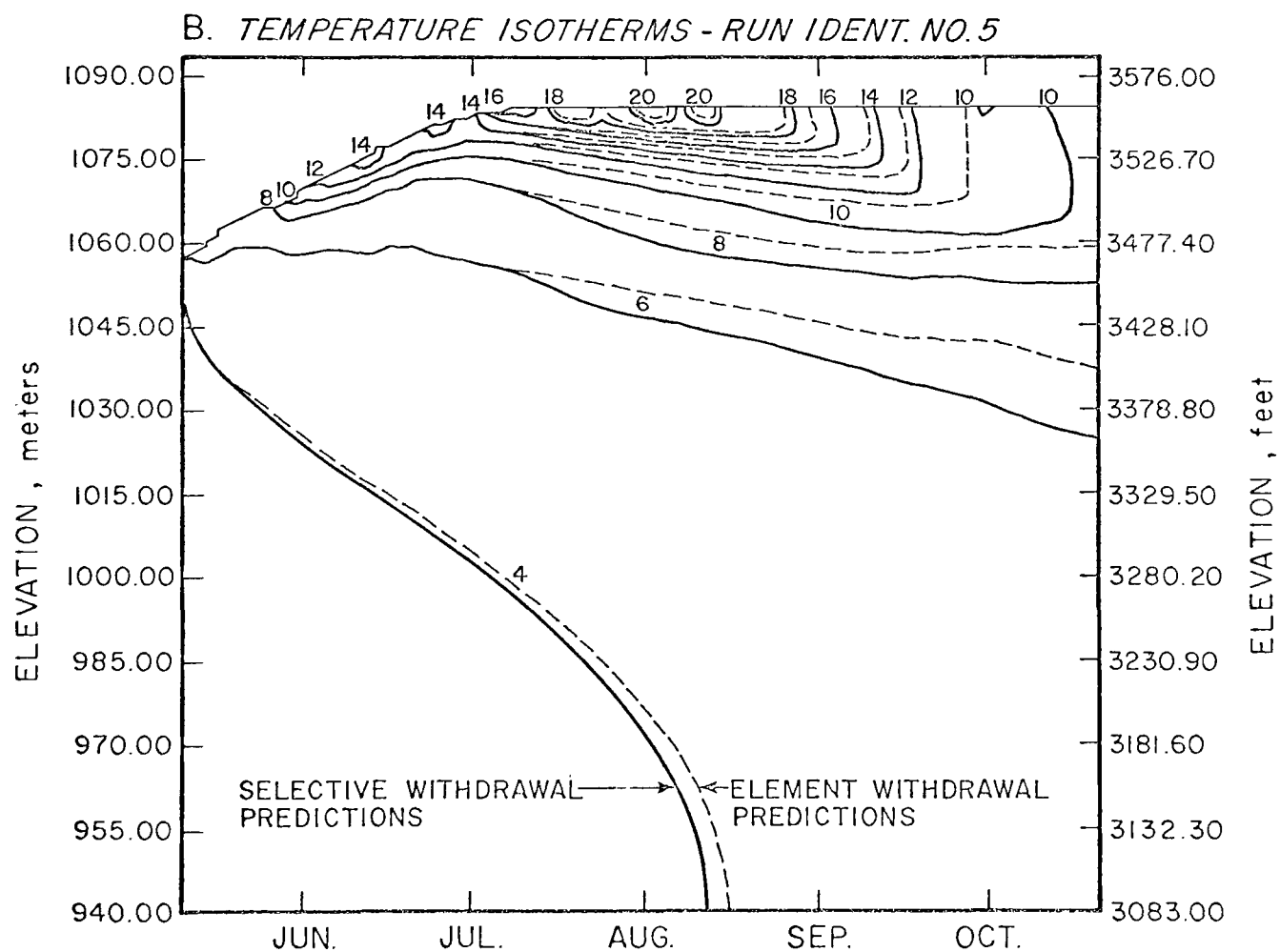
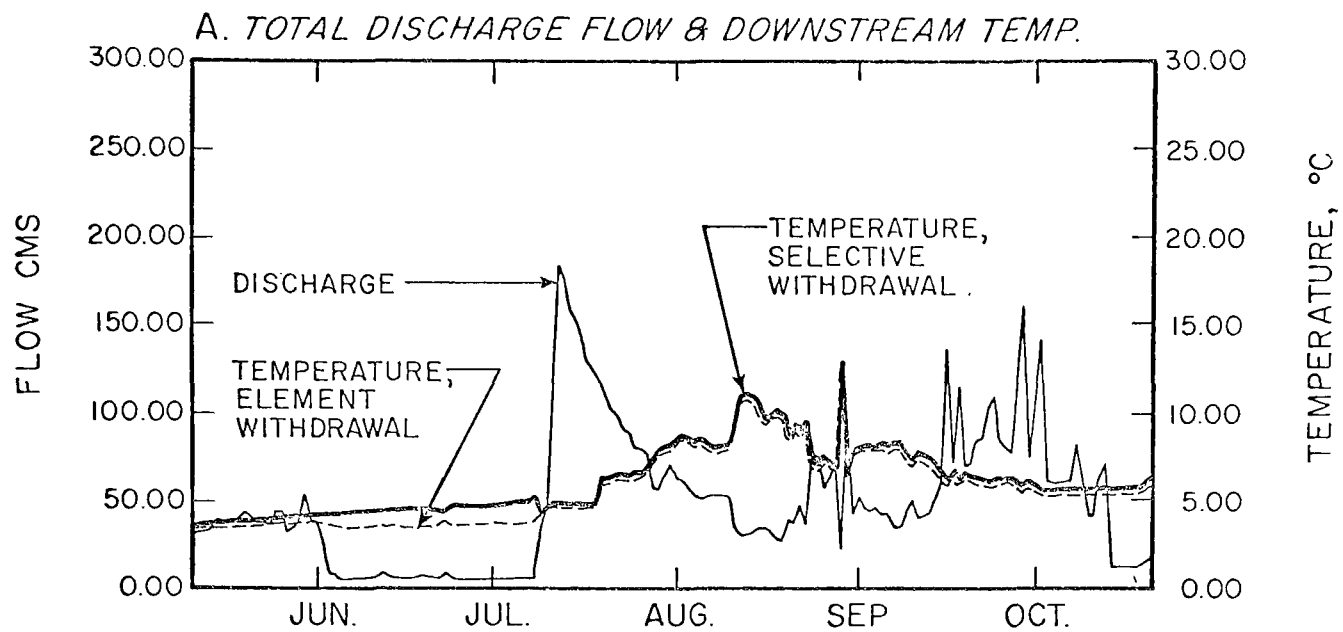


FIGURE 27. Simulated Thermal Regime of Hungry Horse Reservoir, 1965, Using Selective Withdrawal Theory

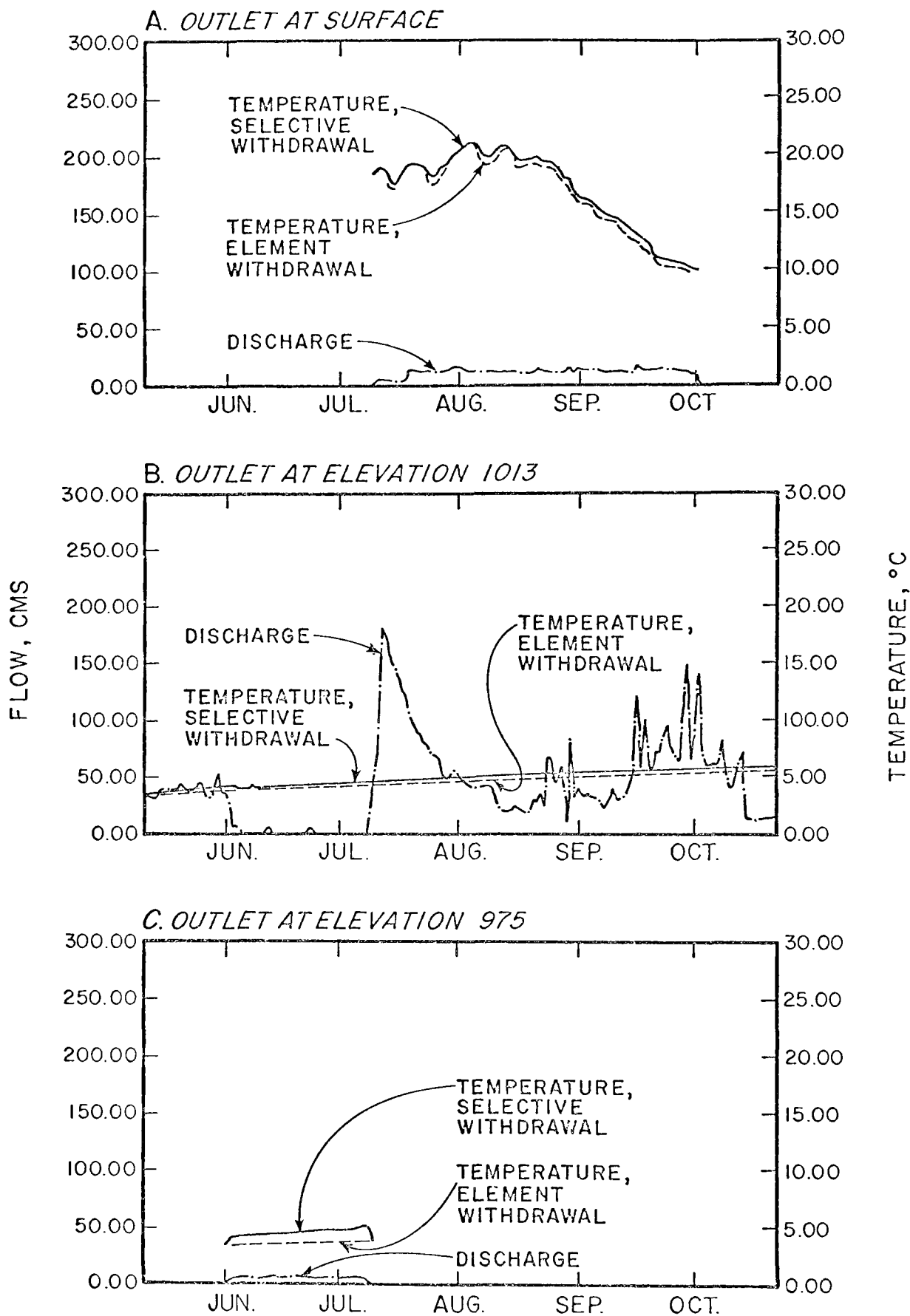


FIGURE 28. Simulated Discharge Temperatures for Individual Outlets as Computed with Selective Withdrawal Theory; Hungry Horse Reservoir, 1965

discharge is sufficiently high, the withdrawal layer will not be deep enough to result in a new withdrawal temperature that is less than that of the element withdrawal case.

The examination of Figure 29 reveals one other observation that is worth discussing. During the period of operation of the discharge tube at elevation 975, the selective withdrawal case produces outflow temperatures significantly higher than does the element withdrawal scheme. The reason for this is that the stability gradient at this point is sufficiently low to cause withdrawal from the entire hypolimnion; consequently, the outflow temperature for the selective withdrawal case represents the mean temperature of the entire reservoir below the thermocline, whereas the outflow temperature for the element withdrawal scheme represents only the temperature of the reservoir at elevation 975.

In summary, while the simulation run incorporating the selective withdrawal theory did not produce the dramatic results expected, it is felt that this was due to the physical nature of the reservoir and its mode of operation, not to a failure of the selective withdrawal theory. This conclusion becomes more clear in the following chapter where two test cases are simulated using the net outflow temperature from the reservoir as the criteria for the operation of the outlets.

VI. MULTIPLE OUTLET STUDIES

As a demonstration of the deep reservoir model's versatility in assessing the consequences of reservoir regulation for downstream temperature control, two test cases were simulated on Hungry Horse Reservoir. These tests were conceived mutually by the FWPCA Study Team and WRE and are as follows.

TEST CASE I

Using the existing outlet configuration in Hungry Horse Reservoir, operate the outlets on a daily basis in such a manner as to produce a prescribed net outflow temperature.

TEST CASE II

Hypothetically, add a second turbine intake to the reservoir. On a daily basis, operate the spillway in the same manner as it was historically operated in 1965 and distribute the remainder of the outflow between the two turbine intakes in such a manner as to produce a prescribed outflow temperature.

For both test cases, the total reservoir outflow was taken as the historical outflow in 1965. The downstream object temperature for the two cases was taken as the observed temperature of the major reservoir tributary, i.e., the temperature of the South Fork of the Flathead River above Twin Creek for the year 1965. The results of these two test simulations are reported below.

TEST CASE I

Test Case I was not the product of whimsical imagination. Rather, it was designed around the fact that, since the construction of Hungry Horse Dam, the reservoir release temperatures have been so cold that the native fish population below the dam has been eliminated. By operating the reservoir outlets in such a manner as to produce a release temperature equal to that of the natural stream, it would be assured that the fish population could be re-established. In addition, the analysis of this type of operation would reveal the hydropower tradeoff required to maintain the downstream fishery.

The simulation results of Test Case I are illustrated in Figures 29 and 30. In order to compare this simulation with the historical case, the results of the selective withdrawal simulation (Figures 27 and 28) have been overlaid. Inspection of Figure 29-A reveals that excellent agreement was obtained between the reservoir release temperature and the object temperature. This result demonstrates that it is possible to operate the reservoir in a manner such that the required downstream temperature control can be achieved. One exception, however, must be taken to this general statement. While the test case shows that spillway

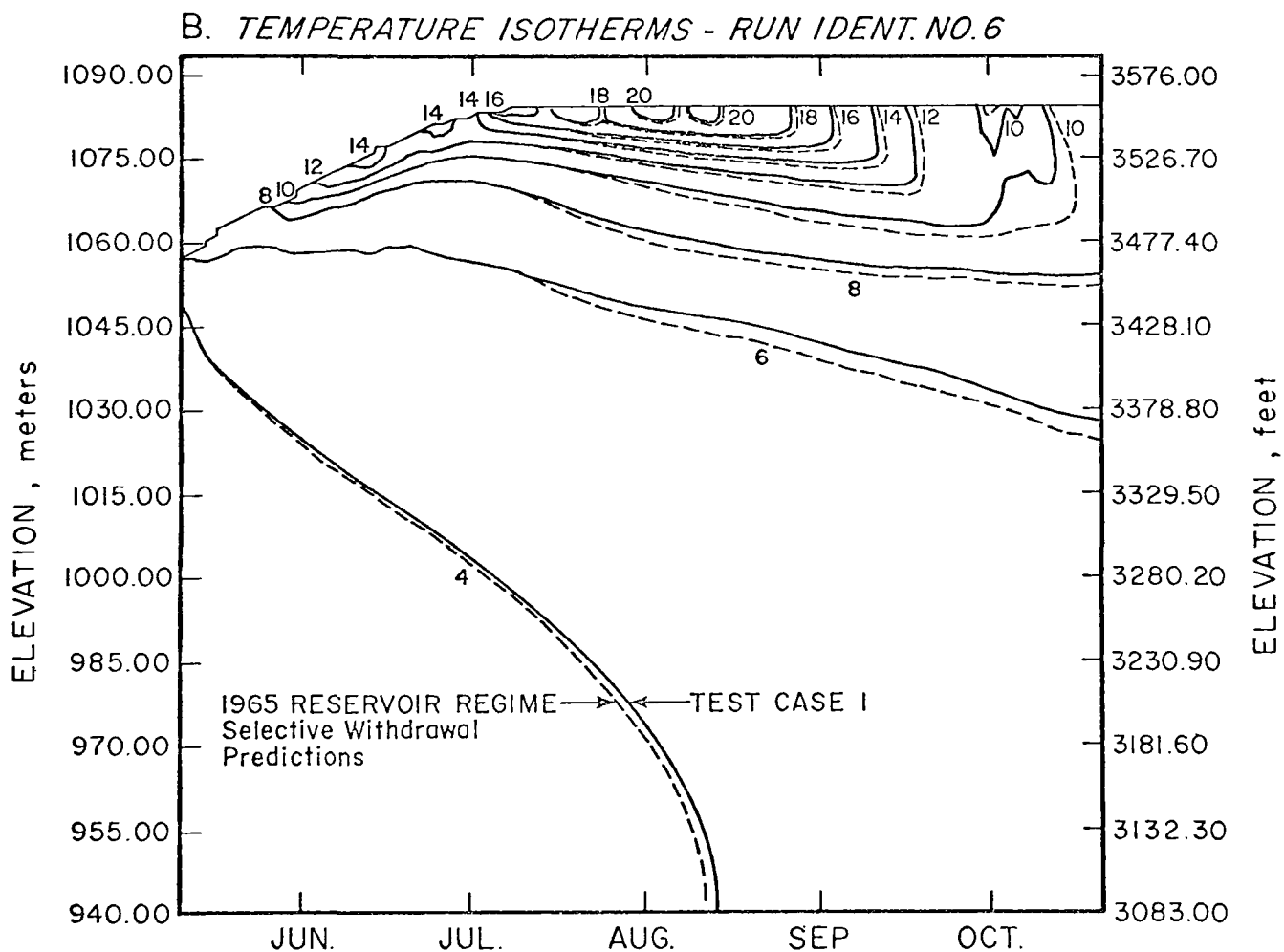
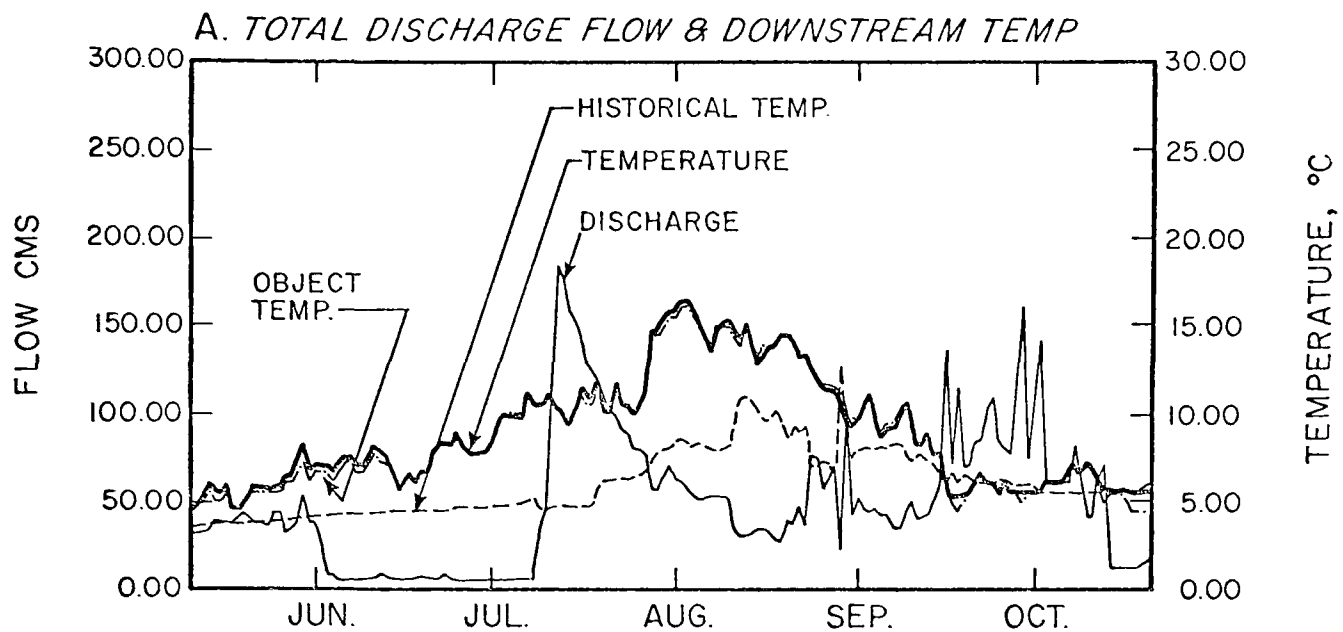


FIGURE 29. Simulated Thermal Regime of Hungry Horse Reservoir 1965, with Modified Reservoir Release Scheme

operation was required in the early part of the summer, this could not have been possible physically, since the water surface was below the spillway crest prior to 24 June. Consequently, in practice, the object temperature would not have been met during the period 11 May to 24 June but rather, the outflow temperature would have been the same as that recorded historically. This exception does not detract, however, from the general result.

Examination of Figure 29-B indicates that changing the operation schedule of the outlets had no significant effect on the thermal regime of the reservoir except to raise slightly the reservoir isotherms toward the middle and end of the simulation period.

To evaluate the magnitude of the power tradeoff required to maintain the object temperature, reference is made to Figure 30 which illustrates the release rate and temperatures of the individual outlets. The outlet at elevation 975 is not shown since it was not operated in this simulation. If the amount of power production is taken as a linear function of the turbine discharge rate, Figure 30 indicates that the hydropower production on a day-to-day basis has been reduced approximately 40 percent from its historical value over the period from 7 July to 27 August; thereafter the percentage loss decreases until by 13 September the loss is insignificant. The loss of revenue from hydropower, as measured in terms of turbine discharge rates, has, so to speak, gone over the spillway. These dollars lost must be weighed against the dollars (and intangibles) gained through re-establishment of the fishery below the dam, and other benefits of downstream temperature control.

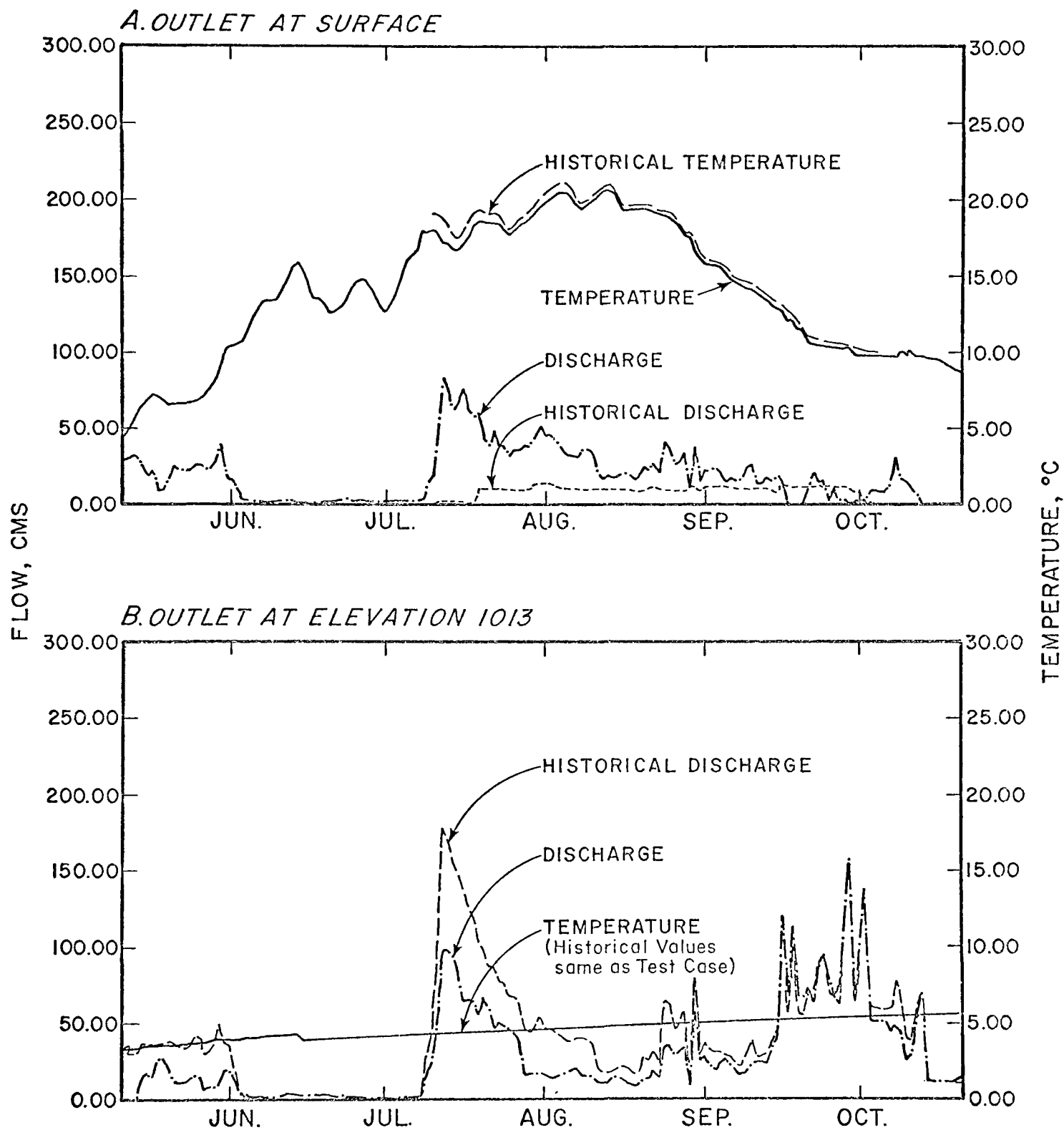


FIGURE 30. Discharges and Discharge Temperatures for Individual Outlets with Modified Reservoir Release Scheme; Hungry Horse Reservoir, 1965

The examination of Figure 30-A reveals that, at the beginning of the high spill period in July, the spill temperature for Test Case I was significantly lower than the historical value, even though the thermal regime of the reservoir was identical during this time for both cases as evidenced by Figure 29-B. This observed phenomenon is the result of applying selective withdrawal theory to the surface outlets and provides the culmination of the discussion in Chapter V which alluded to this Figure. In this case, the withdrawal layer was of sufficient depth (six meters) to produce a net outflow temperature significantly lower than the observed surface water temperature.

TEST CASE II

The second test case was hypothetical in that it was assumed that a second turbine intake was available for power generation. The objective of this test case was to determine if it was possible to distribute the 1965 historical power demand between the two sets of turbines and still achieve the release temperature objective. Consequently, the hypothetical intake was located at elevation 1055 which is the highest elevation at which it could be placed and remain submerged over the simulation period. The results of this simulation are illustrated in Figures 31 and 32. Again, as in Test Case I, the 1965 historical simulation with the selective withdrawal scheme has been overlaid for comparison purposes.

Inspection of Figure 31-A reveals that the object temperature could not be achieved during June, July, and August. While the release temperatures during this period were one to two degrees Centigrade higher than the historical release temperature, they fell from one to six degrees Centigrade below the object temperature. Hence, it is concluded that 1965 power demand and the object temperature could not have been simul-

taneously satisfied with two fixed turbine intake locations. If the power demands were to be met, it appears that a set of multiple intakes would have been required in order to meet the object temperature.

Figure 31-B indicates that the inclusion of a second turbine intake did not significantly alter the thermal regime of the reservoir.

The breakdown of temperatures and discharges through the individual outlets is illustrated in Figure 32. It is apparent from Figures 32-B and 32-C that the reason why the object temperatures could not be met during the summer months was that the reservoir temperature at elevation 1055 was not high enough. Moreover, the only time of the year when the lower turbine intake was required was in the fall when the upper portions of the reservoir were warmer than the object temperature.

The two test cases described above have been demonstrative of the types of analysis which can be performed for re-evaluating the operating rules for existing reservoirs and for aiding in the design of outlet placement in proposed reservoirs. Such analyses (and there are many that could be performed depending upon the particular problem which may be encountered) would not be possible without a tool like the deep-reservoir model. In fact, this is the real value of the model. Its utility lies not in its ability to reproduce historical data but rather in its potential for planning and management through its prediction capabilities

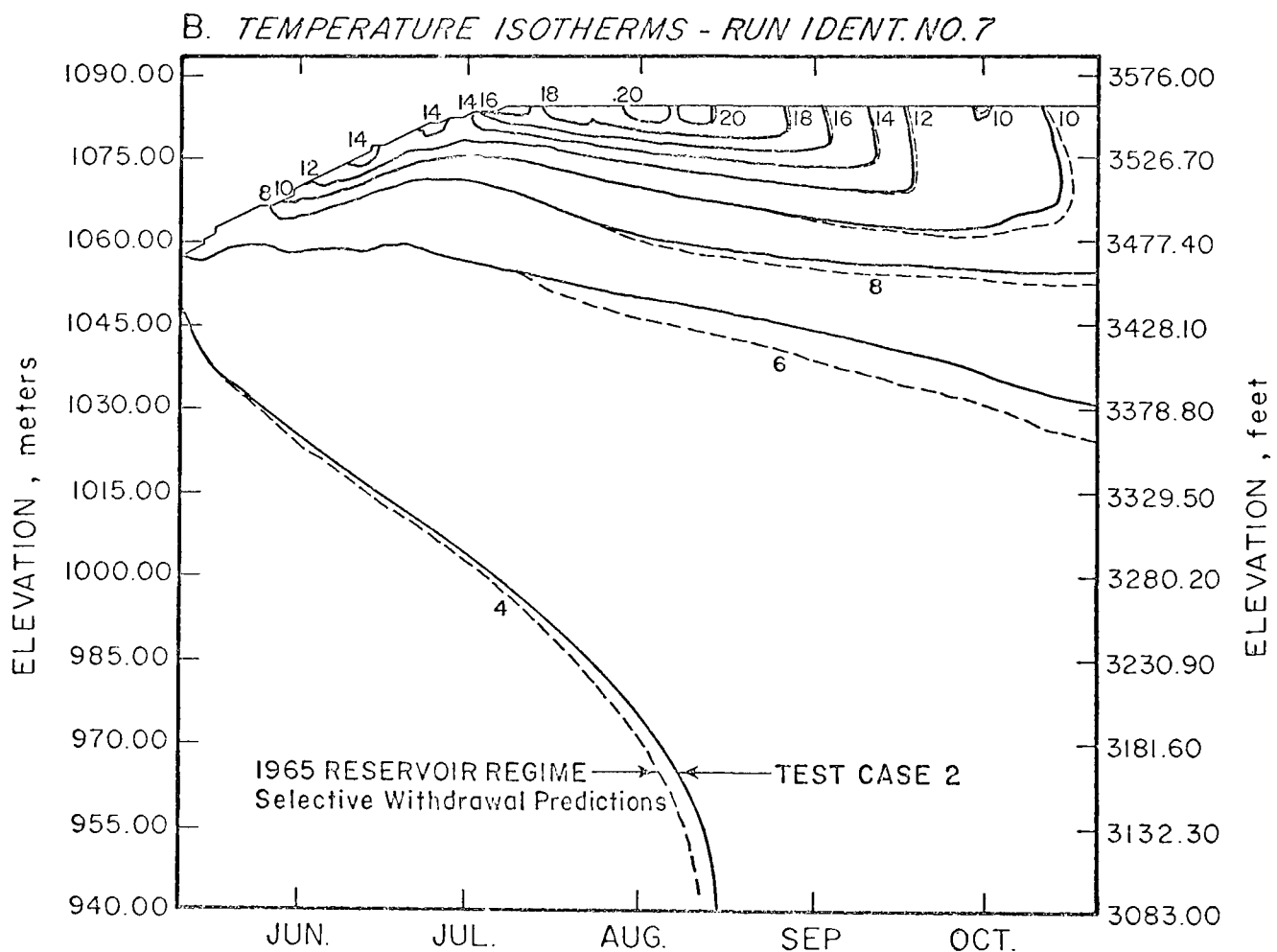
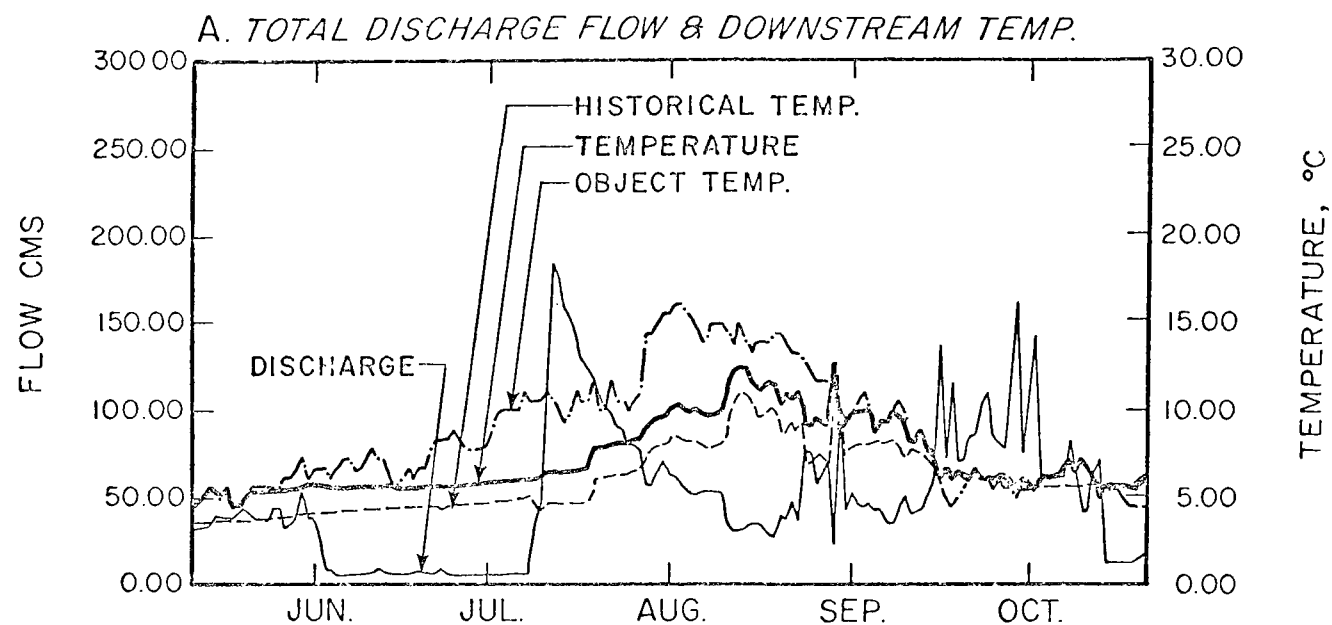


FIGURE 31. Simulated Thermal Regime of Hungry Horse Reservoir, 1965, with Addition of Additional Turbine Intake

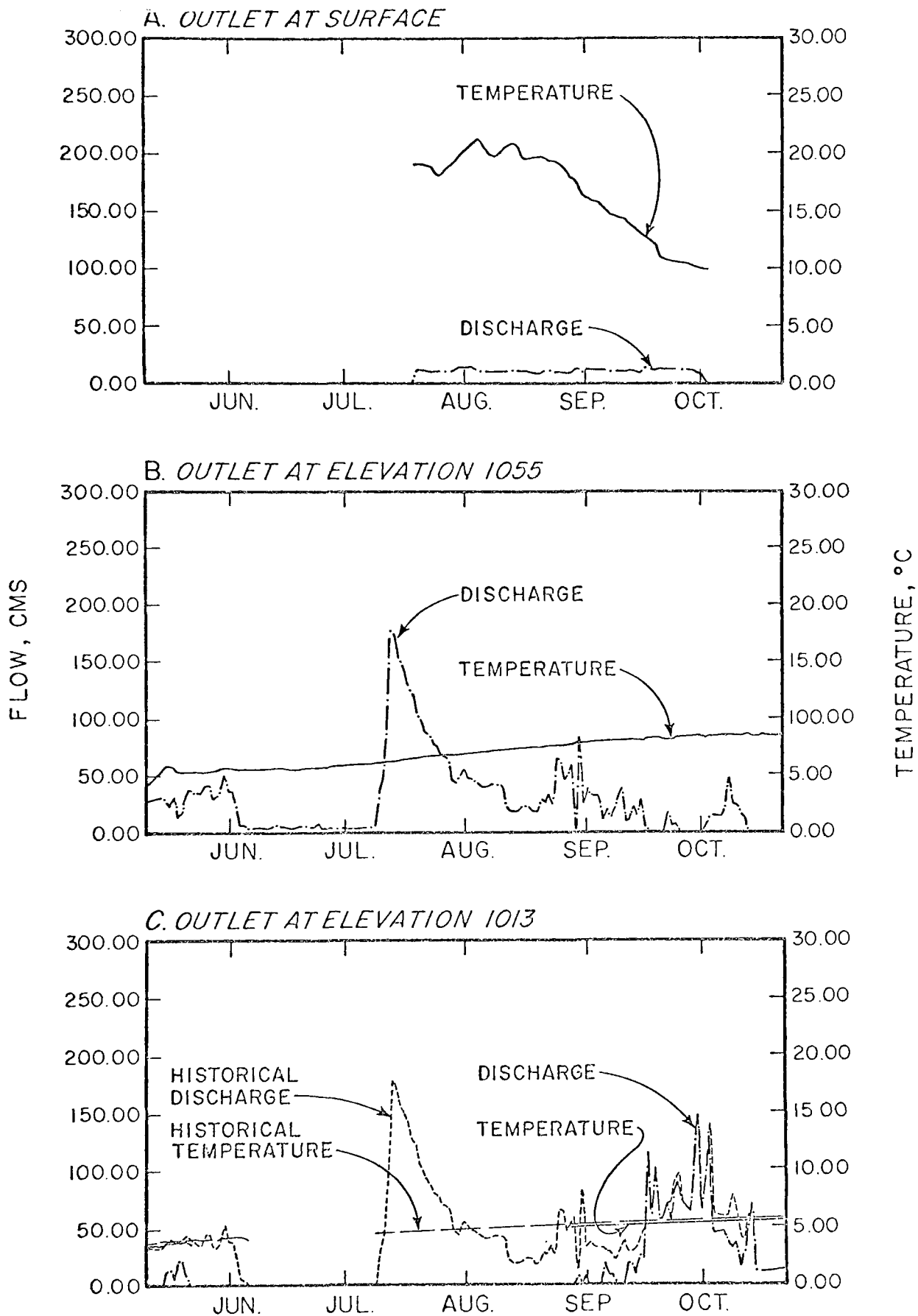


FIGURE 32. Discharges and Discharge Temperatures for Individual Outlets with Addition of Additional Turbine Intake; Hungry Horse Reservoir, 1965

VII. SUMMARY AND CONCLUSIONS

GENERAL

The major accomplishments emanating from the efforts expended in Part I of the research were the incorporation of selective withdrawal theory into the model, as related in Chapter V, and the refined functional description of the eddy conductivity coefficient as given by equation 18. In addition, refining the method for introducing inflows into the model, and the incorporating the minor model refinements as described in Chapter III, have enhanced the operational sophistication of the solution technique. It is felt that these improvements represent a major step forward in generalizing the model's capability to simulate deep reservoirs.

The model, at its present level of development, has essentially eliminated the need for reliance on prototype thermal profiles for evaluating the empirical coefficients in the eddy conductivity function; consequently, its potential as a prediction and design tool for proposed reservoirs has been substantially increased. The two example test cases in Chapter VI served to demonstrate this potential in design as well as to indicate the value of the model for re-evaluating the operating rules of existing reservoirs. Thus, the deep reservoir model, as developed to this point, meets the requirements imposed by objectives 1 and 2 stated

in the INTRODUCTION, and is considered to be adequate for the types of analyses contemplated by the FWPCA Study Team. The supplement to this report supplies pertinent information regarding the operation of the model and the interpretation of its output.

LIMITATIONS

While the deep reservoir model has been significantly generalized and upgraded from its originally derived state, it is not without limitations and these limitations must be omnipresent in the mind of the user if the results of simulation runs are to be properly interpreted. The primary limitation of the model is that it is one-dimensional. While the solution describes a three-dimensional body of water, keeping complete inventory of all water and energy in the system, it permits the internal transfer of heat and mass to occur only along the vertical axis of the reservoir. Such a solution implies that the reservoir properties are constant, or uniform, throughout a horizontal plane. Although this implication is reasonable for the majority of deep reservoir problems of interest, exceptions will be encountered. On the basis of the experience gained through the several applications of the model, these exceptions are expected to occur when the discharge to volume ratio becomes more than about 3 yr^{-1} , or when the reservoir geometry is atypical, e.g. and extremely long reservoir, such as Lake Roosevelt, or a severely branched reservoir with significant inflows in the branches. On terms of the densimetric Froude number as defined by equation 2 in Chapter II, which simultaneously accounts for the discharge volume ratio and the reservoir geometry, the applicability of the model should be questioned if Fr is on the order of 0.1 or greater.

A second limitation is associated with the selective withdrawal theory. The theory, as incorporated into the model, assumes that the reservoir outlets are slots which extend laterally across the face of the dam. The error of this assumption is not known at present; however, the tests on Fontana, Hungry Horse, and Detroit reservoirs, as related in Chapter V, tend to indicate that it is not a serious problem.

Finally, the functional form of the eddy conductivity coefficient must be used with caution until more experience is gained through the application of the model to additional reservoirs. Since time and money constraints limited the developmental investigations to Hungry Horse Reservoir, it was impossible to form generalized functional descriptions for three of the empirical parameters.

The first of these parameters is $A_0(t)$, the value of the eddy conductivity at the water surface as a result of wind mixing. This value is probably a function of the wind speed, wind direction, and reservoir surface geometry. Its value could not be investigated since no wind mixing was observed on the reservoir.

The second parameter is the value b in equation 18-B. While a value was obtained for Hungry Horse Reservoir and is recommended for use at the present time, it is possible that this value could be a function of the turbulence level of the hypolimnion, particularly in reservoirs with larger discharge to volume ratios. Although it is felt that this parameter requires further study, it is believed that the use of the recommended value will not cause misleading conclusions to be drawn in general modeling applications.

The third parameter which was not generalized was the value of $A_H(t)$, the hypolimnetic value of the eddy conductivity. While this parameter was shown to vary with the inflow-outflow relationship in the hypolimnion, the conclusions were too weak to generalize without further study. However, as in the case of the parameter b , the recommended value should suffice as a reasonable approximation until additional investigations on different reservoirs can be conducted.

RECOMMENDATIONS

Notwithstanding the limitations described above, WRE believes that the current version of the deep reservoir model constitutes the most generally applicable model available at the present time for predicting the thermal regime of stratified reservoirs. However, some amount of additional refinement would greatly enhance its prediction capabilities. This refinement is specifically concerned with the generalized definition of the three empirical parameters $A_O(t)$, b , and $A_H(t)$, contained in the eddy conductivity function. To this end, it is recommended that a set of reservoirs be analyzed in order to derive generalized descriptions for $A_O(t)$, b , and $A_H(t)$. The reservoir set should display the following characteristics:

1. Differing geometrical shapes;
2. Various discharge to volume ratios;

3. Wind mixing should be evident in some of the reservoirs; and
4. Each reservoir must have the required complement of data, including thermal profiles, for effecting a "backward" simulation in order to determine observed eddy conductivity coefficients for the reservoir.

The incorporation into the deep reservoir model of generalized expressions for these three parameters would constitute the ultimate development of the model consistent with its one-dimensional limitation.

PART II

SIMULATION OF WEAKLY STRATIFIED RESERVOIRS

VIII. INTRODUCTION

The weakly-stratified reservoir is characterized predominantly by isotherms which are tilted along the longitudinal axis of the reservoir. This tilting results primarily because of the low residence time of the reservoir coupled with a large length-depth ratio for the reservoir, i.e., because of the large Froude number (see Chapter III). The predominant hydraulic phenomenon which affects the degree of tilting is the interflow within the reservoir which possesses sufficient inertia to disrupt the density structure of the reservoir from its static equilibrium state.

As noted in Chapter II, the description of the weakly-stratified reservoir requires that the variation of the reservoir properties be specified in two dimensions; namely in the vertical direction, and along the longitudinal axis of the reservoir. The approach taken herein has been to divide the reservoir longitudinally into several segments and to assume that the heat and mass transfer phenomena within each segment can be described by the deep reservoir model. Thus, the weakly-stratified reservoir is envisioned as a set of deep reservoirs connected in series. Each "reservoir" is coupled

to the one above and below by the requirements for heat and mass continuity within the reservoir as a whole. By solving the vertical temperature distribution in each segment and comparing the profiles of adjacent segments, it is possible to describe the thermal properties of the reservoir in the two required directions.

The idea of longitudinal segmenting is not unique to this model. In particular, Jaske (25), in his recently published model of Lake Roosevelt, has used a segmenting scheme that is nearly identical to the one proposed here. Without going into detail, the basic differences between his model and the model presented here are:

1. the method of handling heat transfer across the air-water interface,
2. the description of the heat and mass transfer between adjacent segments,
3. the formulation of the mechanisms of internal heat transfer in the vertical direction (Jaske hypothesizes molecular diffusion of heat while the WRE model employs a turbulent transfer mechanism), and
4. the numerical solution scheme.

In addition, Jaske's model, in its present state of development, cannot handle a reservoir with fluctuating water surfaces whereas this poses no problem in WRE's model.

In the chapters which follow, the details of segmenting the reservoir and of interfacing adjacent segments with respect to heat and mass transfer are given. The prototype application of the model is demonstrated by a simulation of Lake Roosevelt for the year 1967.

IX. SEGMENTING THE RESERVOIR

NOMENCLATURE

In the following text, reference will often be made to the words *segment* and *element*. *Segment* is used to denote a certain reach in the reservoir. Since the heat transfer characteristics of each segment will be represented by the deep reservoir model, it is necessary to divide each segment vertically into a number of *elements*. These elements are conceptually identical to the elements of the deep reservoir model. Figure 33 illustrates schematically a reservoir divided into segments and elements.

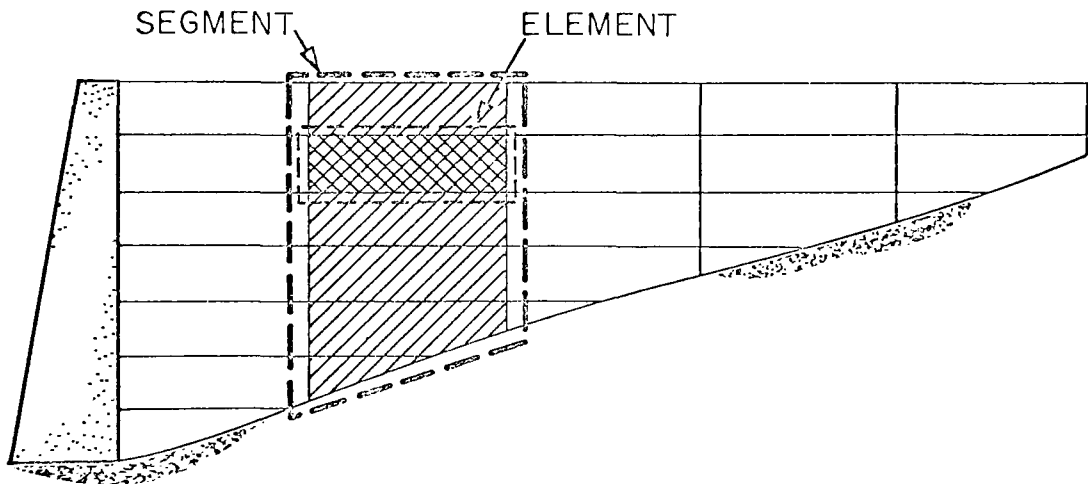


FIGURE 33 Schematic Illustration of a Reservoir Divided Into Segments and Elements

PROCEDURE

The purpose of segmenting the weakly-stratified reservoir is to break it into a set of units each of which can be considered to behave essentially like a deep reservoir, i.e., the isotherms within the segment can be considered to be approximately horizontal. While the decisions regarding the number of segments into which the reservoir is to be divided and the location of the physical boundaries of each segment are primarily subjective, there are at least four criteria upon which these decisions should be based. These criteria are:

1. reservoir geometry;
2. residence time within the segments;
3. points of tributary inflow; and
4. desired longitudinal resolution of the isotherms.

Proper attention to these factors will eliminate much of the guesswork from the segmenting process.

GEOMETRICAL CONSIDERATIONS

It is important for two reasons that a suitable number of reservoir cross sections be available for examination. First, the location of the endpoints of the reservoir segments depends upon the channel geometry; and, secondly, these cross sections will be used later to determine the volume-stage relationship for each segment. Ideally, the sections should be taken at points in the reservoir where there are significant changes in channel geometry, e.g., at narrow points, at wide points, and in bends.

The best modeling will result if the ends of the segments are in straight sections of the channel and are of small cross section since the horizontal flow will be defined best through these sections. The broader sections lying within the segment will be characterized by lower horizontal velocities and are more suitable for representation by the deep reservoir model.

RESIDENCE TIME

The residence time of the reservoir flow within a segment (the volume displacement time) is a very important consideration because, if the residence time is less than the simulation time step, a violation of the necessary conditions for a valid heat budget for the segment can result. Consequently, some estimate must be made of the *shortest* expected residence time within each segment. In general, this event will occur during the peak discharge period. This period of high flows usually occurs before the onset of the stratification period; hence, it can be assumed that the reservoir is in motion over its entire depth and the residence time can be computed as the ratio of the segment volume to the maximum expected daily value of discharge. It should be noted however, that during the stratification period the flow does not generally extend over the entire reservoir depth, but rather is confined to some fraction of the depth. Thus, while the total flow may not be large, if it is sufficiently concentrated within some vertical range of depths, the resulting velocities could be large enough to cause the flow to travel completely through a segment during a simulation time step,

even though the residence time is sufficient for the peak flow period. If this situation is encountered during the simulation runs, the segment lengths can be extended or the simulation time step shortened. In most cases, the latter procedure is the most expedient remedy.

TRIBUTARY INFLOWS

Consideration of the points of tributary inflow in segmenting the model is not critical; however, some consideration of them in the initial segmenting of the model should produce better results. At certain times of the year, an individual tributary, as a result of its temperature or density, may create an interflow in the reservoir at an elevation independent of that of the main body of the flow. This phenomenon is best handled in the model if the tributary is introduced at about the middle of the reach because if it does not enter the reservoir in the region of the mainstream interflow, it may very well experience an internal lateral spreading in the upstream direction as well as downstream.

LONGITUDINAL RESOLUTION OF ISOTHERMS

A fourth consideration in segmenting the reservoir is the resolution that is desired in describing the longitudinal variation in the elevation of the isotherms. Since the deep reservoir model is applied to each segment, there results one temperature at each elevation for each segment. Consequently, the more segments there are in the reservoir, the more resolution is obtained in determining

the position of the isotherms. On the other hand, if the segments are too small, the representation of the segment by the deep reservoir model becomes less accurate; hence, resolution within the segment decreases. The choice of segment size at this point is subjective, however, on the basis of experience with the deep reservoir model, it is felt that the best longitudinal resolution can be obtained, consistent with adequate internal resolution within the segment if the minimum residence times are set up as about one day. This, of course, implies a simulation time step of about one day, the interval that was previously recommended in Part I.

To summarize the segmenting procedure, the most important physical considerations are:

1. placement of the segment ends in narrow straight portions of the channel; and
2. assurance that the residence time of any segment does not exceed the simulation time step interval.

In addition to the guidelines prescribed above, however, technical sagacity is an important asset to the segmenting process, since many of the required decisions are subjective.

X INTERFACING ADJACENT RESERVOIR SEGMENTS

Interfacing as discussed in this chapter is the process of transferring heat and mass between adjacent reservoir segments. In contrast to the reservoir segmenting process, the interfacing is executed internally in the weakly stratified reservoir model and thus, requires no action on the part of the individual. The discussion which follows describes the method of interfacing as programmed into the model.

Since the deep reservoir model, as applied to an individual segment, is one-dimensional along the vertical axis, a horizontal flow distribution is not explicitly defined within the segments. Rather, it is implicitly defined by specifying the flow distribution across the upstream and downstream interfaces. Consequently, it is the interfacing criteria which determines the horizontal flow pattern through the reservoir.

In the absence of a fundamental description of unsteady flow in a thermally stratified impoundment, it becomes necessary to surmise the true nature of the flow on the basis of existing results from steady state theory and experiment. Through such conjecture, it is possible to arrive at several plausible schemes for describing the horizontal flow distribution within the reservoir. The method described here is one of these schemes. While it is by no means a complete answer to the problem, it is believed that the method does provide an adequate description of the horizontal flow through a weakly stratified reservoir.

It has been tacitly assumed that the horizontal flow through the reservoir may be characterized as an interflow, i.e., a flow that is vertically confined between two elevations in the reservoir. The difference in elevations which defines the *thickness* of the interflow is generally less than the reservoir's depth. This assumption is based upon work done by Jaske (26) on Lake Roosevelt and upon theoretical and experimental investigations as reported by Long (27) and Yih (22). Since the location of the interflow and its thickness are governed by momentum forces, buoyancy forces, and the degree of stratification, the interfacing criteria must also reflect these factors. In addition, heat and mass continuity must also be maintained across the interface.

MOMENTUM AND BUOYANCY CONSIDERATIONS

The location of the interflow on the vertical axis of the reservoir is governed jointly by the momentum of the flow and by buoyancy forces. The momentum force tends to propel the fluid along horizontal lines or planes; however, as the interflow travels through the reservoir on this plane, it will experience vertical buoyancy force as a result of the tilted isotherms. The net path which is assumed by the interflow will be determined by the resultant of these two forces.

In an effort to take the buoyancy and momentum forces into account in the reservoir model, it has been assumed that the interflow within a reservoir segment is contained between two horizontal planes, thereby conserving momentum within the segment. At the interface

between adjacent segments, however, there is an abrupt change in the elevation of the interflow. Upon crossing the interface of the upstream segment, it is assumed that the interflow centers itself about the elevation z' in the downstream segment where the temperature is equal to the arithmetic mean temperature of the outflow from the upstream segment. The change in elevation at the interface is a step-wise attempt to account for vertical movement of the interflow as a result of buoyancy forces.

INTERFLOW THICKNESS

The thickness of the interflow is known to be functionally dependent upon the discharge and the degree of stratification; hence, it is a function of the densimetric Froude number. In the absence of a better definition, Debler's criteria as discussed in Chapter V of Part I has been used to evaluate this thickness. Using equation 21, the interflow thickness D can be evaluated as

$$D = 2d = 2(2.04) \left[\frac{Q/w}{2\sqrt{gE'}} \right]^{1/2} \quad (27-A)$$

or

$$D = 2.88 \left[\frac{Q}{w \sqrt{gE'}} \right]^{1/2} \quad (27-B)$$

where Q is the total discharge across the upstream interface of the segment, and w and E are the reservoir width and stability, respectively, at the elevation z' as defined in the preceding paragraph. With the flow spatially centered at z' , the upper and lower elevations bounding

the flow are in general, $z' + \frac{1}{2} D$, and $z' - \frac{1}{2} D$, respectively. Exceptions occur when $z' + \frac{1}{2} D$ is higher than the water surface, or when $z' - \frac{1}{2} D$ falls below the reservoir bottom. In these cases, D remains the same but the interflow layer is shifted up or down as required to contain it within the vertical reservoir boundaries.

MASS CONTINUITY

Mass continuity within the reservoir is maintained as follows: a mass balance is first performed on the reservoir as a whole and the water surface elevations are determined. It is assumed that the water surface is horizontal throughout the reservoir. Given the water surface elevation for each time step, it is then possible to do a mass balance around each segment beginning with the segment farthest upstream and working downstream toward the dam. Given the inflow to the farthest upstream segment as the mainstem river flow, the storage equation is applied and the outflow from that segment is computed. This outflow becomes the inflow to the next segment. The solution is repeated for successive segments until the last segment is reached. Segments with tributaries must include the tributary inflow as part of the total inflow. If the overall mass balance has been done correctly, the outflow computed for the segment abutting the dam will be identically equal to the reservoir outflow.

HEAT CONTINUITY

Since the thickness of the interflow generally will be different on each side of the interface, the temperature distributions will also be different. Approximating the temperature distribution within the interflow as a linear function of the elevation, the temperature distribution of the inflow into the downstream segment can be given as

$$T_i' = m(z_i' - z_0') + b \quad (28)$$

where the primes indicate properties associated with the downstream segment. z_0' is the elevation at the bottom of the interflow zone, and b is defined as T_0 , the temperature of the bottom element within the interflow zone in the upstream segment.

The value of m must be determined in such a manner that heat continuity is maintained across adjacent segments, i.e.,

$$\sum_n \rho c Q_{Ii}' T_i' = \sum_n \rho c Q_{Oj} T_j \quad (29)$$

where Q_{Ii}' is the inflow to the i^{th} element of the downstream segment, Q_{Oj} is the outflow from the j^{th} segment in the upstream element, and n is the number of elements in the interflow zone. As before, the primes indicate properties associated with the downstream segment. If Q is the total discharge across the interface of the adjacent segments, the velocity, u , which has been assumed constant over the interflow zone,

can be defined as

$$u = \frac{Q}{A} = \frac{QL}{V} = \frac{Q_{0j}L}{V_j}, \text{ and} \quad (30-A)$$

$$u' = \frac{Q}{A'} = \frac{QL'}{V'} = \frac{Q_{Ii}'L'}{V_i'} \quad (30-B)$$

where L is the length of the segment, A is the mean cross-sectional area of the interflow zone within a segment, V is the volume of the segment occupied by the interflow zone, and V_i is volume of the i^{th} element in the interflow zone. Solving the right-hand equality of equation 30 for Q_{0j} and Q_{Ii}' gives

$$Q_{0j} = Q \frac{V_j}{V}, \text{ and} \quad (31-A)$$

$$Q_{Ii}' = Q \frac{V_i'}{V'} \quad (31-B)$$

Finally substituting equations 28 and 31 into equation 29, there results the following definition of the slope m :

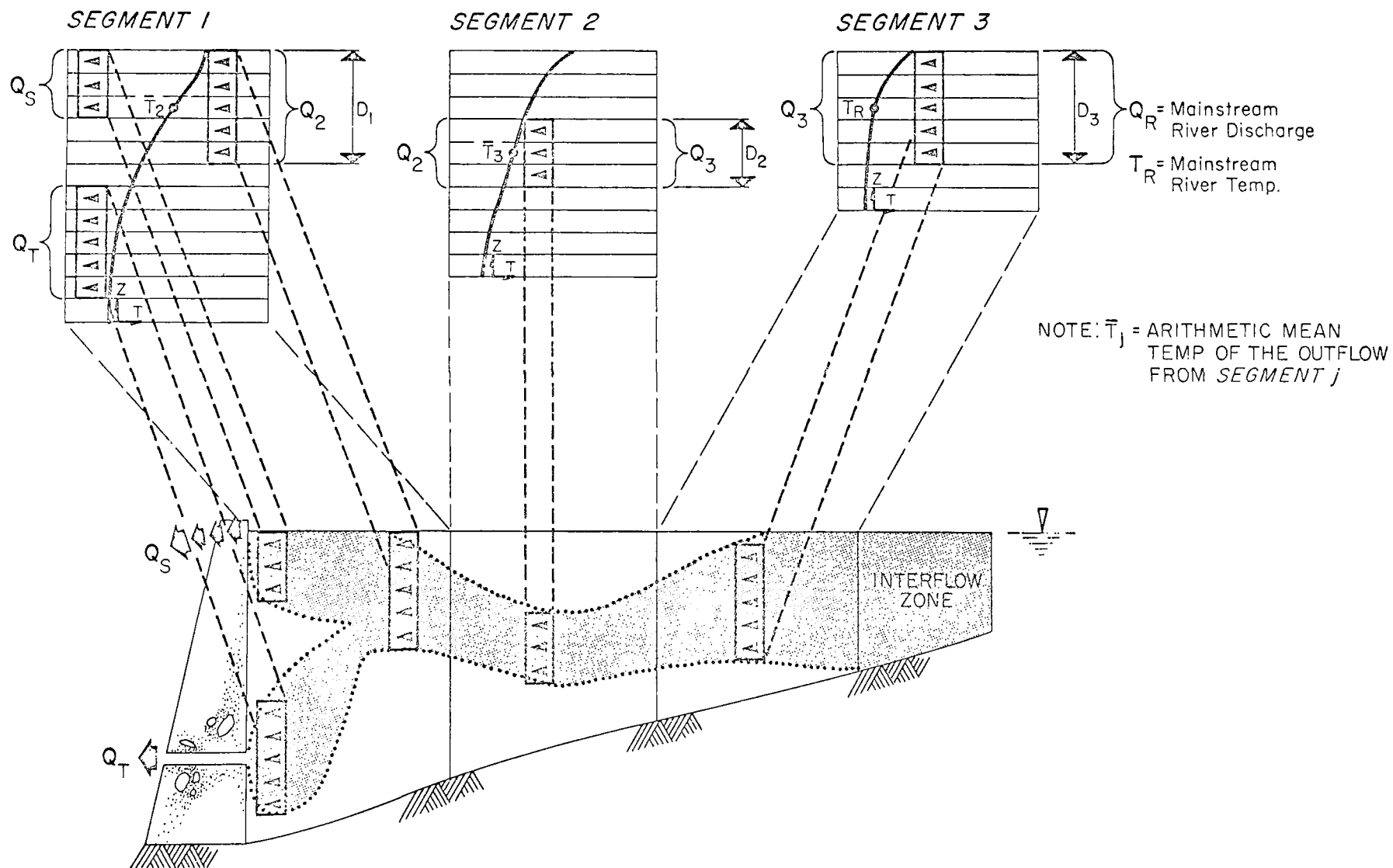
$$m = \frac{\frac{1}{V} \left(\sum_n V_i T_i - T_o \right)}{\frac{1}{V'} \left(\sum_{n'} V_i' z_i' - z_o' \right)} \quad (32)$$

Substituting equation 32 for m in equation 30 and taking the value of b as T_o gives a temperature distribution to the interflow entering the upstream face of a reservoir segment that assures the maintenance of heat continuity across the segment interfaces.

The interfacing criteria as described above is summarized schematically in Figure 34-A for a reservoir with three segments. The assumed relationship between the properties of the segmented model and the prototype is illustrated in Figure 34-B. Note that the interflow zone in Segment 3 is centered vertically at the elevation where the temperature is equal to that of the mainstem. Note also that the outflow from Segment 1 is governed by the selective withdrawal criteria as described in Chapter V of Part I.

Tributary inflows to the segments are accounted for in the heat budget in the following way. If the elevation at which the inflow enters the segment falls within the interflow zone, the flow is added to the total flow at that elevation. If the elevation falls outside the region of interflow, the tributary is then considered as an independent interflow and handled in the same manner as described above. If, at any segment, the two interflow layers coincide, the flows are then combined at that segment and treated as a single interflow through the remainder of the reservoir.

A. MODEL REPRESENTATION



B. PROTOTYPE

Figure 34. Relationship of the Interflow Properties of the Model to Those of the Prototype Reservoir

XI APPLICATION TO LAKE ROOSEVELT

The weakly-stratified reservoir model, as developed in the preceding three chapters, was based on the knowledge that presently exists with regard to the thermal behavior of such water bodies. The test of its validity required that an appropriate prototype reservoir be chosen and simulated. Lake Roosevelt, behind Grand Coulee Dam, was chosen as the test case for the following reasons: 1) the amount of data and its accuracy are the best available; and 2) since this reservoir is the most important weakly-stratified reservoir in the Columbia River System, it is imperative that the FWPCA Study Team has a working model of this reservoir as a part of its Columbia River Thermal Effects Study. The details and results of this simulation are given below.

GENERAL INFORMATION

Lake Roosevelt is located in the mainstem of the Columbia River in Northeastern Washington (see Figure 1). At full pool, this reservoir backs up the Columbia River from Grand Coulee Dam to the

Canadian Border, a distance of nearly 150 miles. The impoundment, which has a usable storage capacity of 5.23 million acre-feet and a total capacity of 9.56 million acre-feet, is used for power development and irrigation. Irrigation water is diverted from the reservoir at Grand Coulee Dam and pumped through a lift of about 280 feet for a distance of two miles into Banks Lake. From there it is distributed through a system of canals to the Bureau of Reclamation's Columbia Basin Project.

As was the case for Hungry Horse Reservoir, time and money constraints required that the period of simulation be limited to a single year. The year 1967 was recommended by the FWPCA Study Team as the period for which the data base was most reliable. The simulation period was further reduced to a length of 76 days since thermal profiles were taken in the reservoir only between 11 July and 25 September of that year. This period is considered adequate, however, since it covers the time from the onset of stratification within the reservoir to a time that is well into the cooling phase of the annual thermal cycle.

PHYSICAL AND THERMAL DATA

A plan view of Lake Roosevelt is shown in Figure 35. From this Figure, it is seen that there were some 92 cross-sections available in the reservoir proper. These sections, which were composited

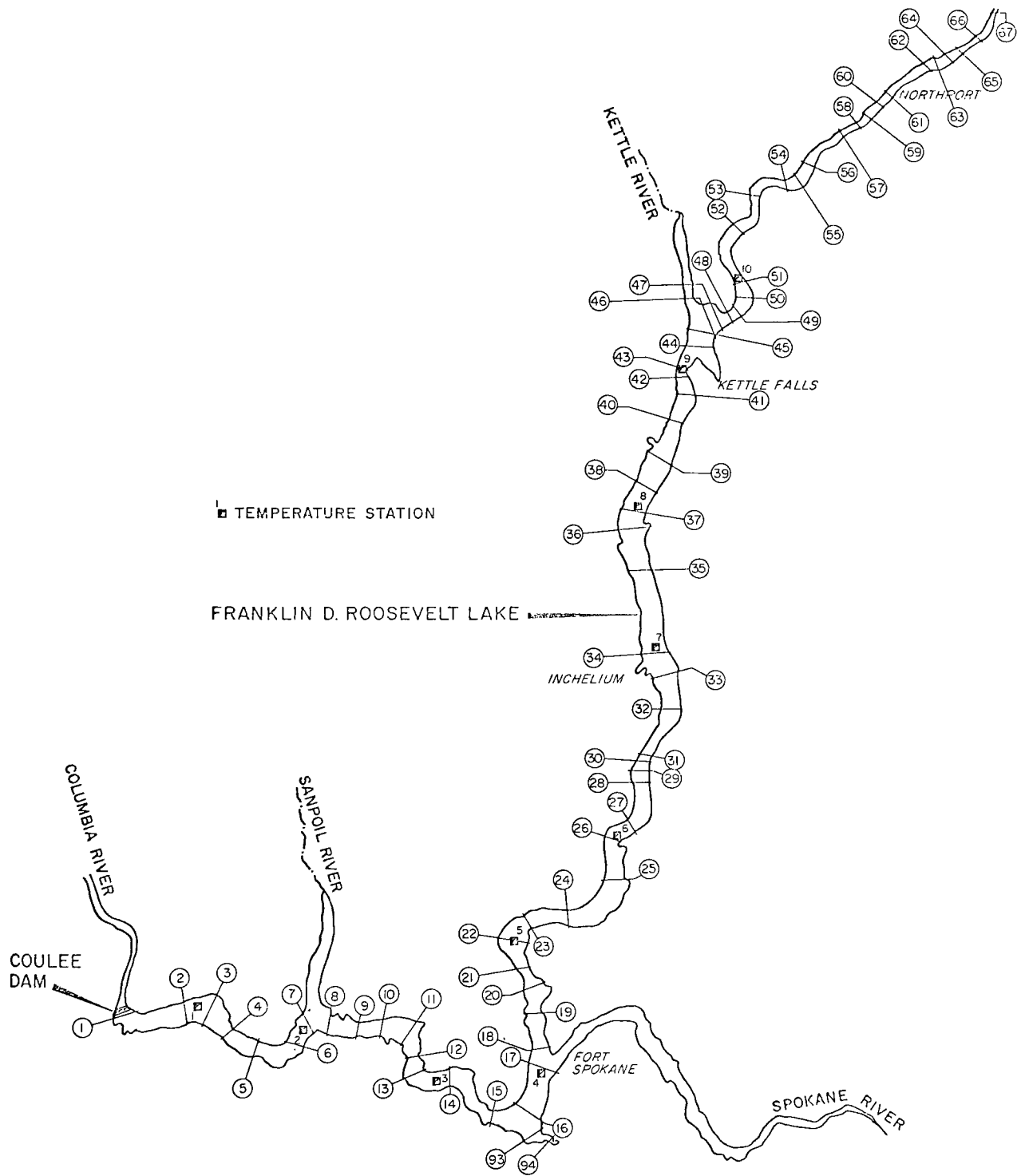


Figure 35. Plan View of Lake Roosevelt

by the FWPCA Study Team from a set of sounding maps, were taken at each reservoir bend and at each point of significant change in channel geometry.

Gaged inflows to the reservoir are the Columbia River mainstem, Kettle River, Colville River (entering at Kettle Falls), and the Spokane River. Ungaged tributaries contribute less than 0.05 percent to the total flow. Additional physical and thermal data were summarized in Table 3. Unfortunately, there were no temperature data on the reservoir outflows; consequently, it was not possible to compare the computed outflow temperatures to observed values.

METEOROLOGICAL DATA

In the absence of meteorological observations at Lake Roosevelt, it was necessary to transpose the data from Spokane, Washington. The use of these point values in the model was equivalent to assuming uniform meteorological conditions to exist over the entire length of the reservoir. While neither the transposition nor the assumption of uniform meteorology is untenable for average daily values of solar radiation and cloud cover, there is some question as to the validity of transposing air temperatures, humidity data, and windspeeds from Spokane to Lake Roosevelt let alone assuming them to be uniformly constant over the entire 150 mile reservoir length. Moreover, the windspeeds taken at Spokane were measured at a distance of 100 feet above the ground. Consequently, it was necessary to

TABLE 3

PHYSICAL AND THERMAL INFORMATION

Lake Roosevelt

PHYSICAL DATA

Location (Grand Coulee Dam): Latitude 47°57', Longitude 118°59'

Elevation: 393 meters (full pool elevation)

Intake Elevations:	Outlet Tubes	285 meters
		316 meters
		346 meters
	Penstock Intakes	318 meters
	Diversion Intake	364 meters

Spillway Type - 504 meter crest with drum gates;
located in middle half of dam.

Elevation of Crest 384 meters

Mean Gaged Inflow:	Columbia River	2785 CMS
	Kettle River	82 CMS
	Colville River	8 CMS
	Spokane River	230 CMS

Average Reservoir Discharge
to Volume Ratio: 8.30 yr⁻¹

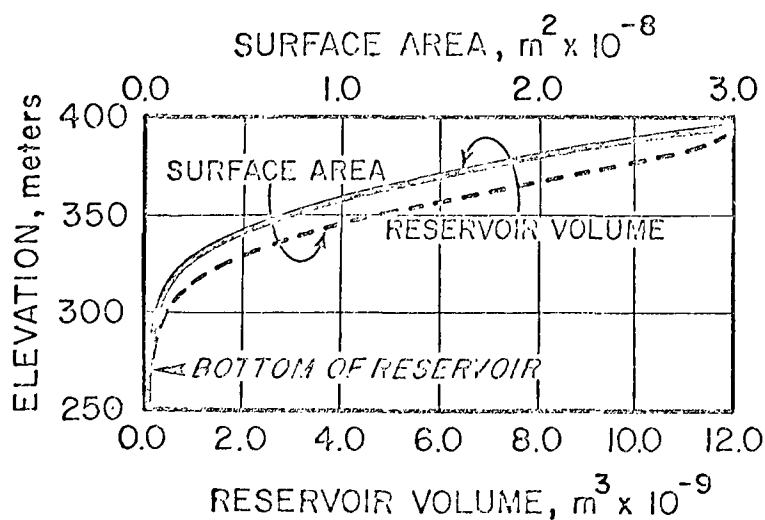


TABLE 3
(Continued)

TEMPERATURE DATA

Reservoir:	Temperature profiles for each of the ten stations shown in Figure 35 at about 7 day intervals.
Tributaries:	Columbia River, mean daily temperature at International Boundary. Kettle River, synthesized mean daily temperature from FWPCA. Colville River, assumed at same temperature as Kettle River. Spokane River, mean daily temperature of the river at Long Lake about 30 miles upstream from Lake Roosevelt.

adjust the evaporation coefficient to a value such that the computed evaporation rates for the reservoir were equal to the average values of evaporation observed in the areas surrounding Lake Roosevelt. This adjusted value was taken as 1.3×10^{-9} mps/mb/mps. The solar radiation extinction coefficient within the reservoir was estimated at 0.691 m^{-1} which gives 99.9 percent extinction at a depth of 10 meters. The extinction depth was based on secchi disk measurements of 10 meters that were taken in the reservoir.

SEGMENTING THE RESERVOIR

Following the guidelines established in Chapter IX, Lake Roosevelt was divided into six segments as illustrated in Figures 36 and 37. The downstream faces of the segments were located in narrow and, as often as was practical, in straight sections of the reservoir channel. The compromise in placing the interfaces in straight portions of the channel was necessitated by residence time considerations.

Residence times for each segment are given in Table 4. It is observed that the minimum residence time in Segment 6 is less than one day, which is not particularly desirable, since it is less than the recommended simulation time step. There are two solutions to this situation as previously stated in Chapter IX: 1) increase the reach length; or 2) decrease the simulation time step. In this instance, however, neither of these steps was taken for the following reasons. First, as seen in Figure 36, Segment 6

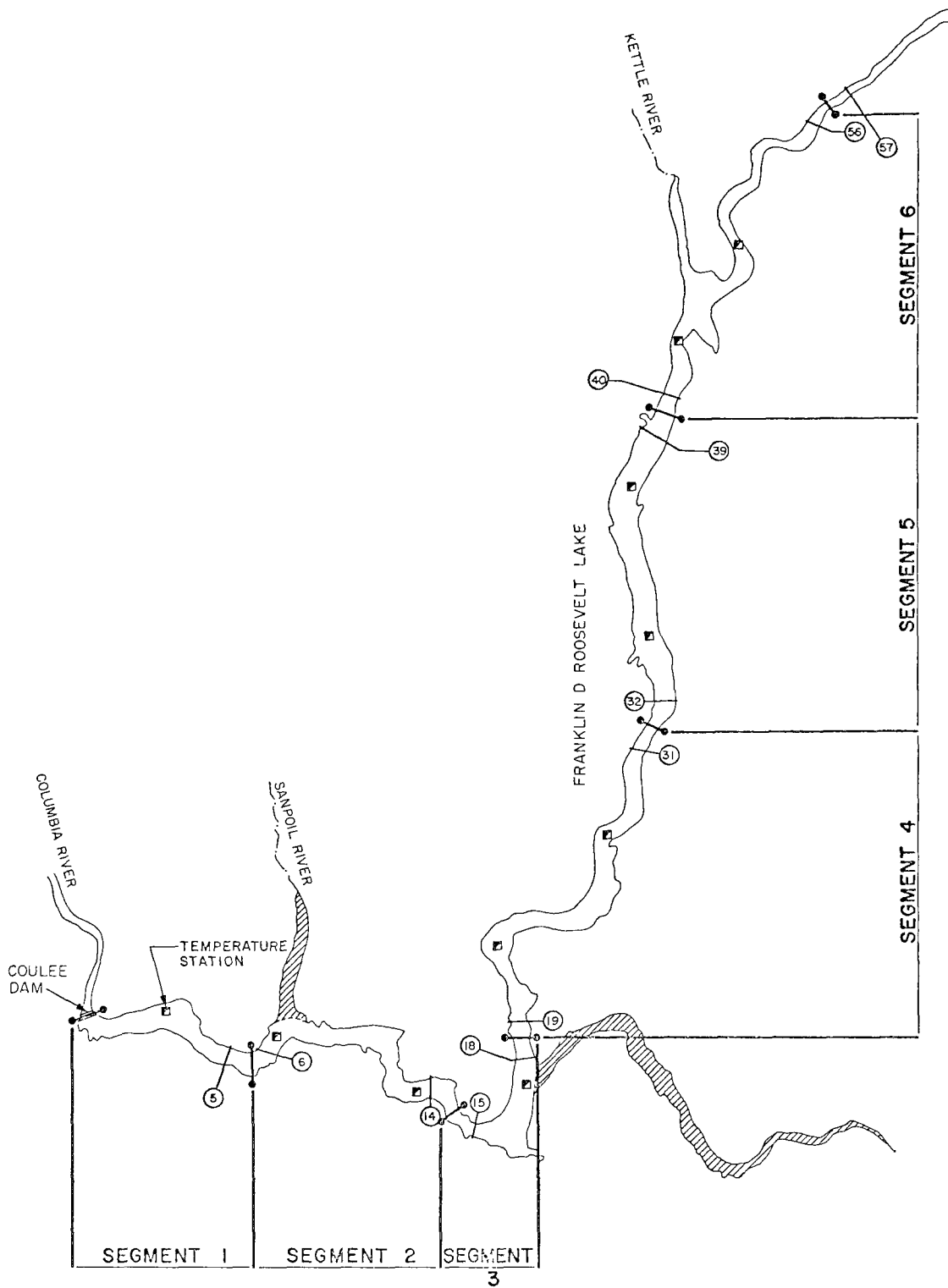


Figure 36. Plan View of Lake Roosevelt as Segmented for Simulation Model

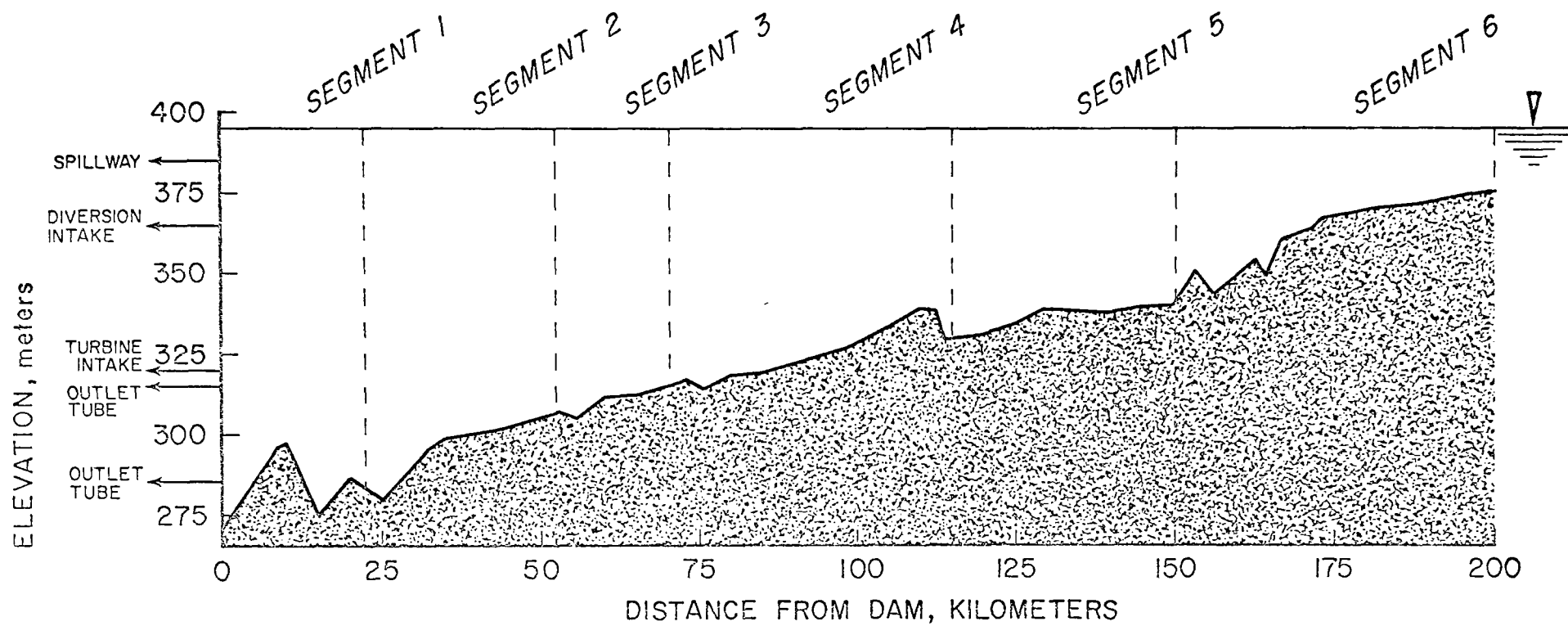


Figure 37. Reservoir Segments in Profile View, Lake Roosevelt

is already quite long (≈ 27 miles); to increase its volume sufficiently to give a minimum residence time of one day would require the reach length to be extended another 50 percent. Such a reach would be too long to be realistically modeled. Second, the peak discharge period occurs about the middle of June which is prior to the onset of stratification. Hence, the small energy budget violations which occur during this period are not serious. By the end of June when stratification begins to set in, the reservoir discharge has decreased to a value such that the residence times are greater than one day.

TABLE 4
RESIDENCE TIMES FOR INDIVIDUAL SEGMENTS
IN LAKE ROOSEVELT

SEGMENT	RESIDENCE TIME, days		
	average	maximum	minimum
1	7.4	26.0	1.9
2	8.1	28.6	2.1
3	5.0	17.6	1.3
4	8.7	30.5	2.3
5	7.6	26.8	2.0
6	3.2	11.1	0.8

Since the reservoir above station 57 is essentially completely mixed, it was not explicitly included in the simulation. Rather, the temperature changes through this upper reach were determined by the

FWPCA Study Team through the application of their river-run model between the Canadian border and station 57. The temperatures thus predicted at station 57 were used as the input temperatures to Segment 6.

Referring again to Figure 36, note that the Sanpoil and Spokane arms of the reservoir have not been included as part of their appropriate segments. The reason for excluding these arms is that the model simply includes their properties as being a part of the properties of the main channel. This, of course, alters the characteristics of the interflow through these segments. If it is felt necessary to include such arms in the simulation, they should be considered as separate reservoir segments and should be interfaced to their appropriate segments in the main channel. Such a refinement was not considered necessary in this simulation since previous studies on the reservoir have indicated that these arms do not significantly affect the thermal structure of the main body of the reservoir. Consequently, the Sanpoil arm is completely unaccounted for in the simulation. The Spokane arm is also neglected; however, the Spokane River is introduced as a tributary to Segment 3 using the temperatures and discharges recorded at Long Lake.

SIMULATION RESULTS

For each of the reservoir segments shown in Figures 36 and 37, the volume-stage and area-stage relationships were determined from cross-section data. The thermal regime of the Lake Roosevelt was then simulated over the 77 day period from 11 July through 25 September 1967. As with the deep reservoir model, the performance of the weakly-stratified reservoir model was judged on the basis of its ability to reproduce the observed temperature profiles in the reservoir. Typical results for four days during the simulation period are illustrated in Figure 38 which shows the computed and observed profiles for each reservoir segment, the elevation of the isotherms along the longitudinal axis of the reservoir, and the position of the flowing layer within the reservoir. Note that there were two observed profiles in Segments 2, 4, and 5.

GENERAL OBSERVATIONS

A comparison of the observed and computed temperature profiles in Figure 38 indicates that the model simulates, quite well, the general progression of the thermal events in Lake Roosevelt, and that it does, in fact, produce tilted isotherms. The only outstanding discrepancy between the simulated results and those observed in the prototype is that the reservoir tends to cool too rapidly toward the end of the simulation period (see Figure 38-D). Even so, over the 77 day simulation period, the maximum deviation of the computed temperature from those observed was 2.6 °C; the average deviation for the period was less than 1.3 °C.

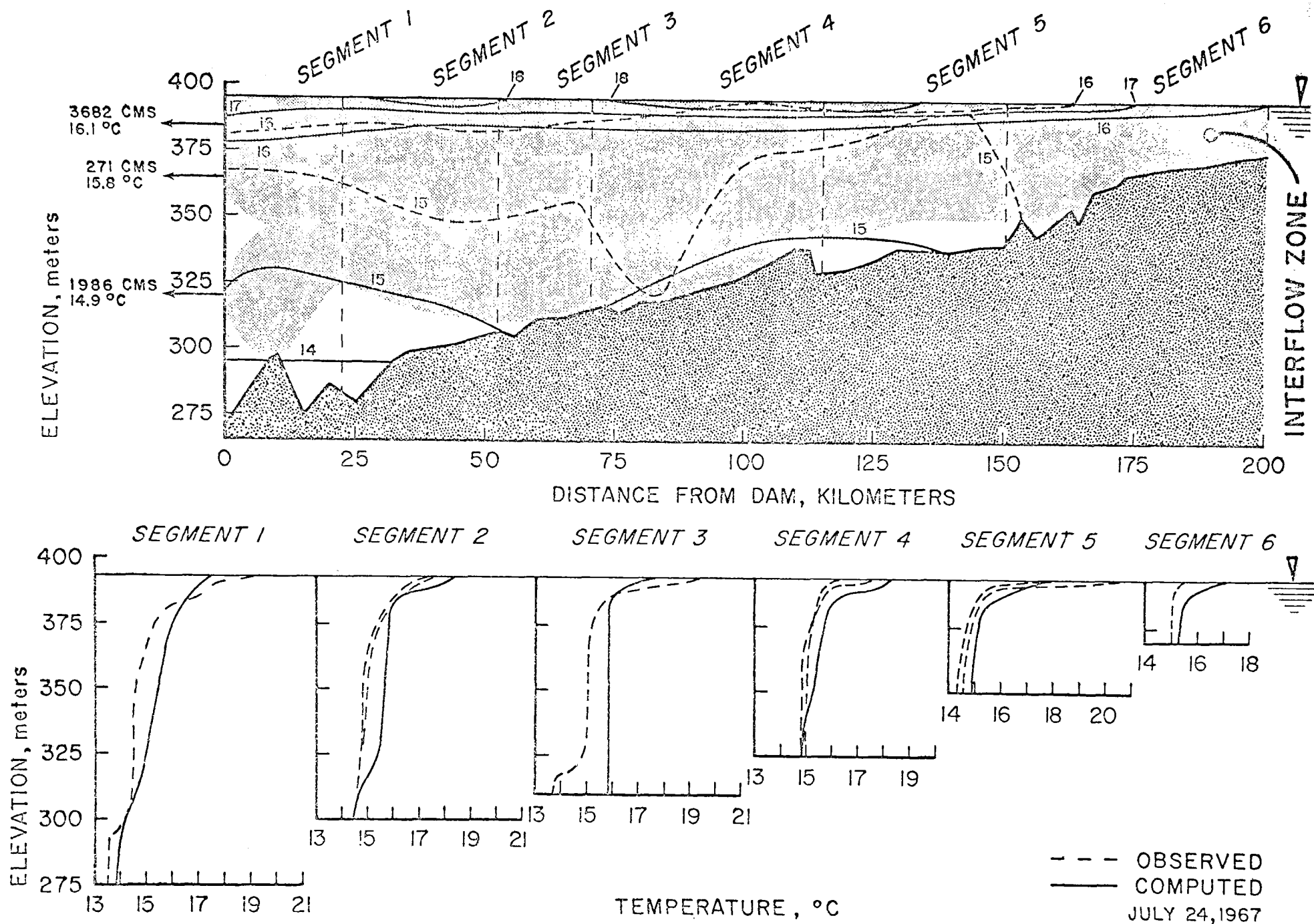


Figure 38-A. Typical Results from Simulation of the Thermal Regime of Lake Roosevelt, 1967

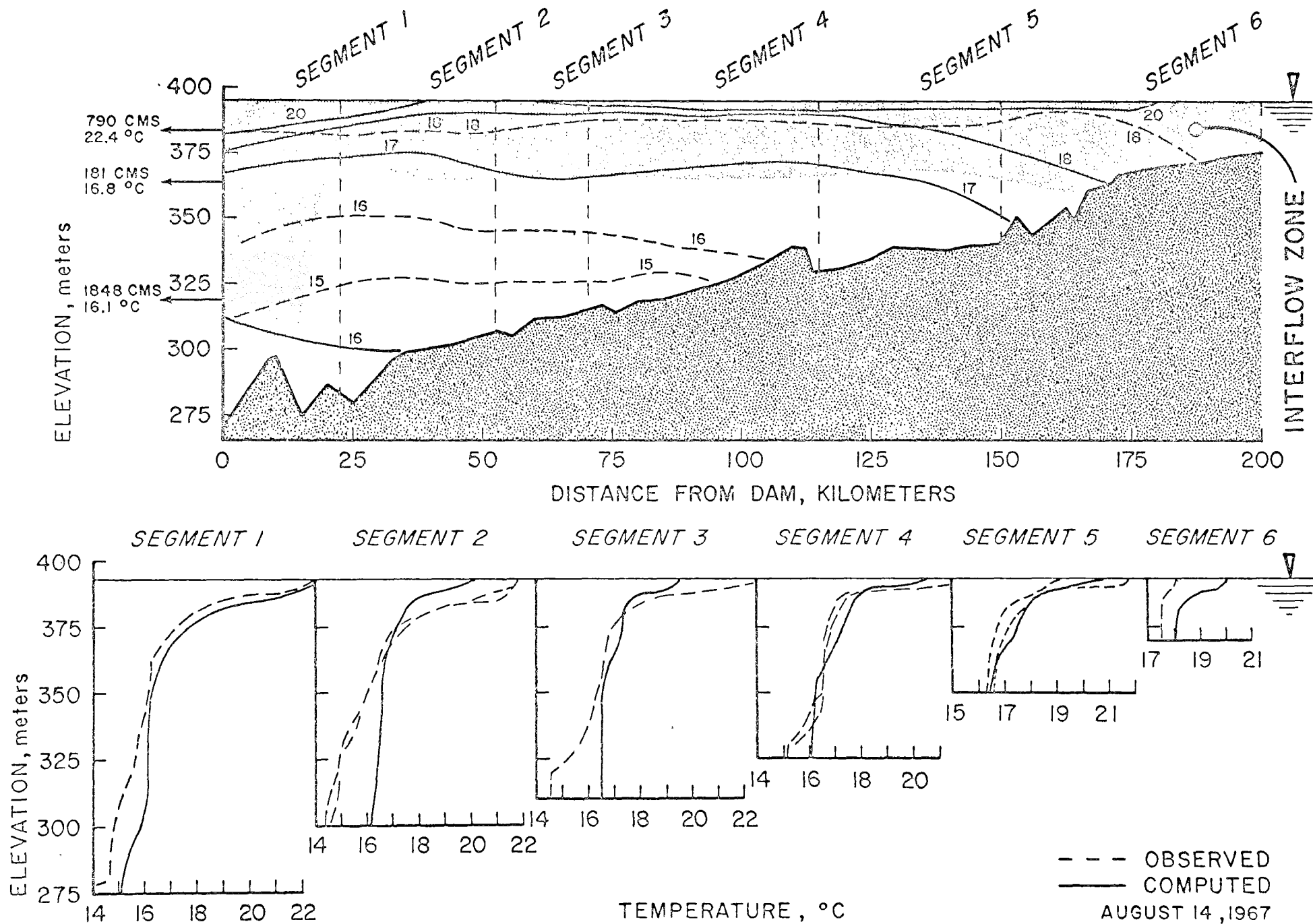


Figure 38-B. Typical Results from Simulation of the Thermal Regime of Lake Roosevelt, 1967

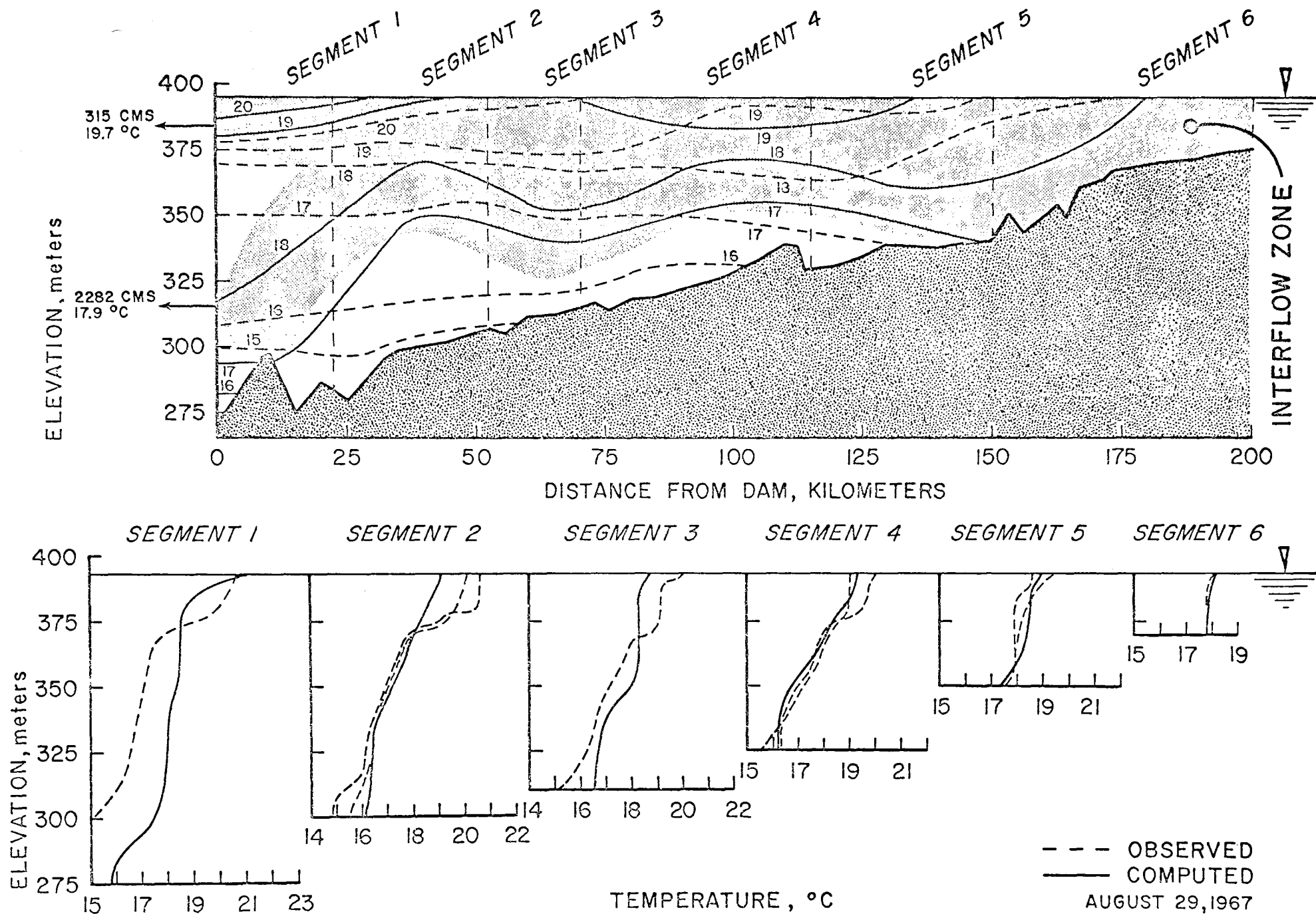


Figure 38-C. Typical Results from Simulation of the Thermal Regime of Lake Roosevelt, 1967

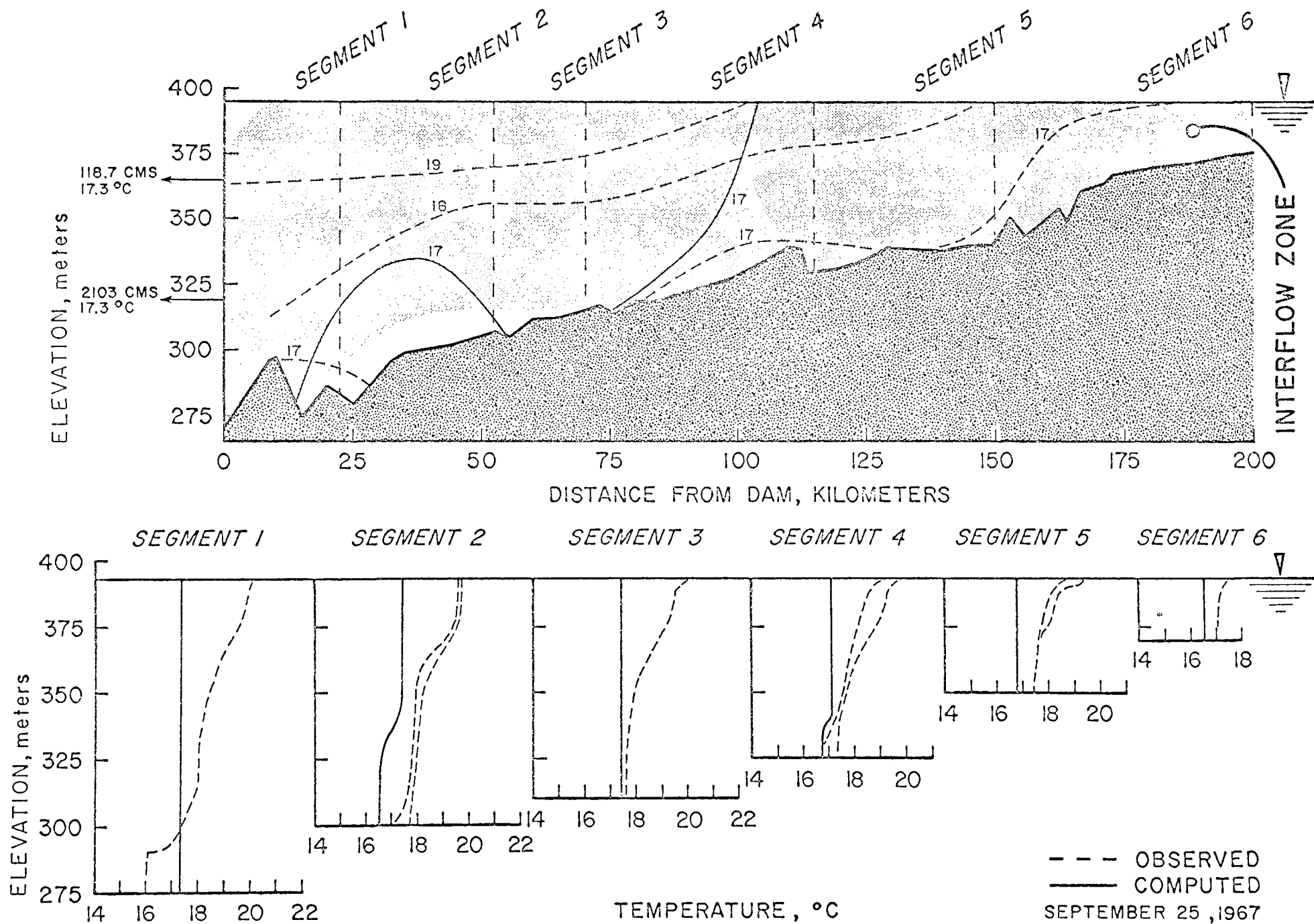


Figure 38-D. Typical Results from Simulation of the Thermal Regime of Lake Roosevelt, 1967

The behavior of the reservoir interflow during the simulation period is interesting. Referring again to Figure 38, it is observed that during July, when the temperature gradients are small, the flowing layer extends over most of the reservoir depth. As the intensity of the reservoir stratification increases, the bottom of the flowing layer moves progressively higher in the reservoir until it assumes the position indicated on 14 August. Thereafter the reservoir begins to cool and the bottom of the flowing layer begins to move downward as observed on 29 August. Finally in late September the intensity of the stratification has become sufficiently weak so that the flowing layer once more extends over the total reservoir depth. This is a rather important phenomenon because it indicates that during the period when the reservoir surface layers are the warmest, this surface water is being drawn off and discharged through the outlets. Consequently, the release temperatures from the reservoir would be expected to be significantly warmer than the mean temperature in a horizontal plane at the elevation of the reservoir outlet. According to Jaske (26) this phenomenon was, in fact, observed during the 1963 operation of the Columbia River Cooling Program undertaken by the Hanford Operation.

Finally, it is noted that the Spokane River (which, except for the mainstem, is the largest tributary inflow to the reservoir) did not appear as a separate interflow at any time during the simulation period. Segment 3 was purposely made small in order to account for this phenomenon should it occur; however, the river temperature was such that the tributary always entered the reservoir at an elevation contained within the primary interflow zone.

SPECIFIC OBSERVATIONS

In comparing the computed and observed profiles, one should be aware that the computed profiles are constructed from the average daily values of temperatures on horizontal planes within the segment while the observed profiles are composed of instantaneous point values. As a result of the unsteady nature of the reservoir on an hour to hour basis (outlet operation, internal waves, lateral temperature variations, diurnal surface heating and cooling, etc.), the instantaneous observed profiles may be expected to deviate from their average daily values by 0.5 °C in the reservoir depths and by 1 to 2 °C at the surface. While these deviations are not an important consideration when comparing profiles at some distance below the water surface, they are quite significant when comparing surface temperatures. Since the reservoir profile measurements were taken during the day, it is reasonable to expect that the observed surface temperatures are somewhat higher than the average daily surface temperature. Allowing for this amount of variability in the observed surface temperatures, it is surprising how closely the computed and observed values compare, especially when it is recalled that point meteorological data, measured at Spokane, was assumed to apply over the entire reservoir.

The examination of the computed and observed profiles for the several reservoir segments revealed that there was often a temperature difference of 1.5 to 2.0 °C in the profiles near the bottom of Segments 1, 2, and 3. Several examples of this behavior can be seen in Figure 38. It is now thought that this deviation resulted from neglecting the effect of the Spokane arm of the reservoir in the model simulation. As the reservoir interflow warms, there is a significant quantity of cold water stored in this arm that flows

out through the reservoir mainstem and is replaced by the warmer water of the interflow. Neglecting to account for this cold water outflow is equivalent to short circuiting the main reservoir interflow through Segment 3. Consequently, the simulated rate of heating downstream is greater than that observed in the prototype. Unfortunately, there was insufficient time to thoroughly investigate this problem; however, some studies of a very preliminary nature indicated that if the volume properties of the Spokane arm are lumped together with those of Segment 3, the simulation of the lower portions of the temperature profiles in Segments 1, 2 and 3 would be improved.

Another feature of the simulation which requires discussion is the accelerated cooling in the fall of the year. This behavior, which can be observed in Figure 38-D, actually starts sometime between 5 and 12 September, and is thought to occur for one or more of the following reasons: 1) the simulated rate of heat loss through the air-water interface is too large; 2) the present method of describing the velocity and temperature distribution of the interflow is incorrect; or 3) the storage effect of the Spokane arm is not taken into account. Again time restricted the amount of effort which could be devoted to this problem; however, on the basis of one of the test runs, some insight was gained on possible ways to decrease the simulated rate of cooling.

In order to acquire a better understanding of why the simulated rate of reservoir cooling was greater than that observed in the prototype, a test run was executed in which the convective mixing (mixing that results when negative temperature gradients form in the reservoir)

was suppressed. Figure 39 shows a typical shape of the resulting profiles. It is readily apparent that heat is being lost through the air-water interface; hence, it was most logical to suspect that this simulated heat loss rate was too large; i.e., the meteorological data was incorrect. However, a check of the reliability of the data by the FWPCA Study Team resulted in nothing suspicious. Moreover, the success with which the surface temperatures were modeled during the warming period inspired confidence in the reliability of the data during the cooling period. Thus, the possibility of bad meteorological data was discarded as a consideration.

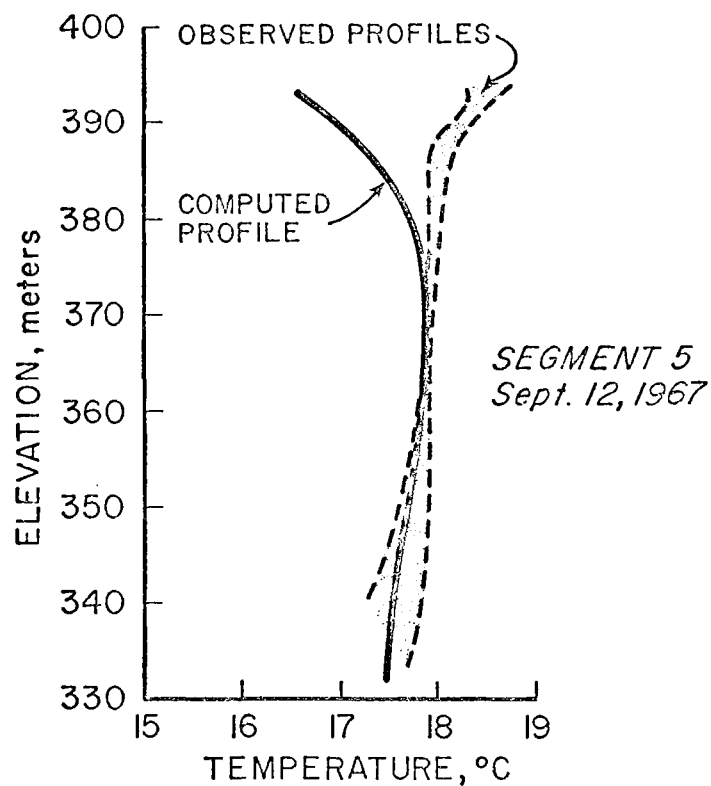


FIGURE 39. Typical Shape of Computed Temperature Profile during Cooling Period when Convective Mixing is Suppressed

A second, and more probable, explanation of the cooling phenomena is the manner in which the temperature is distributed through the interflow as it crosses the segment interfaces. It was assumed that this distribution is linear. However, if it is not linear, the effect of the linearization is to displace heat from the reservoir surface to a lower depth as seen in Figure 40. The net result is to induce artificial surface cooling. Rather than linearize the temperature profile the actual profile should be used; however, as noted in Chapter X, this is a more difficult task and requires additional bookkeeping which was not required in the linearization scheme.

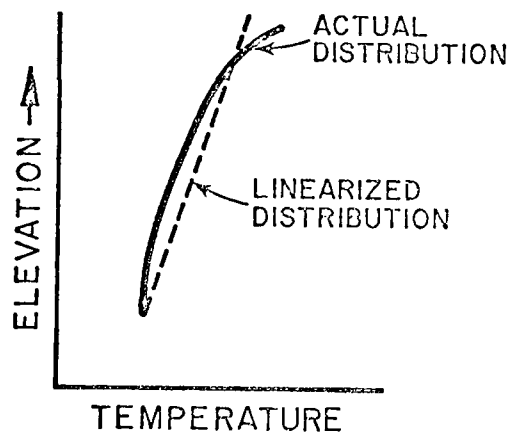


FIGURE 40. Effect of Linearization on the Temperature Distribution of the Interflow

A third possible explanation for the observed cooling involves consideration of the horizontal velocity distribution within the interflow. As presently developed, it is assumed that the velocity distribution is uniform in the interflow zone and zero outside of this zone. If the simulated reservoir velocities are larger near the surface than in the prototype, an excessive amount of surface heat will be carried out of the reservoir by longitudinal advection. This additional heat loss, coupled with the loss of surface heat to the atmosphere, would produce an accelerated cooling rate. A recent report by Jaske (25) contains actual measurements of the velocity profile in Lake Roosevelt during 1967. These measurements indicate that the horizontal velocity in the reservoir near the surface is significantly lower than that observed deeper in the interflow zone. The incorporation of such a velocity distribution into the model would significantly decrease the cooling rate. Unfortunately, this data was not available at the time when the reservoir model was being developed; consequently, the uniform velocity distribution was assumed due to the lack of a more suitable definition.

Finally, the short-circuiting through Segment 3, which results from neglecting the Spokane arm, is thought to contribute to the accelerated cooling in Segments 1, 2 and 3. The effect of neglecting this arm in the fall is just the opposite of that which results from neglecting it in the spring. As the Columbia River cools, there is a significant amount of warmer water in the Spokane arm that is replaced by the cooler Columbia River flow and flows out through the reservoir mainstem. Neglecting this storage effect causes the cooler water to arrive at the lower reaches of the reservoir too early in the fall,

thereby causing Segments 1, 2, and 3 to cool more rapidly in the model than in the prototype. Unfortunately, there was insufficient time to investigate this phenomena, even in a preliminary way.

REMARKS

On the basis of the results from the 1967 test simulation, it is believed that, on the average, the weakly-stratified reservoir model can simulate the temperature regime of Lake Roosevelt within 1.5 °C of the true values; however, deviations as high as 2.6 °C might be expected during fall cooling. As such, the model is considered to be adequate for the types of analyses contemplated in the FWPCA Columbia River Thermal Effects Study except possibly during the period of cooling when its adequacy is judged as marginal.

If the accuracy of the model during the fall cooling portion of annual temperature cycle is judged acceptable, the model can be used for simulating the annual thermal cycle of the reservoir within the confidence limits specified above. Moreover, several years may be simulated in succession without concern over the possibility of carryover error in the heat budget from year to year since the Columbia River discharge is sufficient to completely displace the old reservoir water between the end of the fall cooling cycle and the onset of warming the following spring.

If efforts are made to improve the model during the cooling period, it is suggested that the description of the temperature profile of the interflow at the interface between adjacent segments be refined

first, since of all the probable factors contributing to the accelerated cooling in the model, it is thought that linearizing the temperature profile of the interflow is probably the most significant. Secondly, the effects of the Spokane arm should be investigated in more detail. It is thought that the effects of this arm can be adequately represented if its volume-stage characteristics are simply lumped together with those of Segment 3. Finally, the velocity distribution of the interflow is considered to have the least influence on the rate of cooling. Consequently, it is suggested that this refinement be given the lowest priority in further development of the model.

XII SUMMARY AND CONCLUSIONS -- PART II

GENERAL

The weakly-stratified reservoir model as developed and tested in the preceding four chapters was based on the assumption that a weakly-stratified reservoir can be visualized as a series of deep reservoirs. Adjacent "reservoirs" are coupled to one another by the requirement for conservation of heat and mass in the reservoir as a whole. The longitudinal flow in the reservoir was considered to be a density current the thickness of which was determined by Debler's criteria. The vertical placement of the interflow was established on the basis of its mean temperature and the elevation at which that temperature existed in the reservoir.

A test of the model on Lake Roosevelt over a 77 day period from 7 July through 25 September 1967 showed that, in general, the model simulated with reasonable accuracy the thermal regime of the reservoir; however, some difficulties were encountered in simulating the reservoir during the period of cooling in September.

On the basis of the test case related in Chapter XI, it is concluded that the weakly stratified reservoir model, as developed herein, is adequate for the types of analyses contemplated in the FWPCA Columbia River Thermal Effects Study, except during the period of cooling in the fall of the year. During this period, the adequacy of the model is considered marginal. Preliminary studies indicate, however, that a refinement of the temperature distribution in the interflow zone should significantly improve the model's capability to simulate the fall cooling period.

On the basis of evidence gathered through the test runs on Lake Roosevelt, it was concluded that the Spokane arm of the reservoir does affect the thermal regime of the reservoir and that a better representation of the temperature profiles near the reservoir bottom in Segments 1, 2, and 3 could be obtained if the storage effect of the Spokane arm was accounted for in the model. In addition, inclusion of the storage effect should improve the simulation during fall cooling although the extent of the improvement is not known.

RECOMMENDATIONS

At this juncture, it might be well to point out that the conclusions drawn concerning the applicability and limitations of the weakly-stratified reservoir model have been derived from observation of the results of a simulation of Lake Roosevelt over a single 77 day period. While it is believed that these observations and the resulting

conclusions are basically valid, it is strongly recommended that the first priority in FWPCA's use of the model be the simulation of Lake Roosevelt for different years (preferably two or three) during which internal temperature measurements are available. These simulations would serve to establish additional confidence in the model and to confirm its weaknesses as pointed out above.

Assuming the weaknesses noted in Chapter XI are confirmed and that it is desired to improve upon the accuracy of the model in its present form, the following steps are recommended:

1. Include the Spokane arm in the reservoir by simply lumping its volume-stage characteristics with those of Segment 3. This step is recommended first since it is the simplest to do. If simple inclusion of the volume-stage relationship improves the simulation in Segments 1, 2, and 3, it should be retained. If not, it should be dropped and further investigation deferred until after the refinement of the temperature distribution of the interflow.
2. The description of the temperature distribution of the interflow as it enters the upstream face of a segment should be reformulated to reflect more precisely its actual distribution. It is believed that this refinement would, at least, make the accuracy of the model during fall cooling consistent with that over the remainder of the year; in addition, it is also expected that the simulation would be improved over the entire year.

3. The velocity distribution of the interflow zone should be reformulated on the basis of the information that has recently become available on Lake Roosevelt (25). This refinement, however, is presently rated as a low priority since it is not thought that a better description of velocity distribution would significantly improve the model's accuracy.

CAVEAT

Since the weakly-stratified reservoir model was developed from general concepts and theory, it should be applicable to any reservoir falling within the weakly-stratified reservoir class as defined in Chapter II. However, the only test which has been made of its validity is the simulation of Lake Roosevelt as reported herein. Hence, its general applicability remains to be proven through the simulation of several other reservoirs of the weakly-stratified class. Subsequent to the establishment of its general applicability the model could then be used with confidence as a planning and analysis tool for proposed reservoirs and for reservoirs having insufficient thermal data for verification purposes.

XIII LIST OF REFERENCES

1. "Water Temperature; Influences, Effects and Control," Proc., 12th Pacific Northwest Symposium on Water Pollution Control, U.S.P.H.S., Corvallis, Oregon, 7 November 1963.
2. Klein, L., *River Pollution II. Causes and Effects*, Butterworths, London, 1962.
3. Hutchinson, E. G., *A Treatise on Limnology*, Vol. 1, Geography, Physics, and Chemistry, John Wiley and Sons, Inc., New York, 1957.
4. Wurtz, C. B., and Renn, C. E., "Water Temperature and Aquatic Life," Department of Sanitary Engineering and Water Resources, The Johns Hopkins University, June, 1965.
5. McKee, J. E., and Wolf, H. W., "Water Quality Criteria," State Water Quality Control Board, Sacramento, California, Publication No. 3-A, 1963.
6. Laberge, R. H., "Thermal Discharges," *Water and Sewage Works*, Vol. 106, December, 1959, p. 536.
7. Hynes, H. B. N., *The Biology of Polluted Waters*, Liverpool University Press, Liverpool, 1960.
8. Collins, W. D., "Temperature of Water Available for Industrial Use," U. S. Geological Survey Water Supply Paper 520(f), U. S. Govt. Printing Office, Washington, D. C.
9. Sylvester, R. O., "Effects of Water Uses and Impoundments on Water Temperature," Proc., 12th Pacific Northwest Symposium on Water Pollution Research, Corvallis, Oregon, 7 November 1963, p. 6.

10. Churchhill, M. A., "Effects of Density Currents in Reservoirs on Water Quality," *Journal of Water and Sewage Works*, 30 November 1965.
11. "A Ten Year Hydro-Thermal Power Program for the Pacific Northwest," Bonneville Power Administration, Portland, Oregon, January 1969.
12. "Summary Report on Nuclear Power Plant Siting in the Pacific Northwest for Bonneville Power Administration," Battelle Memorial Institute, Pacific Northwest Laboratories, Richland, Washington, 1967.
13. "The Treaty with Canada for Joint Development of the Columbia River," Bonneville Power Administration, Portland, Oregon, 1 December 1965.
14. "A Proposal for Formulation of a General Mathematical Model for the Prediction of Thermal Energy Changes in Impoundments," Presented to the Federal Water Pollution Control Administration Thermal Effects Project, by Water Resources Engineers, Inc., Walnut Creek, California, 7 May 1968.
15. "Prediction of Thermal Energy Distribution in Streams and Reservoirs," Prepared for the Department of Fish and Game, State of California, by Water Resources Engineers, Inc., Walnut Creek, California, Revised Edition, 30 August 1968.
16. "Applications of Mathematical Models for Prediction of the Thermal and Quality Behavior of Lake Washington," Prepared for the Washington Pollution Control Commission by Water Resources Engineers, Inc., Seattle, Washington, November, 1968.
17. Neuman, G., and Pierson, W. J., Jr., *Principles of Physical Oceanography*, Prentice-Hall, Inc., Englewood Cliffs, New Jersey, 1966.
18. Richardson, L. F., "Some Measurements of Atmospheric Turbulence", *Phil. Trans. Roy. Soc., A*, Volume 221, London, 1920.
19. Yih, C-S., "On the Flow of a Stratified Fluid," *Proc.*, 3rd U. S. National Congress of Applied Mechanics, 1958.
20. Debler, W. R., "Stratified Flow into a Line Sink," *Journal of the Engineering Mechanics Division*, ASCE, Vol. 85, EM3, July 1959.

21. Brooks, N. H., and Koh, R. C. Y., "Selective Withdrawal from Density Stratified Reservoirs," Preprint from Proceedings of ASCE Specialty Research Conference on "Current Research into the Effects of Reservoirs on Water Quality," Portland, Oregon, 22-24 January 1968.
22. Yih, C.-S., *Dynamics of Non-Homogeneous Fluids*, The Macmillan Co., New York, 1965.
23. Craya, A., "Theoretical Research on the Flow of Non-Homogeneous Fluids," *La Houille Blanche*, 1949.
24. Duncan, W., Harleman, R. F., and Elder, R. A., "Internal Density Currents Created by Withdrawal from a Stratified Reservoir," A Cooperative Study, Tennessee Valley Authority and U. S. Corps of Engineers, Norris, Tennessee, February 1962.
25. Jaske, R. T., A Three Dimensional Study of Parameters Related to the Current Distribution in Lake Roosevelt, Battelle Memorial Institute, Pacific Northwest Laboratory, Richland, Washington, April 23, 1969.
26. Jaske, R. T. and Snyder, G. R., "Density Flow Regime of Franklin D. Roosevelt Lake," *Journal of the Sanitary Engineering Division*, ASCE, Vol. 93, SA3, June 1967.
27. Long, R. R., "Velocity Concentrations in Stratified Fluids," *Journal of the Hydraulics Division*, ASCE, Vol. 88, HY1, January 1962.

APPENDIX A

MATHEMATICAL MODELS FOR THE PREDICTION OF THERMAL ENERGY CHANGES IN IMPOUNDMENTS

GRAPHICAL OUTPUT ROUTINES FOR OUTPUT FROM PROGRAM TSIP

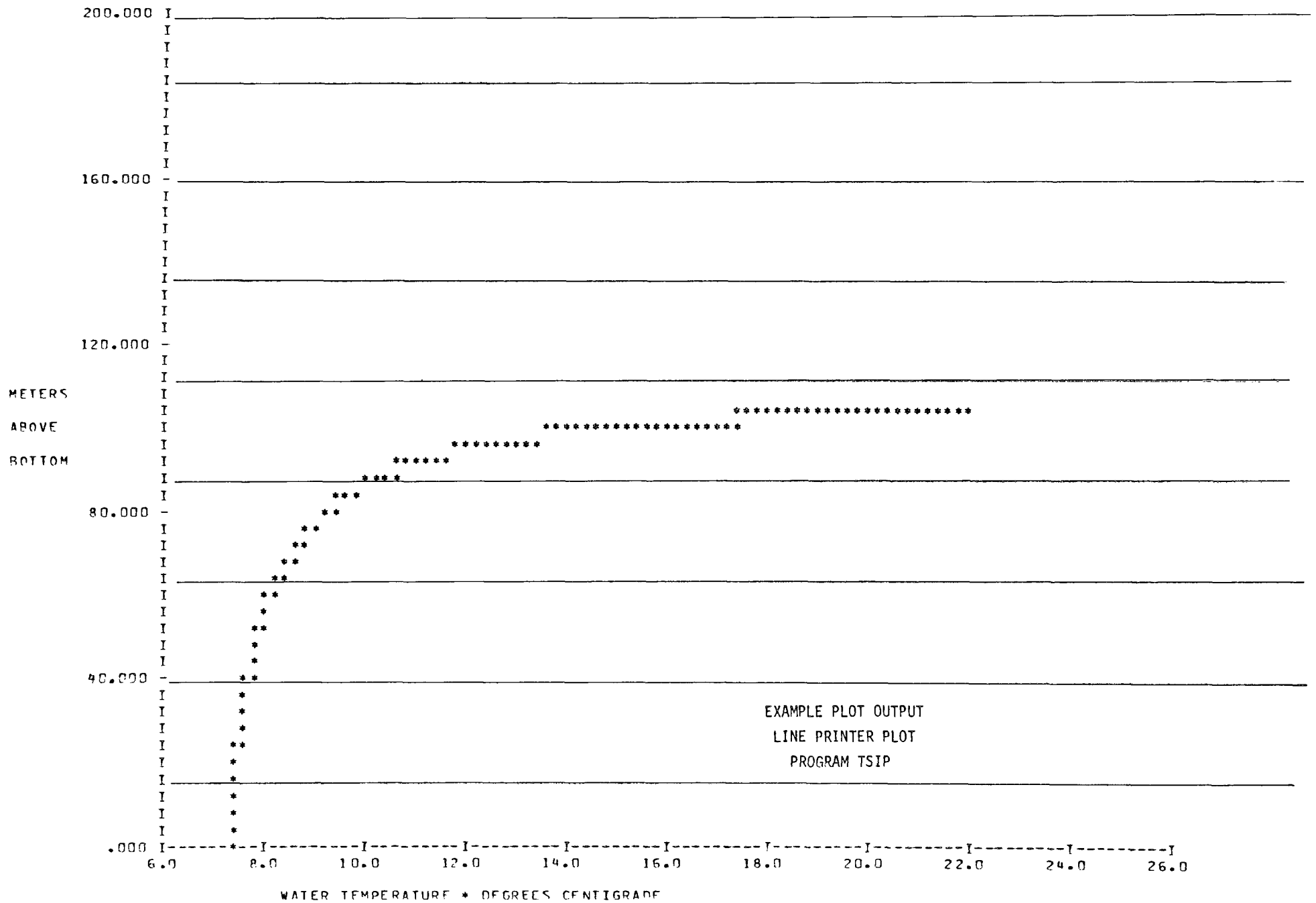
INTRODUCTION

In an effort to enhance the interpretation of the output from program TSIP, two graphical output routines have been included as a part of the computer software package. The first of these routines generates, on the computer system's line printer, a plot of segment temperature vs. depth. This display is produced for each day that printed output is requested. The second output routine, which is a complete and separate program, is programmed to produce pen plots of segment temperature vs. depth for specified days, as well as plots of the temperature and flow of the reservoir system's downstream releases. The pen plots are written for the Calcomp plotting system, and one must have access to such equipment in order to use these routines. The details and requirements for use of these routines are given on the following pages.

LINE PRINTER PLOT

The printer plot will produce a temperature vs. depth plot for each segment for each day that printed output is requested from program TSIP. These plots are produced automatically, and no changes in program input are required for their production. An example of the format of this plot is shown on the next page, and a FORTRAN listing of the plot producing routines is included on subsequent pages. At the present time this plotting routine is included as an integral part of program TSIP. If machine storage requirements become critical to the implementation of TSIP, these routines can be removed without any adverse effects on the actual thermal simulation procedure. The only reference to these routines is the call to SUBROUTINE CURVE from the output section of SUBROUTINE SUBB.

TEMPERATURE VERSUS DEPTH FOR JULIAN DAY 210



FORTRAN PROGRAM LISTINGS
Printer Plots for Program TSIP
Listings for Subroutines

1. CURVE
2. PINE
3. PLOT
4. SCALE
5. LABD

```

SUBROUTINE CURVE(X,Y,NPT,NCV,NPLOT)
DIMENSION X(203,1),Y(203,1),NPT(1)
COMMON/LAB/ TITLE(18),XLAB(11),YLAB(6)
1,HORIZ(20),VERT(6)
C ***** CURVE IS THE ENTRY TO A GENERALIZED PRINTER PLOT ROUTINE. THE
C ROUTINE PLOTS SEQUENTIALLY PAIRED VALUES TAKEN FROM THE X AND
C Y ARRAYS. THE SCALING VALUES FOR BOTH ARRAYS ARE STORED IN THE
C LAST TWO ARRAY LOCATIONS IN THE SAME MANNER AS CALCOMP SCALING.
C
C THE ARGUMENTS IN THE CALLING SEQUENCE ARE DEFINED BELOW...
C
C X...THE ARRAY CONTAINING THE X AXIS COORDINATES OF THE
C POINTS TO BE PLOTTED.
C
C Y...THE ARRAY CONTAINING THE Y AXIS COORDINATES OF THE
C POINTS TO BE PLOTTED.
C
C NPT...THE NUMBER OF POINTS TO BE PLOTTED.
C
C NCV...THIS VALUE IS ALWAYS ONE (1).
C
C NPLOT...USED FOR PLOT IDENTIFICATION, THIS VALUE IS
C PRINTED ABOVE EACH PLOT FOR EACH CALL TO CURVE.....
C
NPTS=NPT(1)*NCV
C
C SET UP X AND Y SCALES
C
AXLEN=10.
CALL SCALE(X,AXLEN,NPTS,1)
AXLEN=5.
CALL SCALE(Y,AXLEN,NPTS,1)
C
C FORM X LABELS AND FACTORS
C
XMIN=X(NPTS+1,1)
DELT X=X(NPTS+2,1)
XLAB(1)=XMIN
DO 260 I=1,10
260 XLAB(I+1)=XLAB(I)+DELT X
XSCAL=100./(XLAB(11)-XMIN)
C
C FORM Y LABELS AND FACTORS
C
YMIN=Y(NPTS+1,1)
DELT Y=Y(NPTS+2,1)
YLAB(6)=YMIN
DO 270 I=1,5
270 YLAB(6-I)=YLAB(7-I)+DELT Y
YSCAL=50./(YLAB(1)-YMIN)
C
C INITIALIZE PLOT OUTLINE

```

```

      NCD=100
      CALL PPLOT(D,D,NCD,NPLOT)
      K = 1
C
C
C          DRAW IN EACH CURVE
      DO 450 L=1,NCV
        IF(NPT(L).EQ.0) GO TO 440
C
C
C          JOINING XO YO AND XT YT
      XO=XSCAL*(X(1,L)-XMIN)
      YO=YSCAL*(Y(1,L)-YMIN)
      NPOINT = NPT(L)
      DO 400 N = 2,NPOINT
        XT = XSCAL*(X(N,L) - XMIN)
        YT = YSCAL*(Y(N,L) - YMIN)
        CALL PINE(XO,YO,XT,YT,K,NPLOT)
        XO = XT
        YO = YT
      400 CONTINUE
      420 CONTINUE
      440 K = K + 1
      450 CONTINUE
C
C
C          OUTPUT FINAL PLOT
      NC=99
      CALL PPLOT(D,D,NC,NPLOT)
      RETURN
      END

```

```

SUBROUTINE PINE(X1,Y1,X2,Y2,NSYM,NCT)
  AXA=X1
  AXB=X2
  AYA=Y1
  AYB=Y2
  N=1
  IF (ABS(AXB-AXA).LT.ABS(AYB-AYA)) GO TO 290
C
C   SET PARAMETERS FOR X DIRECTION
C
  IF (AXB.GT.AXA) GO TO 245
  AXA=X2
  AXB=X1
  AYA=Y2
  AYB=Y1
245 CONTINUE
  IXA=AXA+.5
  IXB=AXB+.5
  IYA=AYA+.5
  IYB=AYB+.5
250 CONTINUE
  IF (IXA.LT.0.OR.IXA.GT.100) GO TO 260
  IF (IYA.LT.0.OR.IYA.GT.50) GO TO 260
  CALL PPLOT(IXA,IYA,NSYM,NCT)
260 CONTINUE
  IXA=IXA+1
  YA=(N*(AYB-AYA))/(AXB-AXA)
  IYA=AYA+YA+0.5
  N=N+1
  IF (IXA.LE.IXB) GO TO 250
  GO TO 400
C
C   SET PARAMETERS FOR Y DIRECTION
C
290 CONTINUE
  IF (AYB.GT.AYA) GO TO 295
  AYB=Y1
  AYA=Y2
  AXB=X1
  AXA=X2
295 CONTINUE
  IXA=AXA+.5
  IXB=AXB+.5
  IYA=AYA+.5
  IYB=AYB+.5
300 CONTINUE
  IF (IXA.LT.0.OR.IXA.GT.100) GO TO 310
  IF (IYA.LT.0.OR.IYA.GT.50) GO TO 310
  CALL PPLOT(IXA,IYA,NSYM,NCT)
310 CONTINUE
  IXA=IXA+1
  XA=(N*(AXB-AXA))/(AYB-AYA)
  IXA=XA+AXA+0.5

```

```
      N=N+1
      IF(IYA-IYB) 300,320,400
320  IXA = IXB
      GO TO 300
400  RETURN
      END
```

```

SUBROUTINE PLOT (IX,IY,K,NCT)
DIMENSION A(51,101),SYM(9)
COMMON /LAB/ TITLE(18),XLAB(11),YLAB(6)
1,HORIZ(20),VERT(6)
DATA SYM / 4H****,4H++++, 4H''''', 4HXXXX, 4H... , 4H2222,
1 4H , 4HIIII, 4H--- /
IF(K-99) 200,220,230
200 A(51-IY,IX+1)=SYM(K)
RETURN
220 CONTINUE
I=0
WRITE(6,103) TITLE,NCT
DO 225 II=1,6
I=I+1
WRITE(6,101) YLAB(II),(A(I,J),J=1,101)
IF(II.EQ.6) GO TO 228
DO 224 JJ=1,9
I=I+1
IF(I.NE.28) GO TO 221
WRITE(6,106) VERT(5),VERT(6),(A(I,J),J=1,101)
GO TO 224
221 IF(I.NE.24) GO TO 222
WRITE(6,106) VERT(1),VERT(2),(A(I,J),J=1,101)
GO TO 224
222 IF(I.NE.26) GO TO 223
WRITE(6,106) VERT(3),VERT(4),(A(I,J),J=1,101)
GO TO 224
223 WRITE(6,100) (A(I,J),J=1,101)
224 CONTINUE
225 CONTINUE
228 CONTINUE
WRITE(6,102) XLAB
WRITE(6,105) HORIZ
100 FORMAT(18X,101A1)
101 FORMAT(F17.3,1X,101A1)
102 FORMAT(F20.1,10F10.1)
103 FORMAT(1H1,20X,18A4,I6/)
105 FORMAT(/30X,20A4)
106 FORMAT(3X,2A4,7X,101A1)
230 DO 250 I=1,50
DO 240 J=1,101
240 A(I,J)=SYM(7)
A(I,1)=SYM(8)
250 CONTINUE
DO 260 J=1,101
260 A(51,J)=SYM(9)
DO 270 I=1,101,10
270 A(51,I)=SYM(8)
DO 290 I=11,41,10
A(I,1)=SYM(9)
290 CONTINUE
RETURN
END

```



```

      IF (AMIN.LT.0.) K=K-1
C
C                                     CHECK FOR MAX VALUE IN RANGE
C
      IF (AMAX.GT.(K+AXLEN)*RANGE) GO TO 330
      I=NPTS*INCT+1
      ARRAY(I)=K*RANGE
      I=I+INCT
      ARRAY(I)=RANGE
      RETURN
C
C                                     IF OUTSIDE RANGE RESET L AND
C
330  L=L+1
      IF (L.LT.11) GO TO 280
      L=2
      N=N+1
340  GO TO 280
C
C                                     SET UP NEGATIVE STEPS
C
350  K=AMAX/RANGE
      IF (AMAX.GT.0.) K=K+1
      IF (AMIN.LT.-(K+AXLEN)*RANGE) GO TO 330
      I=INCT*NPTS+1
      ARRAY(I)=K*RANGE
      I=I+INCT
      ARRAY(I)=-RANGE
      RETURN
400  WRITE(6,100)
100  FORMAT( // 10X, 'RANGE AND SCALE ARE ZERO ON PLOT ATTEMPT' )
      RETURN
      END

```



```

BLOCK DATA
COMMON/LAB/ TITLE(18),XLAB(11),YLAB(6)
1,HORIZ(20),VERT(6)
DATA VERT/4HMETE ,4HRS ,4HABOV,4HE ,4HROTT,4HOM /
DATA TITLE/8*4H ,4H TEM,4HPERA,4HTURE,4H VER,4HSUS ,4HDEPT,
A 4HH FO,4HR JU,4HLIAN, 4H DAY /
DATA HORIZ/4HWATE,4HR TE,4HMPER,4HATUP,4HE * ,4HDEGR,4HEES ,
A4HCENT,4HIGRA,4HDE ,10*4H /
END

```

CALCOMP PEN PLOT

The pen plotting routine graphs certain requested portions of the output from program TSIP. In order to use this routine, an output file (normally a magnetic tape) must be written during the execution of program TSIP. The production of this file is a user defined option, and is accomplished by placing a positive value in columns 61-70 of card number 1 of Card Group II in the input to TSIP. The file thus produced, together with the small amount of card input explained below, constitutes the total input for this program. Examples of the plots produced by the program and its FORTRAN listing are shown subsequent to the following explanation of plot's input and output.

INPUT

The card input to this plotting routine consists of two or more cards as explained below:

<u>CARD NO.</u>	<u>CARD COLUMNS</u>	<u>DATA DESCRIPTIONS</u>
1	1-80 (free field)	Comment to be printed on line printer.
2	1-5	Logical Unit Number upon which the tape written by TSIP is to be mounted for <i>input</i> to the plot routine.
	6-10	Logical Unit upon which Calcomp tape is to be written on <i>output</i> .
	11-15	The total number of days for which segment profile plots are to be produced.
3,4,5*	1-80 (16 fields of 5 columns each)	A list of the days for which profile plots are desired. Up to 48 days may be requested.

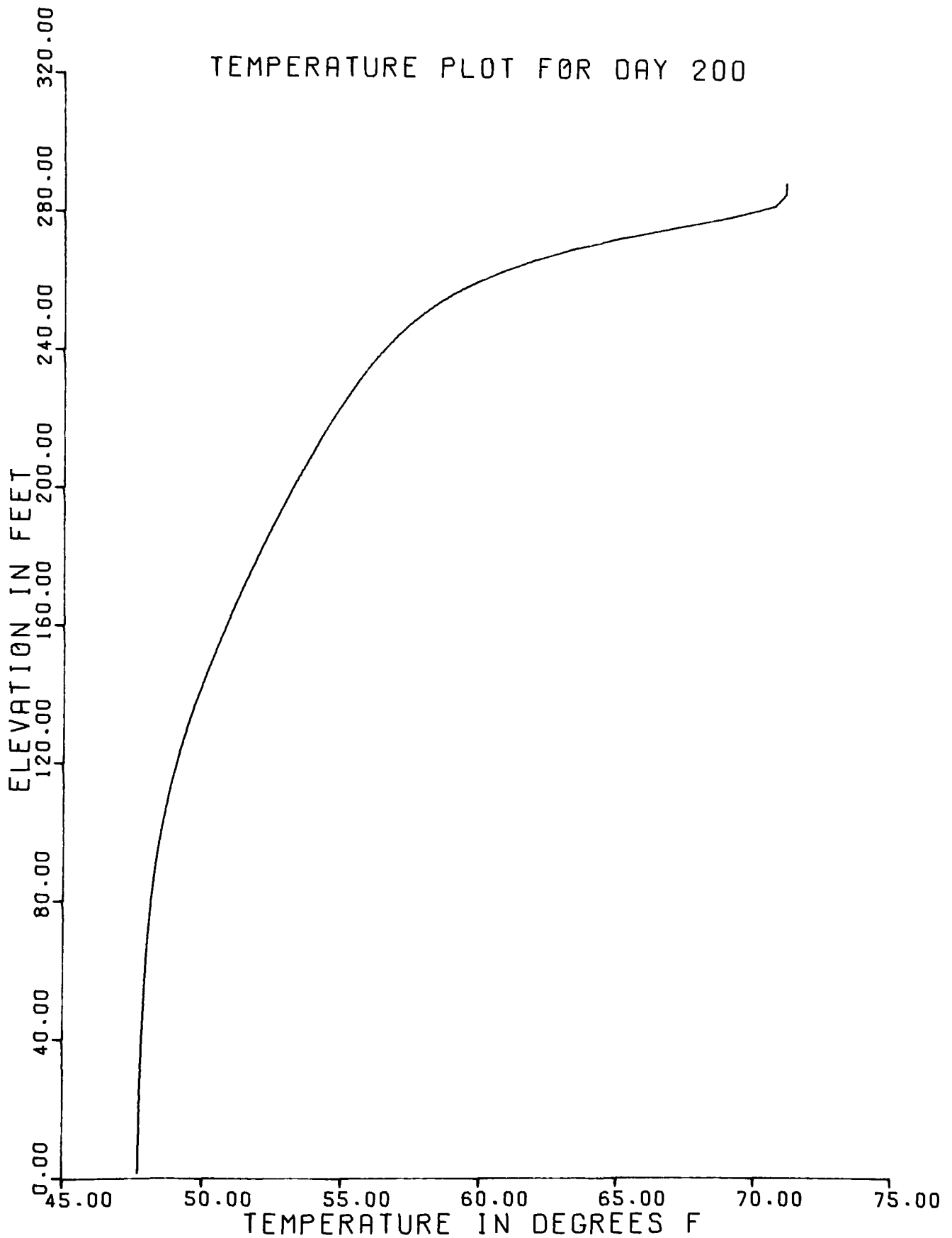
* Use only as many cards as necessary.

OUTPUT

The output from this routine are pen plots of the following items.

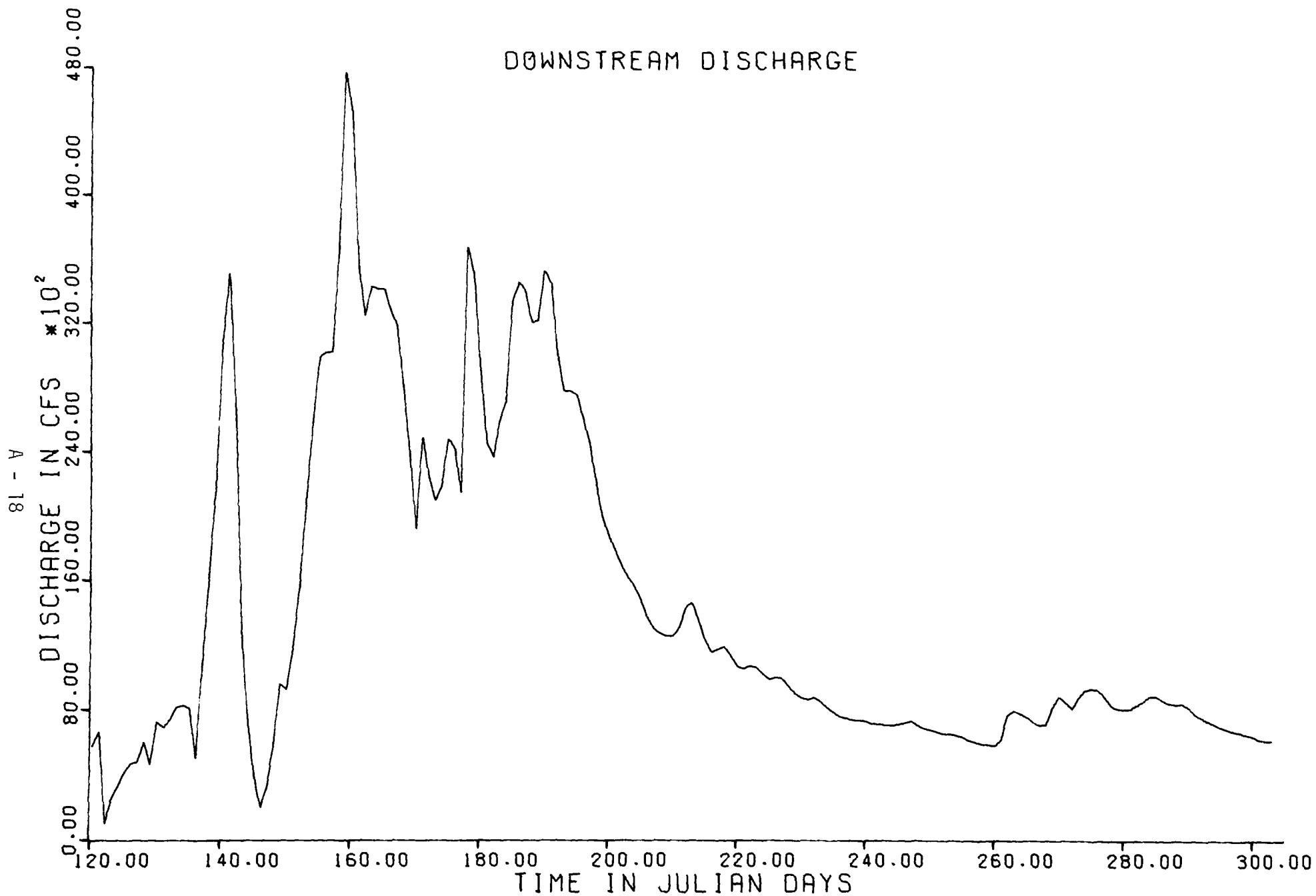
1. Temperature vs. depth for each segment for each day specified.
2. Temperature vs. time for total downstream release.
3. Discharge vs. time for total downstream release.
4. Temperature vs. time for the discharge from each individual outlet.
5. Discharge vs. time for each individual outlet.

TEMPERATURE PLOT FOR DAY 200

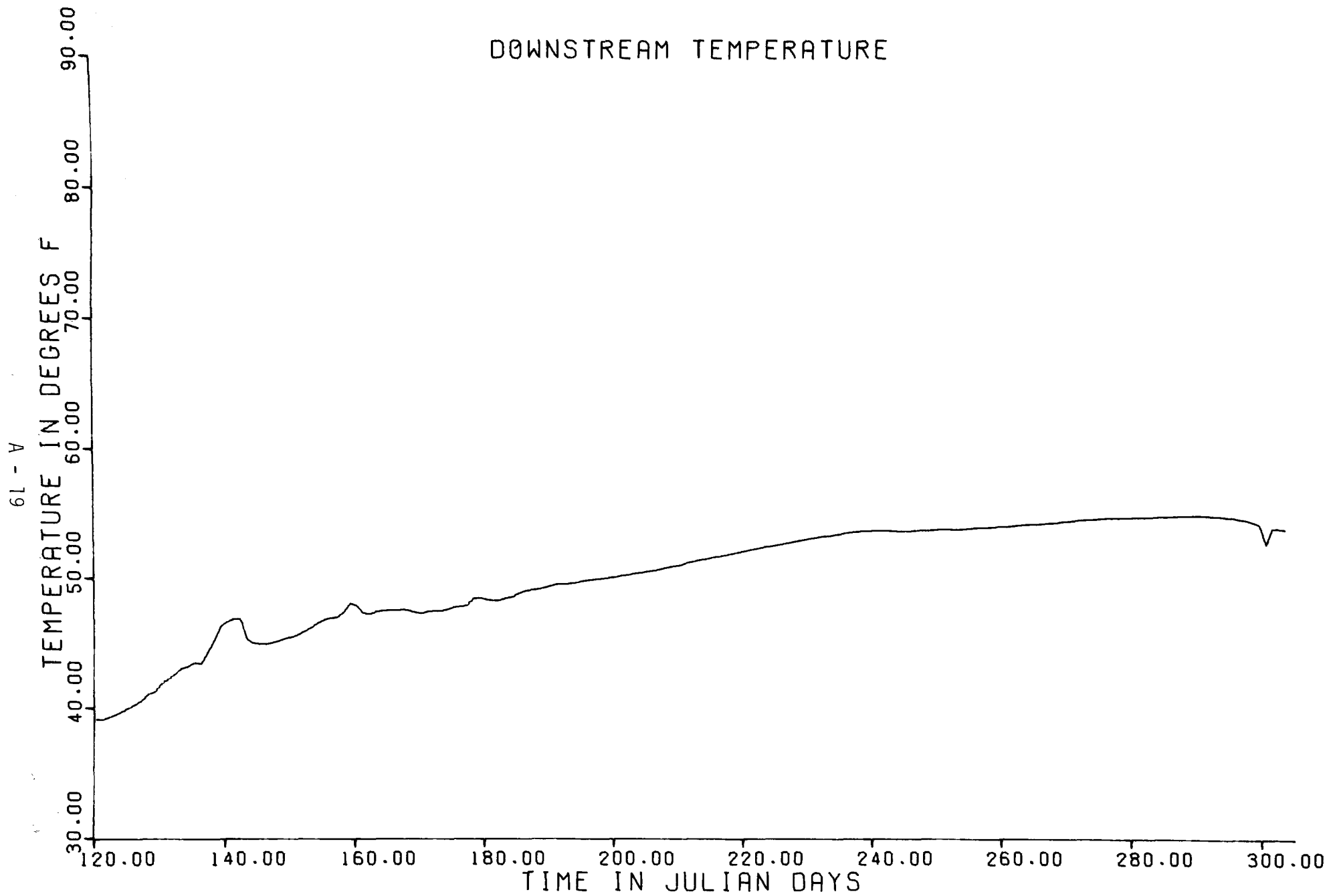


EXAMPLE PEN PLOT OUTPUT

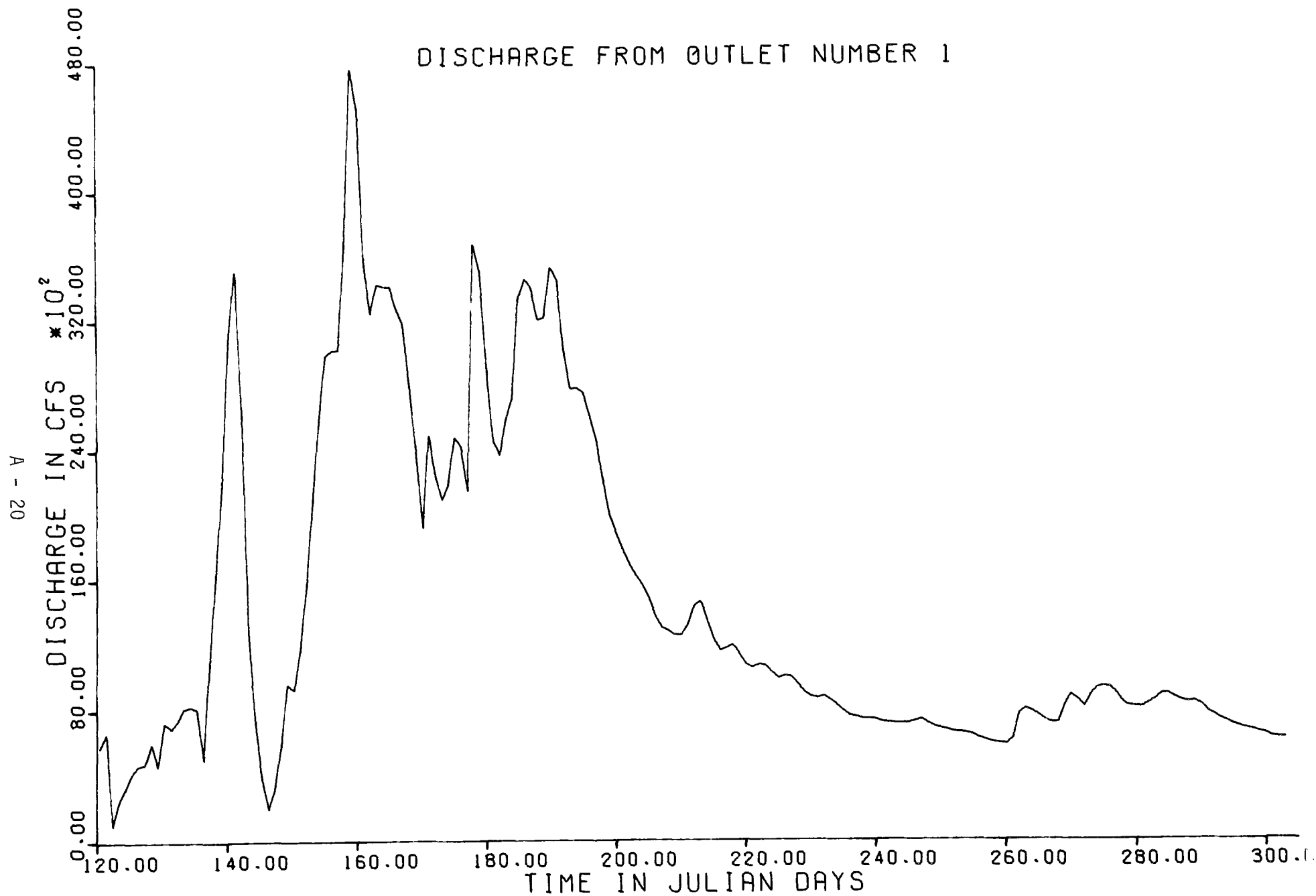
Segment Temperature vs. Elevation



EXAMPLE PEN PLOT OUTPUT
Downstream Temperature vs. Time

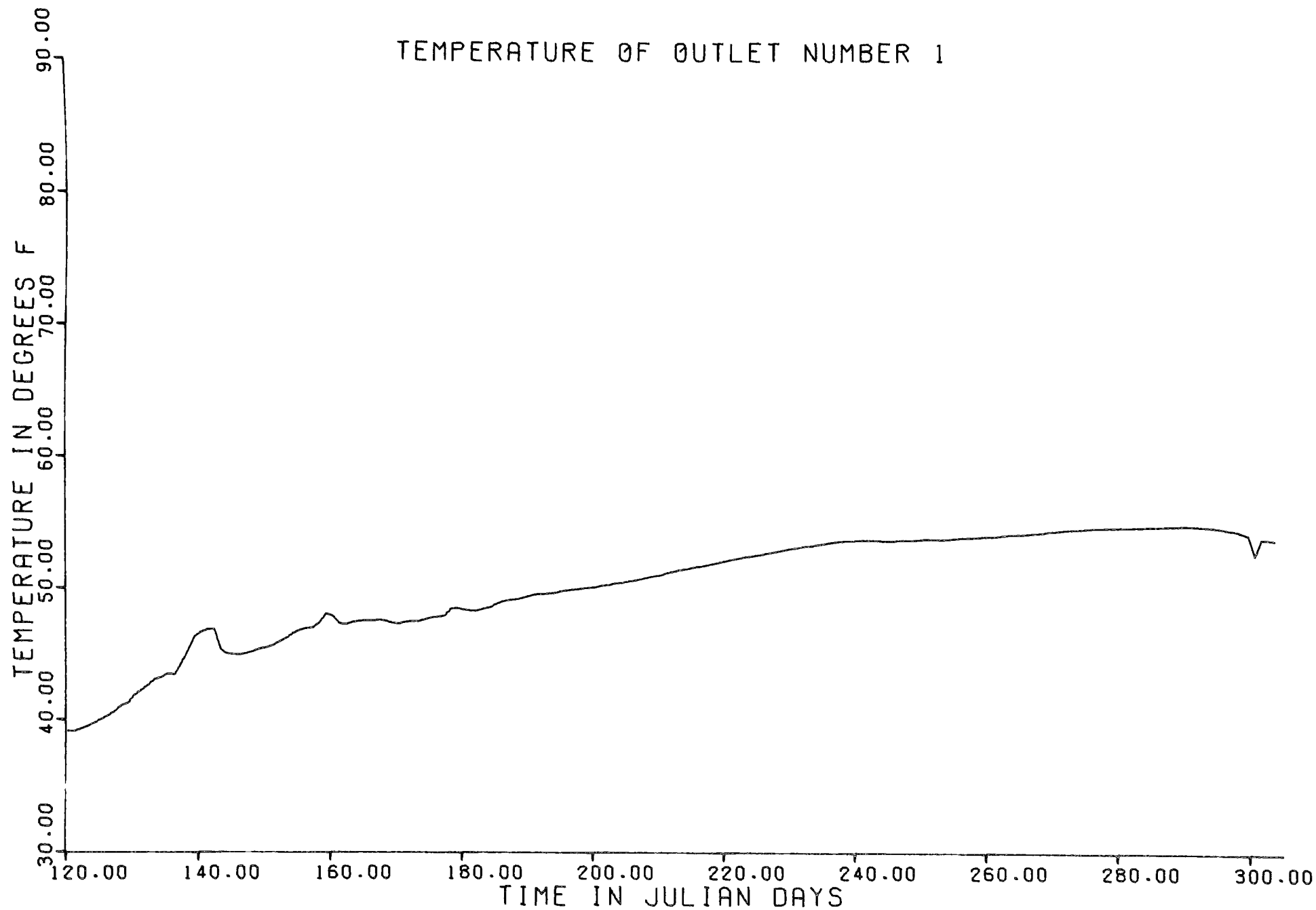


EXAMPLE PEN PLOT OUTPUT
Downstream Discharge vs. Time



EXAMPLE PEN PLOT OUTPUT
Individual Outlet Temperature vs. Time

TEMPERATURE OF OUTLET NUMBER 1



EXAMPLE PEN PLOT OUTPUT
Individual Outlet Discharge vs. Time

FORTRAN PROGRAM LISTING

CALCOMP PEN PLOT FOR OUTPUT FROM PROGRAM TSIP

```

C ***** CALCOMP PEN PLOT FOR OUTPUT FROM PROGRAM TSIP
C
      DIMENSION IBUF(1000), IDOUT(50), X(368), Y(368), QQT(368,5),
A   TOUT(368,5), DST(368), DSQ(368), HEAD(20), T08J(368)

C **** READ AND WRITE CARD INFORMATION

      READ(5,501) HEAD
      WRITE(6,601) HEAD
      READ(5,503) ITAPE, NTP, NSD
      WRITE(6,603) ITAPE, NTP, NSD
      IF( NSD .LE. 0 ) GO TO 103
      READ(5,503) ( IDOUT(J), J = 1, NSD )
      WRITE(6,605) ( IDOUT(J), J = 1, NSD )

C **** SETUP CALCOMP ORIGIN

103 CALL PLOTS(IBUF,1000,NTP)
      CALL PLOT(0.0,-30.0,-3)
      CALL PLOT(0.0,1.5,-3)
      CALL SYMBOL(0.0,0.0,0.21,25HPLOT FOR FWPCA STUDY TEAM
A   90.0,25 )
      CALL PLOT(4.0,0.0,-3)

C **** SETUP AND PLOT REQUESTED TEMPERATURE PROFILES

105 READ(ITAPE) IDAY, LDAY, SDZ, NOUTS, NSEG, NLETS
      WRITE(6,607) IDAY, LDAY, SDZ, NOUTS, NSEG, NLETS
      Y(1) = 3.2808 * 0.5 * SDZ
      TA = 3.2808 * SDZ
      IDAY = IDAY - 1
      DO 125 L = IDAY, LDAY
      READ(ITAPE) ID, NPTS, ( X(J), J = 1, NPTS )
      IF( NSD .LE. 0 ) GO TO 125
      DO 107 K = 1, NSD
      IF( IDOUT(K) .EQ. ID ) GO TO 111
107 CONTINUE
      GO TO 125
111 DO 115 J = 2, NPTS
      Y(J) = Y(J-1) + TA
115 CONTINUE
      DO 119 J = 1, NPTS
      X(J) = 1.8 * X(J) + 32.0
119 CONTINUE
      CALL SCALE(Y(1),8.0,NPTS,1)
      CALL SCALE(X(1),6.0,NPTS,1)
      CALL AXIS(0.0,0.0,24HTEMPERATURE IN DEGREES F,-24,6.0,0.0,
A   X(NPTS+1),X(NPTS+2) )
      CALL AXIS(0.0,0.0,17HELEVATION IN FEET,17,8.0,90.0,
A   Y(NPTS+1),Y(NPTS+2) )
      CALL LINE(X,Y,NPTS,1,0,0)
      CALL SYMBOL(1.04,8.00, 0.14,24HTEMPERATURE PLOT FOR DAY,0.0,24 )
      FPN = ID

```

```

      CALL NUMBER(4.54,8.00,0.14,FPN,0.0,-1)
      CALL PLOT(10.0,0.0,-3)
125  CONTINUE
      READ(ITAPE,END=127) TA
127  IF( NSEG .NE. NLETS ) GO TO 105
      WRITE(6,609)

```

C ***** INPUT AND CONVERT DOWNSTREAM VALUES

```

      NPTS = LDAY - IDAY + 1
      READ(ITAPE) ( ( QOT(J,K), K = 1, NOUTS), J = 1, NPTS )
      READ(ITAPE) ( ( TOUT(J,K), K = 1, NOUTS), J = 1, NPTS )
      DO 145 J = 1, NPTS
      DSQ(J) = 0.0
      TA = 0.0
      DO 141 K = 1, NOUTS
      QOT(J,K) = 35.3145 * QOT(J,K)
      TOUT(J,K) = 1.8 * TOUT(J,K) + 32.0
      DSQ(J) = DSQ(J) + QOT(J,K)
      TA = TA + QOT(J,K) * TOUT(J,K)
141  CONTINUE
      DST(J) = TA / DSQ(J)
145  CONTINUE

```

C ***** GENERATE THE TIME AXIS

```

      X(1) = 0.5
      DO 149 K = 2, NPTS
      X(K) = X(K-1) + 1.0
149  CONTINUE
      TA = IDAY - 1
      CALL SCALE(X,9.0,NPTS,1)

```

C ***** PLOT THE FLOWS AND DISCHARGES

```

      DO 155 K = 1, NOUTS
      TOUT(NPTS+1,K) = 30.0
      TOUT(NPTS+2,K) = 10.0
      CALL SCALE(QOT(1,K),6.0,NPTS,1)
155  CONTINUE
      CALL SCALE(DSQ(1),6.0,NPTS,1)
      MAX = NOUTS + 1
      DO 167 L = 1, MAX
      CALL AXIS(0.0,0.0,19,TIME IN JULIAN DAYS,-19,9.25,0.0,
A   TA,X(NPTS+2) )
      CALL AXIS(0.0,0.0,24,TEMPERATURE IN DEGREES F, 24,6.0,90.0,30.0,
A   10.0 )
      IF( L .GT. 1 ) GO TO 159

```

C ***** PLOT TOTAL DOWNSTREAM VALUES

```

      CALL LINE(X,DST,NPTS,1,0,0)
      CALL SYMBOL(3.08,6.00,0.14,22HDOWNSTREAM TEMPERATURE ,0.0,22 )

```

```

CALL PLOT(13.25,0.0,-3)
CALL AXIS(0.0,0.0,19HTIME IN JULIAN DAYS,-19,9.25,00.0,
A TA, X(NPTS+2) )
CALL AXIS(0.0,0.0,16HDISCHARGE IN CFS,16,6.0,90.0,
A DSQ(NPTS+1),DSQ(NPTS+2) )
CALL LINE(X,DSQ,NPTS,1,0,0)
CALL SYMBOL(3.22,6.00,0.14,20HDOWNSTREAM DISCHARGE,0.0,20)
GO TO 163

```

C ***** PLOT DOWNSTREAM COMPONENTS

```

159 K = L - 1
    FPN = K
    CALL LINE(X,TOUT(1,K),NPTS,1,0,0)
    CALL SYMBOL(2.52,6.00,0.14,28HTEMPERATURE OF OUTLET NUMBER,0.0,28)
    CALL NUMBER(6.58,6.00,0.14,FPN,0.0,-1)
    CALL PLOT(13.25,0.0,-3)
    CALL AXIS(0.0,0.0,19HTIME IN JULIAN DAYS,-19,9.25,0.0,
A TA, X(NPTS+2) )
    CALL AXIS(0.0,0.0,16HDISCHARGE IN CFS,16,6.0,90.0,
A QOT(NPTS+1,K),QOT(NPTS+2,K) )
    CALL LINE(X,QOT(1,K),NPTS,1,0,0)
    CALL SYMBOL(2.52,6.00,0.14,28HDISCHARGE FROM OUTLET NUMBER,0.0,28)
    CALL NUMBER(6.58,6.00,0.14,FPN,0.0,-1)
163 CALL PLOT(13.25,0.0,-3)
    WRITE(6,613) L
167 CONTINUE
    REWIND ITAPE

    STOP

```

C ***** INPUT FORMAT STATEMENTS

```

501 FORMAT( 20A4 )
503 FORMAT( 16I5 )

```

C ***** OUTPUT FORMAT STATEMENTS

```

601 FORMAT( 1H1 / 35X, 55HCALCOMP PLOTTING ROUTINE FOR THERMAL SIMULAT
ION RESULTS // 40X, 20A4 )
603 FORMAT( // 20X, 10HINPUT TAPE I10 / 18X, 12HCALCOMP TAPE I10 /
A 17X, 13HPROFILE PLOTS I10 )
605 FORMAT( /// 23X, 17HPROFILE PLOT DAYS //( I40 ) )
607 FORMAT( // 19X, 11HTAPE HEADER// 21X, 9HFIRST DAY I10 /
A 21X, 9HFINAL DAY I10 / 23X, 7HELEMENT F10.2 /
B 23X, 7HOUTLETS I10 /
C 20X, 10HSEGMENT NO I10 / 20X, 10HOUTLET SEGMENT I10 )
609 FORMAT( /// 40X, 22HPROFILE PHASE COMPLETE )
613 FORMAT( // 40X, 15HCOMPONENT PHASE I2, 12H IS COMPLETE )

END

```

1	Accession Number	2	Subject Field & Group	SELECTED WATER RESOURCES ABSTRACTS INPUT TRANSACTION FORM
			Ø2H, Ø5B	

5	Organization
	Water Resources Engineers, Incorporated Walnut Creek, California

6	Title
	MATHEMATICAL MODELS FOR THE PREDICTION OF THERMAL ENERGY CHANGES IN IMPOUNDMENTS,

10	Author(s)	16	Project Designation
	Orlob, Gerald T., Roesner, Larry A., and Norton, William R.		FWPCA Contract No. 14-12-422, 16130 EXT
		21	Note

22	Citation
	Final Report, FWPCA Contract No. 14-12-422, FWQA Report No. 16130 EXT 12/69

23	Descriptors (Starred First)
	*Reservoirs, *Impoundments, *Water temperature, *Thermal stratification, *Mathematical models, *Heat budget, Computer programs, Columbia River, Stratification, Diffusion, Diffusivity

25	Identifiers (Starred First)
	*Temperature prediction, *Selective withdrawal, Lake Roosevelt

27 *Abstract* A mathematical model developed previously by Water Resources Engineers, Inc., was refined and extended to produce a more generalized model capable of describing the thermal regime of a stratified reservoir under various hydrologic, meteorologic, and hydraulic conditions. Two important refinements of the original model were made: (1) A generalized empirical expression for the eddy conductivity coefficient was derived, and (2) The influence of reservoir stability on the vertical extension of the withdrawal zone for reservoir outlets and the zone of influence for inflows was accounted for.

The refined model accounts for external heat exchange by the usual heat budget components. Internal heat transfer is accomplished by the penetration of short-wave radiation, eddy diffusion, and vertical advection. The model was tested and verified on Hungry Horse Reservoir and is applicable on reservoirs for which the assumption of horizontal isotherms is valid. A method for testing this assumption is given.

The model described above was extended to simulate weakly stratified reservoirs (tilted isotherms). The weakly stratified reservoir is represented as a set of smaller reservoirs (or segments) that are coupled to one another by heat and mass continuity. Each small reservoir is described by the basic model, and the tilted isotherms are produced by connecting the temperature profiles at the longitudinal midpoints of the segments. A test of the segmented model on Lake Roosevelt gave satisfactory results; however, its general applicability remains to be established.

This report was submitted in fulfillment of project 16130 EXT, Contract No. 14-12-422, under the sponsorship of the Federal Water Quality Administration.

Abstractor	Larry A. Roesner	Institution	Water Resources Engineers, Incorporated
------------	------------------	-------------	---